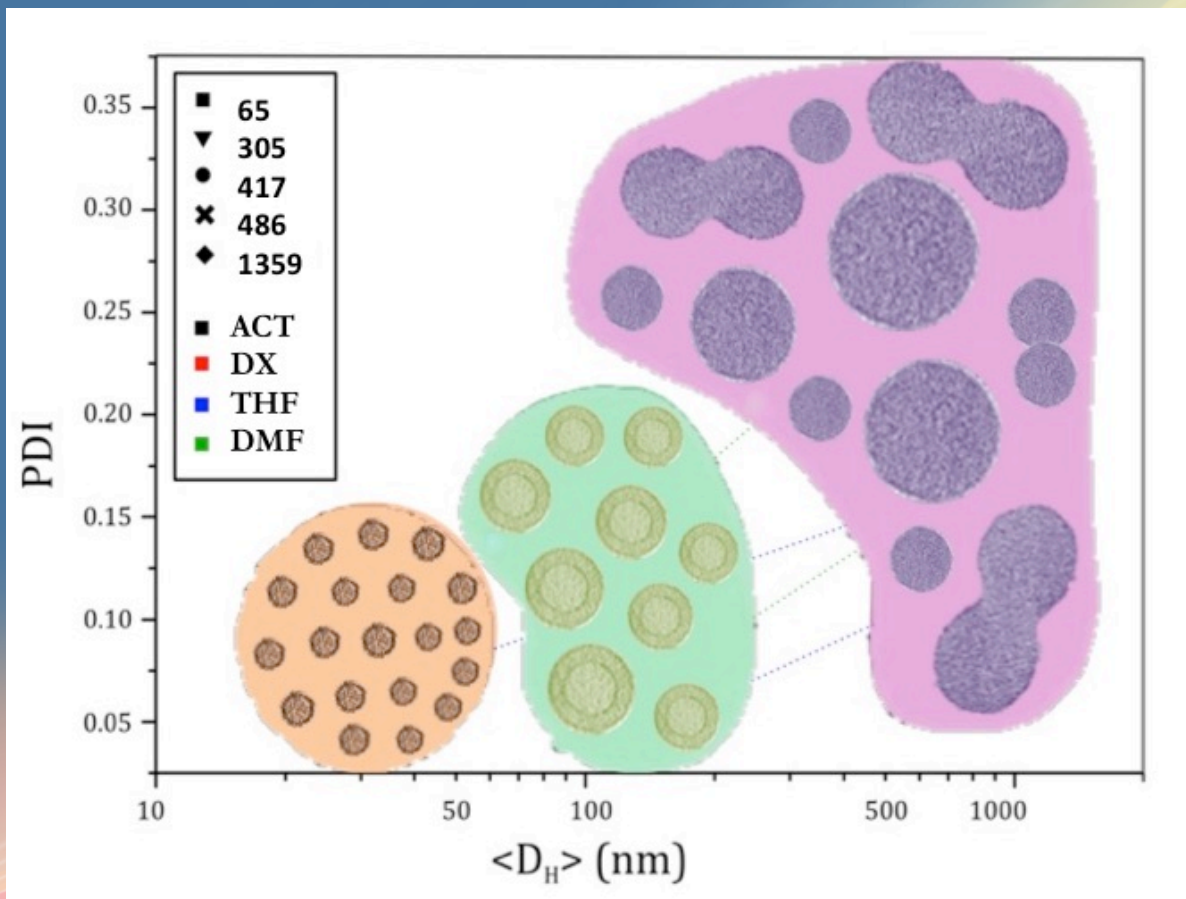


Self-assembly of amphiphilic block copolymers from good solvents: toward a predictive morphologic map for the choice of drug delivery system



Self-assembly of amphiphilic block copolymers from good solvents: toward a predictive morphologic map for the choice of drug delivery system

Daniela Manzone



SCUOLA DI DOTTORATO
UNIVERSITÀ DEGLI STUDI DI MILANO-BICOCCA

Department of Materials Science

PhD School in Nanostructures and Nanotechnology
Cycle XXVIII

Self-assembly of amphiphilic block copolymers from good solvents: toward a predictive morphologic map for the choice of drug delivery system

Surname Manzone **Name** Daniela Maddalena
Registration number 775148

Tutor: Prof. Roberto Simonutti

Coordinator: Prof. Gianfranco Pacchioni

ACADEMIC YEAR 2016/2017

**Dedicated to
my father**

*“There are no ideal conditions in which to write, study,
work or think, but it is only the will, passion and
stubbornness to push a man to pursue his own project.”*

- Konrad Lorenz

Summary

Abstract	7
CHAPTER 1	9
INTRODUCTION	9
1.1 Nanotechnology	9
1.2 Nanomedicine	14
1.3 Block Copolymers	15
1.4 Biopolymers for drug delivery system	16
1.5 Self-assembly of amphiphilic block copolymer from good solvents	21
1.6 References	28
CHAPTER 2	30
SYNTHESIS OF mPEO₁₁₃-<i>b</i>-PLA_x COPOLYMERS BY RING-OPENING POLYMERISATION	30
2.1 Experimental Section	30
2.1.1 Materials	30
2.1.2 Synthetic Methods	30
2.1.3 NMR spectroscopy (NMR).....	33
2.1.4 Gel Permeation Chromatography (GPC)	33
2.1.5 Differential Scanning Calorimetry (DSC)	34
2.2 Results and Discussion	35
2.3 Chapter Summary	44
2.4 References	45
CHAPTER 3	47
SELF-ASSEMBLY OF AMPHIPHILIC BLOCK COPOLYMERS FROM GOOD SOLVENTS	47
3.1 Experimental Section	47
3.1.1 Materials	47
3.1.2 Nanoparticle fabrication	47
3.1.3 Dynamic Light Scattering	51
3.1.4 Transmission Electron Microscopy (TEM).....	57
3.1.5 TEM in cryogenic conditions (cryo-TEM)	59
3.2 Results and Discussion	63
3.3 Chapter Summary	67
3.4 References	68

CHAPTER 4	69
SELF-ASSEMBLY OF AMPHIPHILIC BLOCK COPOLYMERS FROM A MIXTURE OF GOOD SOLVENTS	69
4.1 Experimental Section	69
4.1.1 Materials	69
4.1.2 Preparation of C6-NPs for crossing the blood brain barrier	69
4.1.3 Self-assembly of amphiphilic block copolymers from a mixture of good solvents...	75
4.2 Results and Discussion	77
4.3 Chapter Summary	80
4.4 References.....	81
CHAPTER 5	83
CYTOTOXICITY OF SELF-ASSEMBLED AMPHIPHILIC BLOCK COPOLYMERS NANOPARTICLES.....	83
5.1 Experimental Section.....	83
5.1.1. Materials	83
5.1.2 Nanoparticles Fabrication	83
5.1.3 Cell Cultures	84
5.1.4 Assessment of NP Cytotoxicity.....	84
5.1.5 MTT Assay.....	84
5.2 Results and Discussion	87
5.3 Chapter Summary	92
5.4. References.....	93
CHAPTER 6	94
STUDY ON AGING OF mPEO₁₁₃-b-PLA_x SYSTEM.....	94
6. 1 Experimental Section	94
6.1.1 Materials	94
6.1.2 Aging of mPEO-b-PLA _x system	94
6.1.3 Study on aging of the copolymers mPEO ₁₁₃ -b-PLA _x	96
6.2 Results and Discussion	102
6.3 Chapter Summary	104
6.4. References.....	105
CHAPTER 7	106
7.1 Conclusion and Future Outlook.....	106
7.2 References.....	110
List of Abbreviations	111
Acknowledgements.....	115
Publication list	117
Appendix	118

Abstract

Polymeric nanoparticles (NPs) are very promising “smart carriers” for the future of nanomedicine. The main advantages of polymeric NPs manufactured by self-assembly are: high control of shape and size, high stability and significant increase of the solubility of poorly soluble drugs. Particle morphology can condition cytotoxicity, circulation time in blood, release of drug and removal of NPs from the body and thus improve the therapeutic efficacy. In turn, assembly can be guided by the choice of the environment. In this work, a protocol was developed for the synthesis and characterization of self-assembled polymeric NPs. We selected amphiphilic block copolymers of polyethylene oxide (PEO) and polylactic acid (PLA), two polymers already approved by the US Food and Drugs Administration (FDA) for medical use. The synthesis of the poly (lactic acid block) on a block of poly (ethylene oxide) has been carried out, by means of ROP (Ring Opening Polymerization) using a completely metal-free synthesis, catalyzed by 1,5-diazabicyclo[5.4.0]undec-5-ene (DBU), in order to avoid any problems of poor biocompatibility or allergenicity. The compositional characterization was carried out by solution Nuclear Magnetic Resonance (NMR) and calorimetric properties have been studied by Differential Scanning Calorimetry (DSC). After polymerizing a great variety of PLA chains of different length (PEO₁₁₃-b-PLA_x- with x ranging from 30 to 1359), nanoparticles were assembled from different organic solvents: dimethylformamide (DMF), acetone, tetrahydrofuran (THF) and dioxane, using the technique of nanoprecipitation. NPs were then purified by dialysis and analyzed by Dynamic Light Scattering (DLS), obtaining for each sample a mean hydrodynamic diameter value and a value of dispersion diameters. Particle diameter ranged goes from 40 to 800 nm, with many of the polymers presenting different values as a function of the starting solvent.

A plot of all samples in terms of the DLS variables displayed several clusters, ideally associated to different morphologies.

To verify the corresponding shapes, and then transform the plot into a morphological map that is able to guide the selection of the most promising nanocarriers for medical applications, Cryogenic Transmission Electron Microscopy (cryo-TEM) investigation was necessary. Specifically we mapped the region of simple micelles (low diameter, low PDI) the region of polymersomes was mapped as well. The cytotoxicity tests were performed on all samples and only the largest nanoparticles reduced cell viability.

Additional experiments of uptake and release of drugs were carried out, also through ad hoc assemblies in solvent mixtures that optimize the solubility of the drugs without affecting the morphology of “nanocarriers”. Finally, study of the polymers’ aging obtained through the characterisation by DSC, GPC and NMR were performed.

CHAPTER 1

INTRODUCTION

1.1 Nanotechnology

Nanoscience and nanotechnology take a new approach to science that is based on the understanding and in-depth knowledge of the properties of matter at the nanoscale.

Nanoscience operates within a framework of multidisciplinary investigations involving multiple lines of research, including chemistry, materials science, physics, technology, mechanical engineering and electronics, molecular biology, biophysics, biochemistry, medicine, biology, mechanics and art. For this reason, it is considered a 'horizontal science' (Figure 1.1).¹

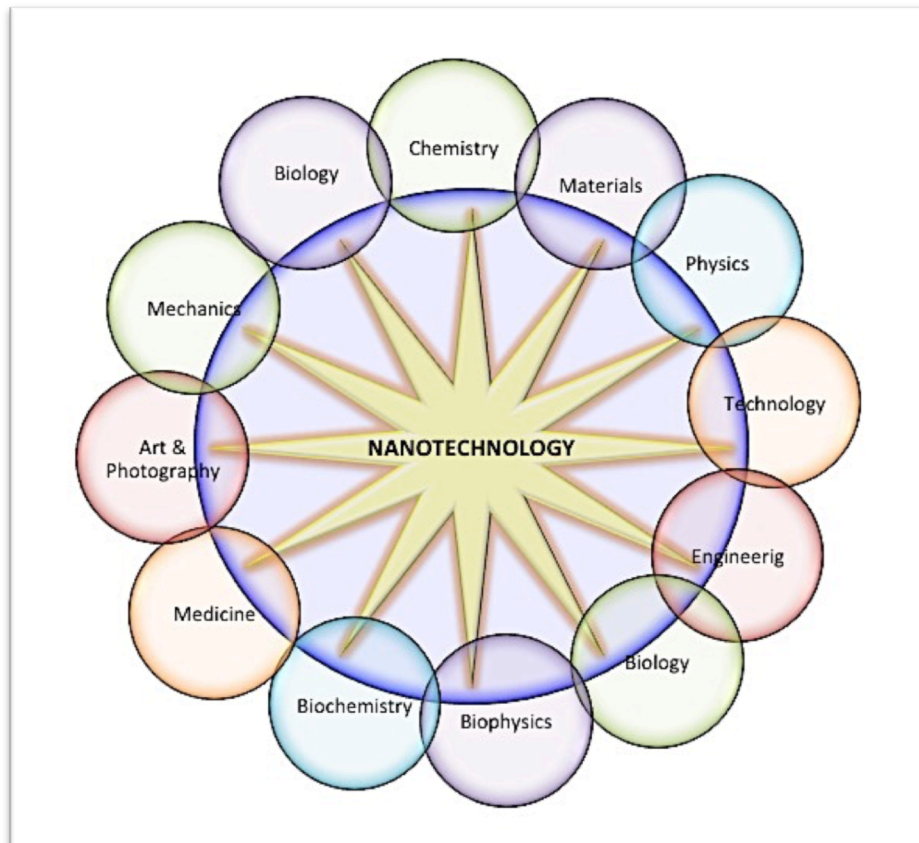


Figure 1.1. Convergence and multidisciplinary in nanotechnology.

The ‘nano’ prefix indicates 10^{-9} ; a nanometer (nm) equals one billionth of a meter, a dimension tens of thousands of times smaller than the diameter of a human hair. At this scale, the chemical-physical properties exhibited by the materials may be surprisingly different from those present at a larger scale (Figure 1.2).

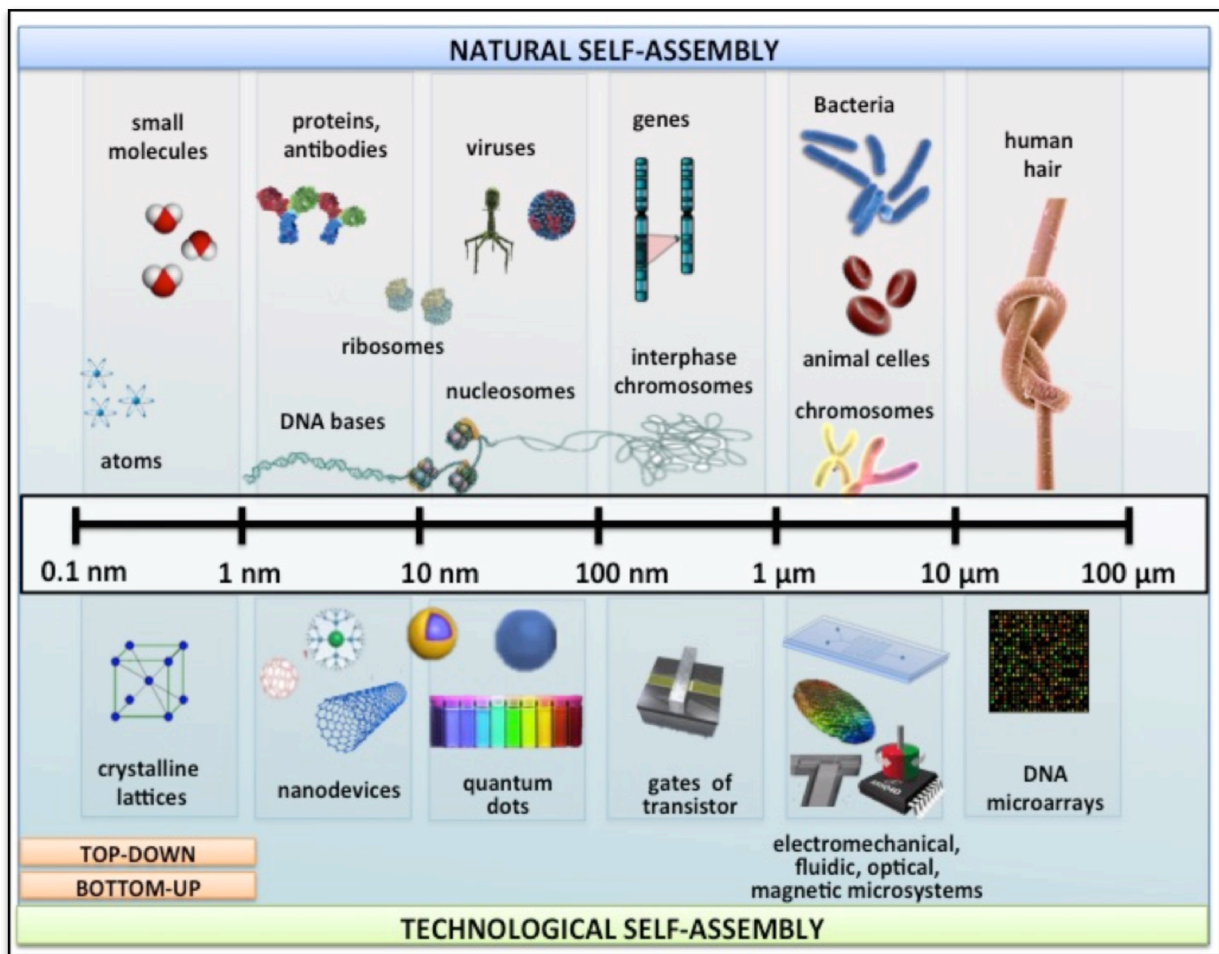


Figure 1.2. Comparison of the scales of various biological and technological objects.

Over the years, the field of nanotechnology began to multiply in numerous sectors of applied studies, such as biomedical, pharmaceutical, electronic, automotive, aerospace, textiles and cosmetology. Nanotechnology has also had a profound impact on art. The research and tools of nanotechnology, and in particular the beauty of microscopic images, have inspired the artists of the ‘invisible world’, of what the human eye cannot perceive (Figure 1.3).

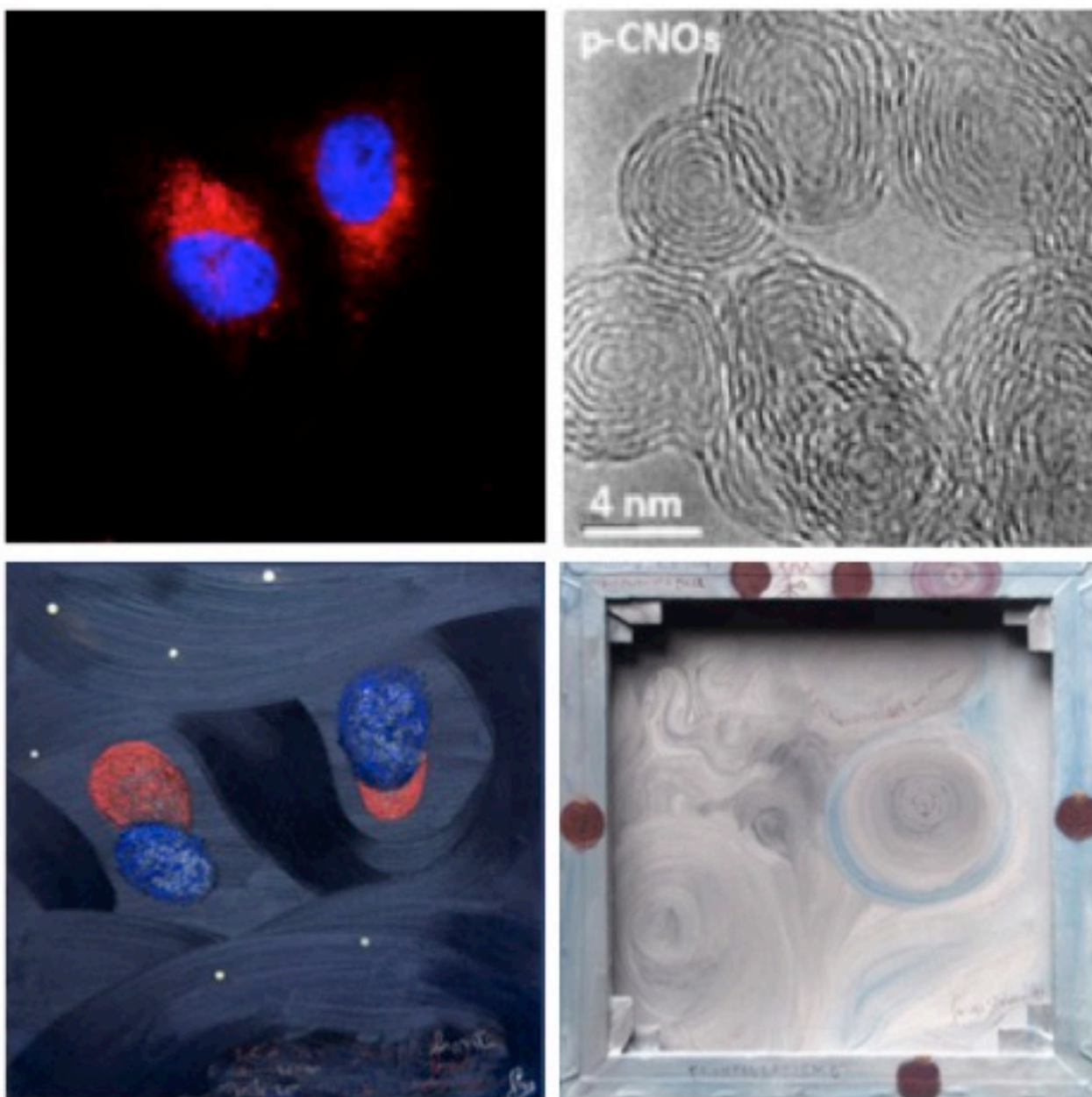


Figure 1.3. High-resolution TEM images of pristine CNOs (top and left); confocal images of azaBODIPY-CNOs in HeLa Kyoto cells (top and right)². Courtesy of Professor Silvia Giordani. *Micro cosmos and peace*, 2014, front and back. Author Giuseppe Siniscalchi. Mixed technique on canvas 40 x 40 cm. Representative work of fronteversismo® art of peace and love for life. Courtesy of Giuseppe Siniscalchi.

Given its industrial importance, the breadth of application areas and continued growth of public and private funding for research in the field of nanotechnology is now universally recognised; many analysts see nanotechnology as the driving force behind a new ‘industrial and technological revolution’ or even a ‘new Renaissance of Science’.^{3,4,5,6}

The increase of public funding and private research and development (R&D) of nanosciences and nanotechnology in recent years reflects the high expectations lying in the successful application of these disciplines. The world's R&D investment in the field of nanotechnology, reported by government organisations, increased at least ninefold between 1997 and 2005, and at least 60 countries have started to invest in this promising field innovation. Mainly advanced industrial countries but also developing nations are engaged in intense R&D activity that is increasingly financed by public funds, which is still considered essential to the support of large efforts from an economic point of view. This research is mainly supported at the private level, by companies that are very present in the industrial fabric of the United States and Japan, where there are companies with great turnover (more than \$500 million), followed by German and UK companies, which have small to medium turnover (tens of millions of dollars). Private companies are not the only institutions active in nanotechnology; research institutes and university organisations play a key role, especially in Europe and Asia.⁷ The growing interest in nanotechnology is also confirmed by the 'proliferation of nanojournals' between 1985 and 2010 (Figure 1.4).⁸

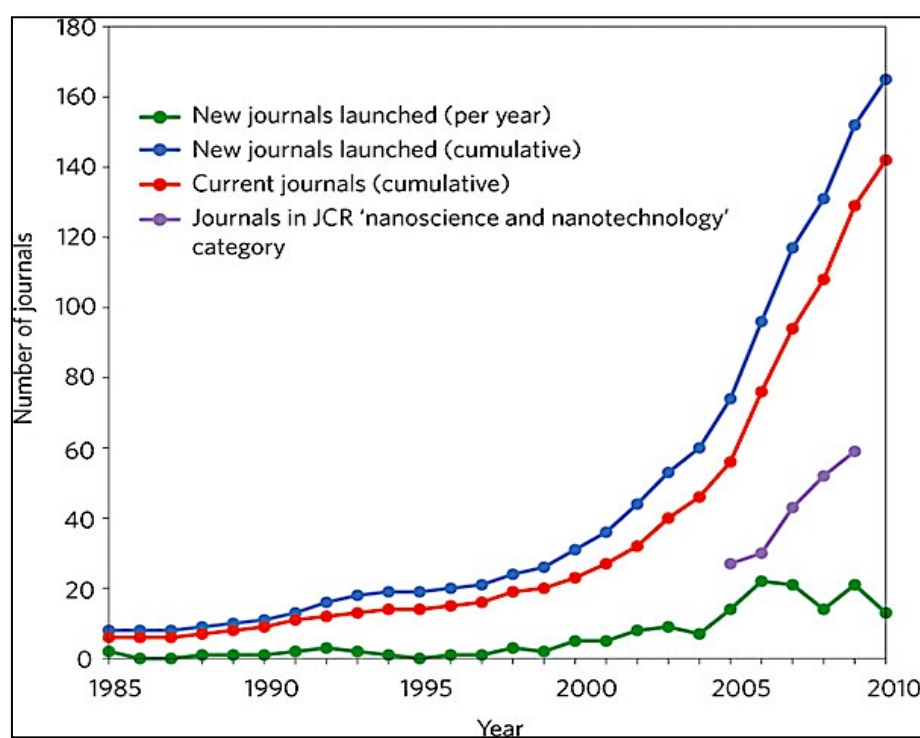


Figure 1.4. Increase in scientific publications 1985–2010.⁸

The actual ability to transfer scientific results obtained in research laboratories to technological applications can be estimated if one considers the change in the number of patents filed by year.

Nanotechnology in medical applications is particularly promising, and significant achievements have been registered in the early diagnosis of many diseases and in modified drug release; the technology also allowing the imaging of cellular traffic monitoring. Further evidence of the biotechnological and pharmaceutical industries' strong impetus toward nanotechnologies is that, interestingly, the number of patents filed per year in nanobiotechnology and nanobiomaterials was constantly growing from 1991 to 2008 (Figure 1.5).⁹

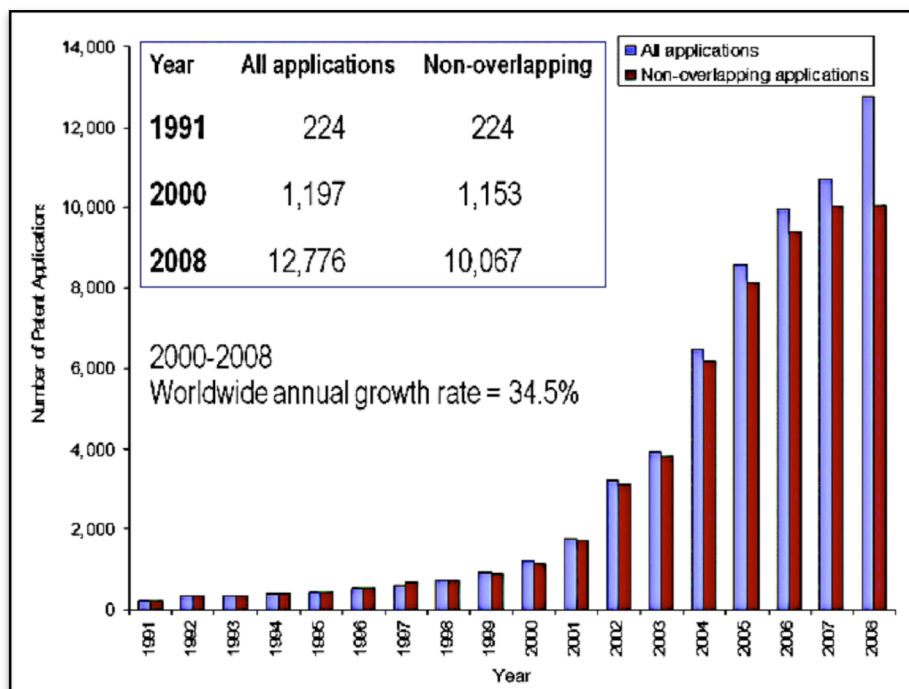


Figure 1.5. Total number of nanotechnology patent applications from 1991 to 2008 in 15 leading patent depositories in the world from 1991-2008. Two sets of data are reported based on the number of all nanotechnology patent applications and the number of non-overlapping nanotechnology patent applications.⁹

According to a recent report the global nanobiotechnology market was valued at about \$28 billion in 2015 and expected to reach about \$42 billion by 2021, growing at a CAGR of 8.5% between 2016 and 2021 (Figure 1.6).¹⁰

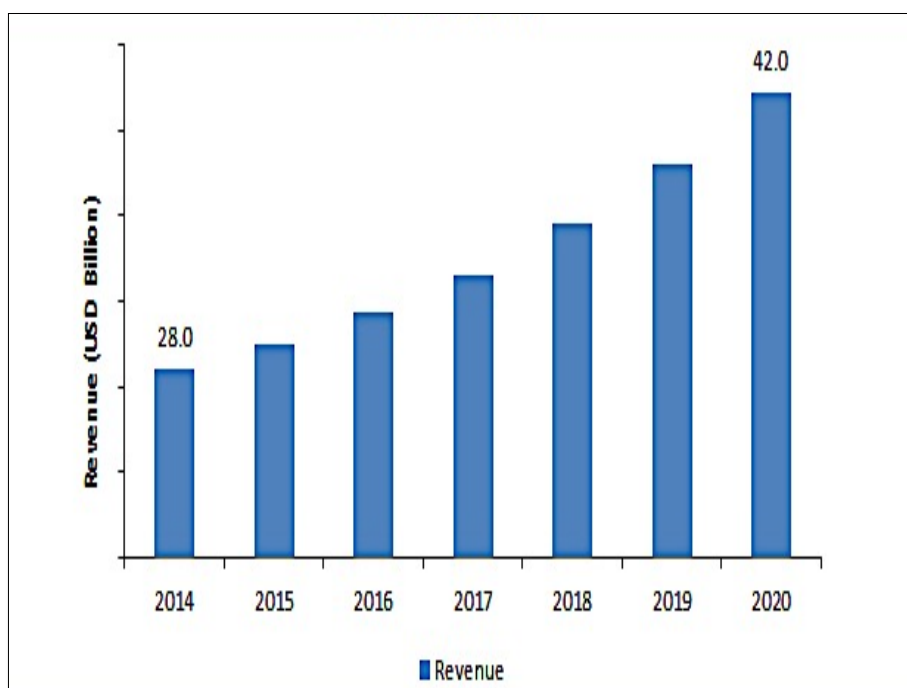


Figure 1.6. Global nanobiotechnology market between 2014 and 2020.¹⁰

1.2 Nanomedicine

The European Science Foundation (ESF) defines nanomedicine as ‘the science and technology of diagnosing, treating, and preventing disease and traumatic injury, of relieving pain, and of preserving and improving human health, using molecular tools and molecular knowledge of the human body’ (ESF 2004).

A more recent definition is that given by the U.S. National Institutes of Health Roadmap for Medical Research in Nanomedicine (NIH 2006), in which nanomedicine is defined as ‘an offshoot of nanotechnology, which refers to highly specific medical interventions at the molecular scale for curing disease or repairing damaged tissues, such as bone, muscle, or nerve’.¹¹

Nanomedicine operates at the same scale of biological mechanisms. A molecule of DNA has a diameter of about 2.5 nm, one of hemoglobin about 5 nm. Human cells have a diameter of 10–20 μm (from a minimum of 4 μm to a maximum of 200 μm).

Benefiting from converging interdisciplinary approaches, nanomedicine aims to provide a valuable set of research tools and clinically useful devices in the field of regenerative medicine, diagnostics, and the development of new approaches to drug delivery. This means that nanometer-size materials and tools can readily enter most cells.

Some aspects, however, remain unresolved, especially from the point of view of safety¹² and regulatory oversight.¹³

1.3 Block Copolymers

A macromolecule in which two or more monomers are incorporated as integral parts of every single macromolecular chain is defined as a copolymer. Both synthetic and natural polymers (proteins, peptides, nucleic acid) play a major role in the life sciences.

Block copolymers (BCPs) are classified by the number of blocks each molecule contains and how they are arranged: linear block copolymers comprise two or more polymer chains in sequence, whereas a star block copolymer contains more than two linear block copolymers attached at a common branch point.

The standard notation for block copolymers is defined by IUPAC guidelines, whereby A-b-B denotes a diblock copolymer of polymer blocks A and B. However, sometimes the b is replaced by the full term block (A-block-B) or alternatively is omitted (A-B). Block copolymers with two, three and more blocks are called diblock copolymers (A-B), triblock copolymers (A-B-A/A-B-C) and star-block copolymers (multi-block).

Thus, an A-B-C linear triblock consists of three monomer types, whereas an ABA linear triblock consists of two monomer types.

In a linear arrangement (Figure 1.7), the blocks are connected end to end; in a star, they are connected via one of their ends at a single junction.¹⁴

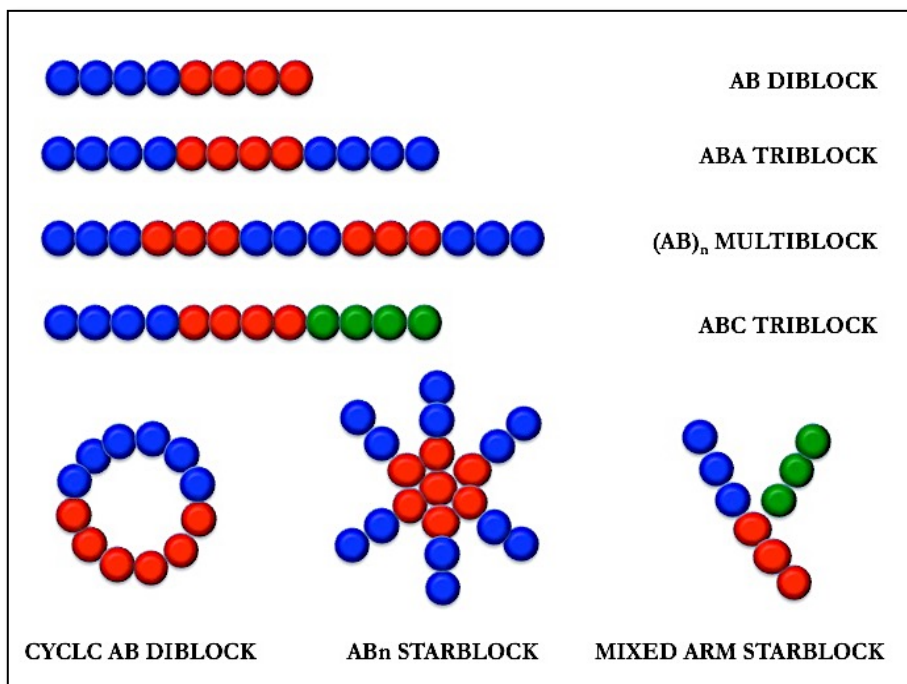


Figure 1.7. Different block copolymer architectures.

1.4 Biopolymers for drug delivery system

Most of the instruments used in nanomedicine as ‘carriers’ of other molecules are called nanocarriers. The use of nanocarriers, for example as conveyors of drugs, is today the epicenter of modern drug delivery strategies. Paul Ehrlich, German pharmacologist, founder of chemotherapy, and winner of the Nobel Prize in Physiology or Medicine, first mentioned this concept in the 19th century. He described a ‘magic bullet’ capable of transporting drugs directly into the target tumor cell so as not to act on the surrounding cells. Different types of drug delivery systems (DDS) have been developed in recent decades, and many are currently under study.¹⁴ Among the different proposed nanocarriers as DDS, there has been particular interest in the following: liposomes, dendrimers, nanocrystals, nanoparticles and polymeric micelles, nanoshells, gold nanoparticles.^{15,16,17,18,19} These systems can be ‘smart made’ by targeting strategies that allow the concentration of the drug only where necessary, enhancing its therapeutic efficacy and limiting the presence in the systemic circulation, with a consequent reduction of side effects. The DDS can also respond to certain stimulations, such as

changes in pH or temperature, or be made in such a manner as to be degraded slowly in the organism (for example, biodegradable polymers) or eliminated by renal filtration.²⁰

Micelles and nanoparticles are colloidal nanocarriers containing a principle actively dispersed, encapsulated, adsorbed or bound to their surface.²¹ Their use is applicable in various fields of nanomedicine, such as imaging in diagnosis or the transport of drugs, nucleic acids and proteins.^{22,23,24} In particular, these nanocarriers are very useful in drug delivery, as they also allow the transport of hydrophobic drugs in biological aqueous environment.^{25,26} Among the many DDS, biopolymers are the most studied due to their biocompatibility and biodegradability. Biopolymers are synthetic polymeric materials obtained from natural substances. It should be emphasised that these materials are often referred to as bioplastics because the term ‘biopolymer’ is used to define the macromolecules produced by living organisms, such as DNA or polypeptides. In this case the term biopolymer is used, considering that it does not refer to the macroscopic material but to the polymer chain. Because of environmental problems in recent years, such as pollution and the cost of waste disposal, interest in biopolymers has grown more and more. In fact, they are almost all biodegradable, so they do not present the problem of disposal. Being synthesised from natural substances, some of them are also biocompatible.

Due to their biocompatibility and biodegradability, biopolymers are much studied in many areas of nanomedicine, such as tissue engineering or drug delivery. The biocompatibility request is easy to understand: anything that is not biocompatible is rejected by the body. For its part, biodegradability allows for devices or nanoparticles that degrade once their function has ended, and they do not deposit in the body.

In the present work, we synthesised and characterised $m\text{PEO}_{113}\text{-b-PLA}_x$, block copolymers that can be used to form nanoparticles for controlled drug delivery.

Poly(ethylene glycol) (PEG) and poly(ethylene oxide) (PEO) are names that refer to oligomers or polymers based on ethylene oxide. The two names are synonyms; historically, however, PEG is used for oligomers with a molecular weight of less than

20,000, while PEO refers to molecular weights above 20,000. Depending on their molecular weight, they can be very viscous liquids (PEO400) or solids (Figure 1.8).

The standard synthesis is the anionic polymerisation by ring opening of ethylene oxide in presence of acidic or basic catalysts. Using this technique, it is possible to achieve very low polydispersity indexes (of the order of 1.01). In any concentration the polymer dissolves very well in water; however, it has amphoteric character, hence it is also soluble in dichloromethane, tetrahydrofuran, ethanol, acetone and chloroform.²⁷

PEO is a biocompatible, non-toxic polymer and has been approved by the U.S. Food and Drug Administration (FDA) for oral and topical applications. It is already widely used in cosmetics, soaps, and in the pharmaceutical and biomedical fields; it is rapidly cleared by the body without undergoing modifications, with disposal rates inversely proportional to the molecular weight of the polymer.^{28,29} Furthermore, it is able to prevent any interaction with the immune system's proteins; for this reason, it is also the ideal material for medical use.³⁰

Poly(lactic acid) (PLA) belongs to the family of aliphatic polyesters and presents excellent physical and mechanical properties. It is classified as a biopolymer, and it is obtained from renewable sources; its repeating unit is a natural product and is fully biodegradable (Figure 1.8).

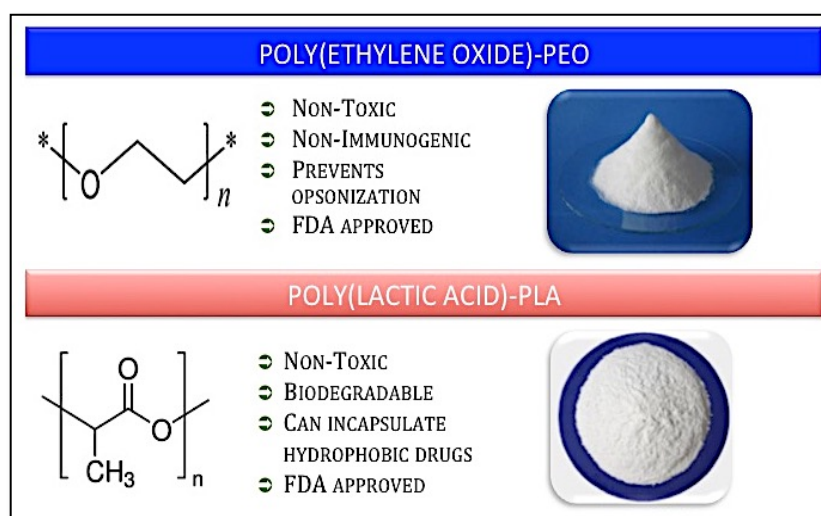


Figure 1.8. Chemical structure and main features of PEO and PLA.

The monomeric unit is lactic acid, a natural molecule isolated for the first time in 1780 by the Swedish chemist Scheele and produced in 1881.³¹

It is a hydroxyacid that possesses a chiral carbon and that therefore may exist in two optically active forms (Figure 1.9); human beings and other animals are able to produce only the isomer L; bacteria, on the other hand, are able to synthesise both the L and the D forms. It is precisely this process of fermentation of carbohydrates by bacteria that is used for the production of these two enantiomers.

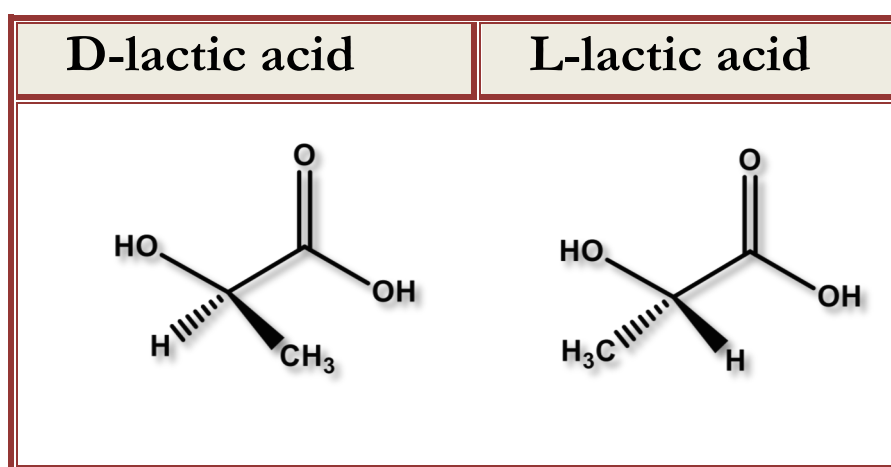


Figure 1.9. Lactic acid enantiomers: structure of D- and L- lactic acids.

One peculiarity of the PLA is that its stereochemistry and the properties of the final material are strictly dependent on the ratio between the two stereoisomers; in fact, the polymer formed only from isomer L appears to be highly crystalline and not very biodegradable, whereas from both stereoisomers a completely amorphous polymer is formed that easily biodegradable.³²

The properties of the polylactide, such as for example the melting point, the mechanical strength and the crystallinity, depend on the stereoisomers present in the polymer and the molecular weight. Even the degradative hydrolysis of the polymer is strongly influenced by the degree of crystallinity; a highly crystalline PLA requires months to be degraded to lactic acid, while an amorphous polymer can be degraded in a few weeks.

The poly (L-lactide) (PLLA) have a melting temperature between 170 ° C and 183 ° C. The introduction in the poly (L-lactide) of D-lactide or meso-lactide impurities leads to irregularities in the structure, then to lower crystallinity and to a decrease of the melting point up to 130 ° C. At the moment when the two stereoisomers are present at 50% (rac-lactide) it has even disappearance of the melting point because the polymer is completely amorphous. The glass transition temperature varies from 55 ° C to 65 ° C in the first case while amorphous polymers obtained from meso-lactide have a temperature of 59 °C.³³

The PLLA is soluble in chlorinated or fluorinated solvents and dioxane, while PDLA is soluble in a much wider variety of organic solvents (acetone, ethyl lactate, pyridine, tetrahydrofuran, ethyl acetate, N, N-dimethylformamide). The polylactides generally precipitate in methanol, ethanol, isopropanol, hexane, heptane and water.

In general, the thermal stability of the aliphatic polyesters is limited. The polylactide degrades at temperatures above 200 °C for phenomena of hydrolysis, oxidation, and transesterification reactions inter- and intra-molecular.

The degradation depends on environmental: temperature, presence of impurities and catalysts, capable of lowering the temperature of degradation).³⁴ During the thermal degradation, reactions can be observed of termohydrolysis, depolymerisation, thermal degradation, and transesterification. The transesterification of inter- and intra-molecular reactions takes place in the polymers at temperatures close to or above the melting point. In the polyesters, these reactions in the polymer melt are very rapid but also take place at temperatures below the melting point.

Finally, the PLA is also subject to degradation at room temperature. The degradation of PLA is through two steps. In the first stage of degradation, the high molecular weight chains undergo a hydrolysis process that leads to shorter chains or oligomers; this reaction may be accelerated by acids or bases and depends on the temperature.³⁵ The second step consists in the degradation by microorganisms that transform the low molecular weight chains into carbon dioxide and water. A typical degradation curve of PLA is shown in figure 1.10.

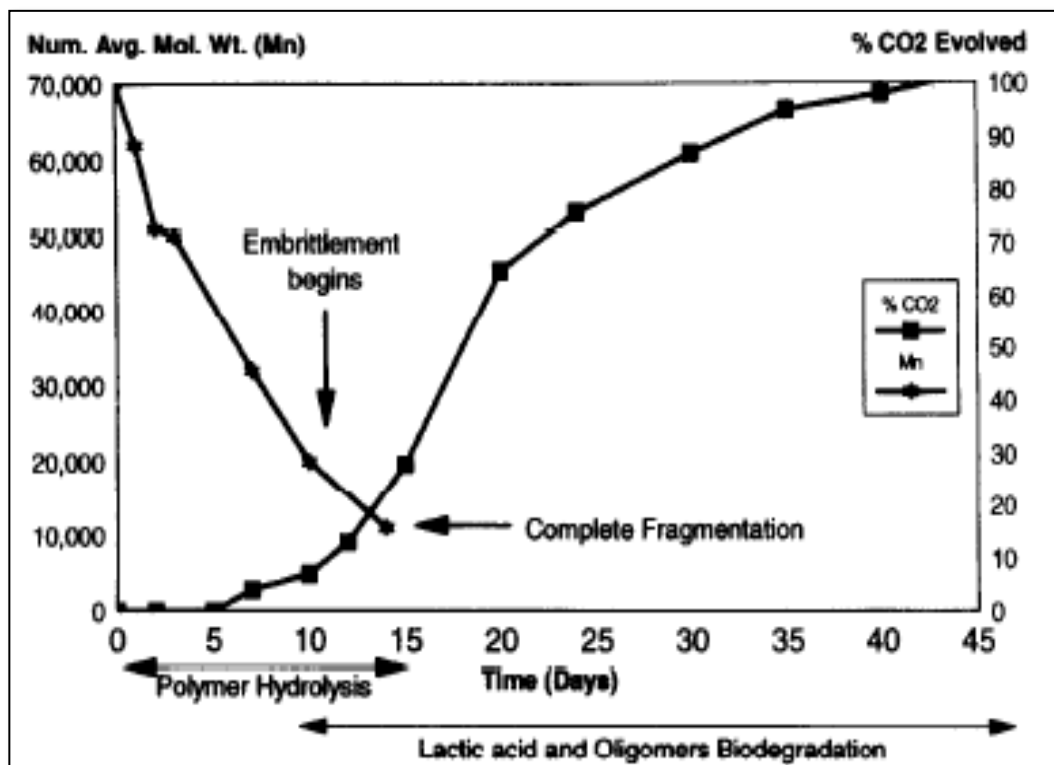


Figure 1.10. Degradation of PLA at 60 °C.³⁵

1.5 Self-assembly of amphiphilic block copolymer from good solvents

Block copolymers are known to self-assemble in block-selective solvents, which solubilise one but not the other block, forming micelles of various shapes. In such a solvent, block copolymer phase behaviour is controlled by the interaction between the segments of the polymers and the solvent molecules as well as the interaction between the segments of the two blocks. A defining property of amphiphilic block copolymers is the ability of individual block copolymer molecules (unimers) to self-assemble into micelles in dilute solutions. The unimers form molecular solutions in water at block copolymer concentrations below that of the critical micelle concentration (CMC). At concentrations of the block copolymer above the CMC, unimer molecules aggregate and form micelles, a process called ‘micellisation’ (Figure 1.11).³⁶

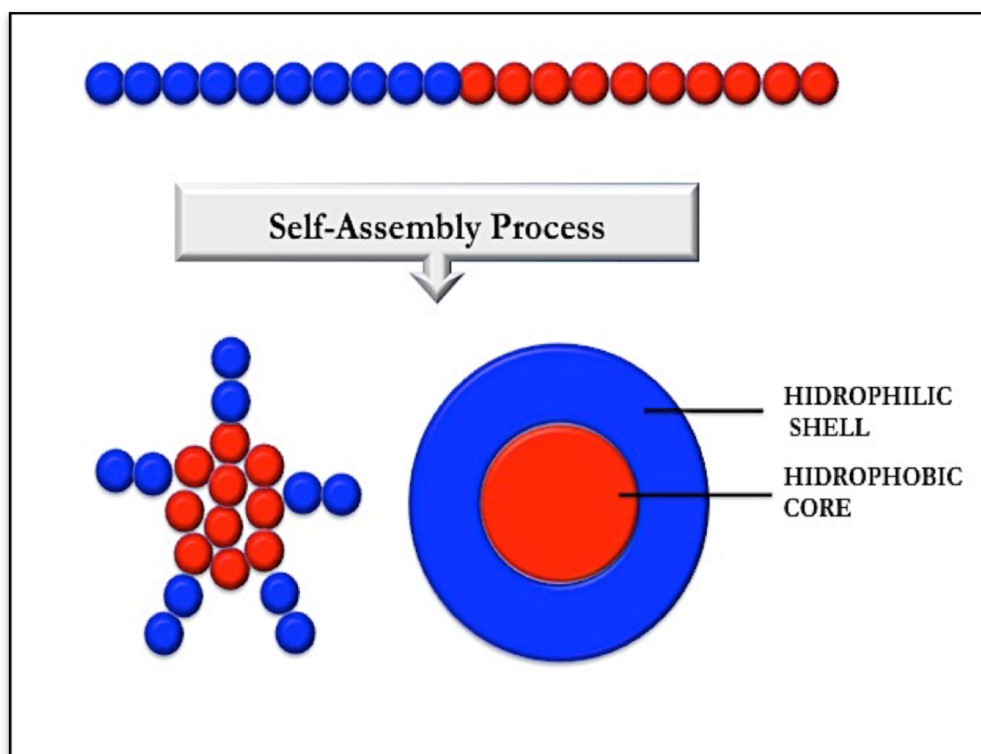


Figure 1.11. Schematic of self-assembled amphiphilic block copolymers into supramolecular nanostructure.

The hydrophobic blocks of amphiphilic copolymers self-associate in aqueous solutions to form supramolecular aggregates consisting of hydrophobic domains surrounded by swollen hydrophilic blocks. Hydrophobic interactions are a fundamental driving force in the assembly of amphiphilic systems, which helps in the macromolecular self-association and the formation of nanoscale-ordered structures through hydrophobic attraction. The number of block copolymer molecules forming one micelle is called the ‘aggregation number’. The hydrophobic core can serve as a ‘pool’ for the incorporation of various hydrophobic compounds into the micelles. As a result of the incorporation into the core, water-insoluble compounds are transferred into the micellar solution, a process called ‘solubilisation’.³⁷ Like surfactants, the micellisation process for block copolymers is mainly governed by two parameters: critical micellisation temperature (CMT) and critical micellisation concentration (CMC). In some instances, micellisation is stimuli-responsive, as in the case of double-hydrophilic AB block copolymers containing two water-soluble blocks. Under normal conditions, double-hydrophilic block

copolymer chains have no tendency to aggregate in aqueous media and are thus observed as unimers. However, in some cases once an adequate stimulus is applied, one of the hydrophilic blocks may become hydrophobic. This transition is generally observed to be reversible and results in a sharp modification of the macroscopic characteristic features of the aqueous medium (Figure 1.12).

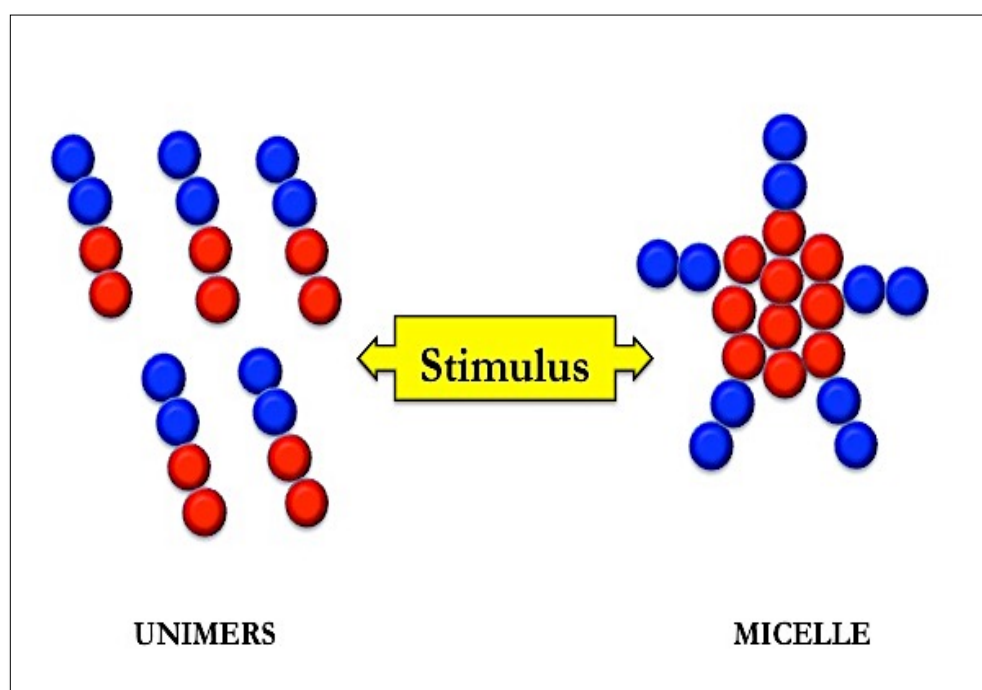


Figure 1.12. Schematic of a stimuli-sensitive micellisation process.

The responsiveness of polymer assemblies to biological stimuli (e.g., pH, reduction-oxidation, enzymes, glucose) and externally applied triggers (e.g., temperature, light, solvent quality) shows particular promise for various biomedical applications, including drug delivery, tissue engineering, medical diagnostics, and bioseparations.³⁸

As a consequence of the immiscibility of the two portions of the polymer chain, block copolymers are able to self-assemble into microphases when they are in mass (bulk) or in solution; in this way different nanostructures of controllable size can be obtained.

The self-assembly driving force is the thermodynamic incompatibility between blocks A and B, which leads to a separation in microphases that maximises the interaction with the related groups while minimising the contact area with the non-related groups.³⁹

Differently from the fluids of low molecular weight, the entropy of mixing per unit volume for various polymers is small; this arises from the fact that it is inversely proportional to molecular weight.

For this reason, even small structural differences between the blocks A and B provide a sufficient contribution to make mixing unfavourable in terms of free energy⁴⁰ (Figure 1.13).

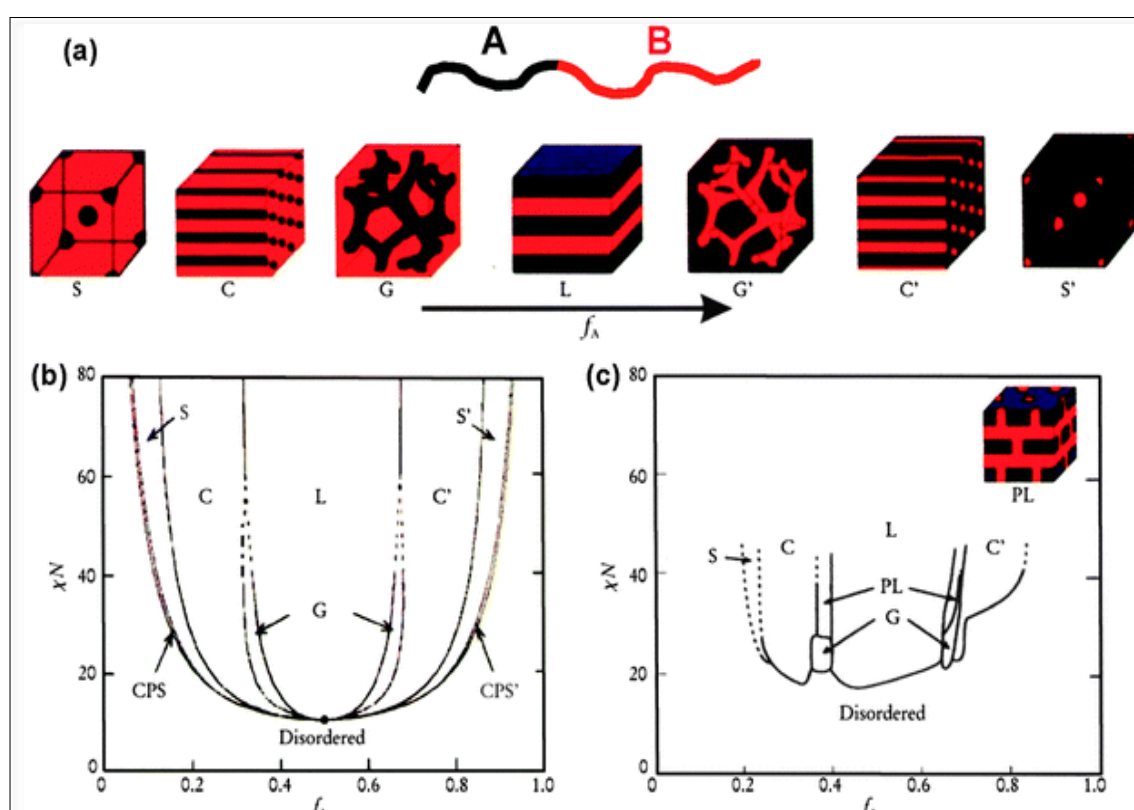


Figure 1.13. (a) Equilibrium morphologies of AB diblock copolymers in bulk: S and S' = body-centered-cubic spheres, C and C' = hexagonally packed cylinders, G and G' = bicontinuous gyroids, and L = lamellae. (b) Theoretical phase diagram showing of AB diblocks predicted by the self-consistent mean-field theory, depending on volume fraction (f) of the blocks and the segregation parameter χN , where χ is the Flory-Huggins segment-segment interaction energy and N is the degree of polymerisation; CPS and CPS' = closely packed spheres. (c) Experimental phase portrait of polyisoprene-*block*-polystyrene copolymers, in which f_A represents the volume fraction of polyisoprene, PL = perforated lamellae.⁴¹

The contribution to the free energy of mixing can be expressed as

$$\Delta G_{mix} \propto \chi_{AB} \cdot \kappa_B T \cdot N \quad (1)$$

where k_B is the Boltzmann constant, T is the absolute temperature, and N is the degree of polymerisation; χ_{AB} is the Flory-Huggins interaction parameter:^{40,41}

$$\chi_{AB} = \frac{z}{\kappa_B T} \left[\varepsilon_{AB} - \frac{1}{2} (\varepsilon_{AA} + \varepsilon_{BB}) \right] \quad (2)$$

where Z is the coordination number, and ε represents the internal energies of the systems AA, AB and BB. If χ_{AB} is positive, there is net repulsion between the monomers A and B; if it is negative, the free energy tends to make them mix.

For a typical pair of monomers in which there are no strong interaction specifications, χ_{AB} is positive and smaller than unity.

The parameter that determines the curvature of the structures is defined by the form (packing factor parameter) and depends on the area of interface between the hydrophilic block and the hydrophobic a_0 ; the volume v occupied by the hydrophobic chains; and l_c , their maximum length:⁴²

$$p = \frac{v}{a_0 l_c}$$

Different morphological structures correspond to different values of this parameter (Figure 1.14). The energy balance of the interaction between blocks and solvent determines the values of this parameter where the system is stable, and thus ultimately determine the shape that particles assume in dispersion.

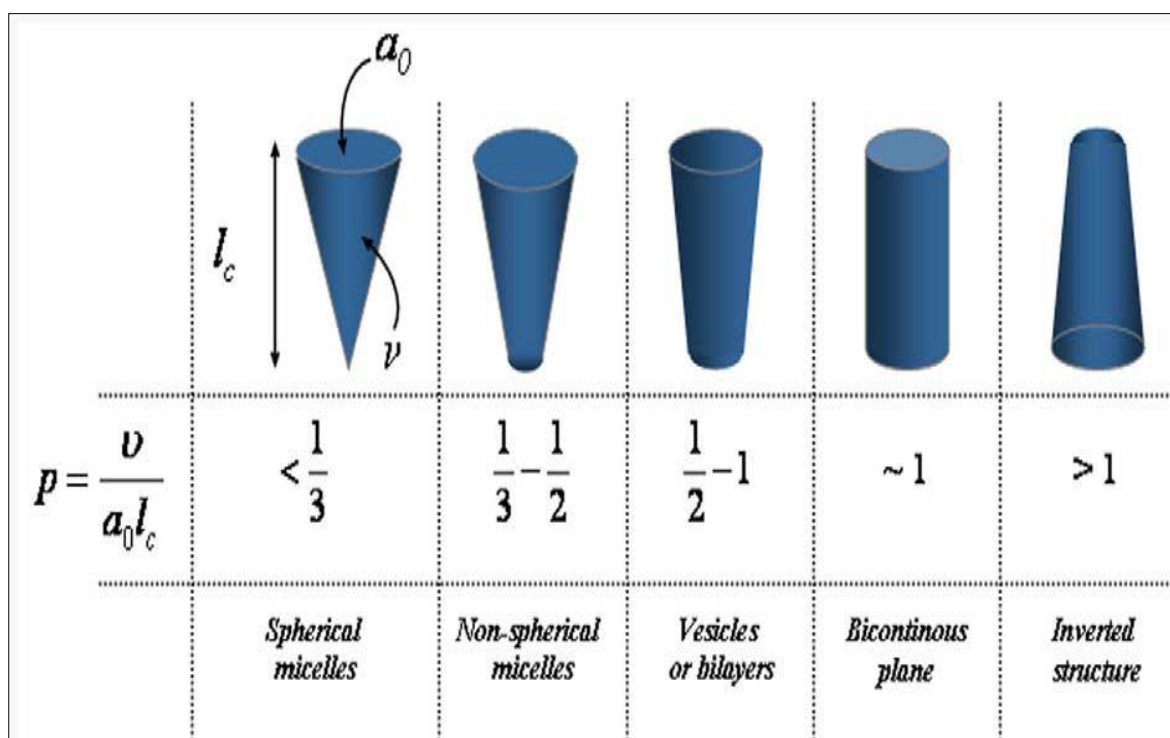


Figure 1.14. Dependence of the final micellar structure by intrinsic molecular parameters a_0 , l_c , and v of the hydrophobic block.

Following these general principles, several morphologies were obtained by the self-assembly of block copolymers in solution. When the hydrophilic chain is prevalent, the core-corona micelle is strongly favoured by thermodynamics. Instead, using an hydrophobic part much larger than the hydrophilic part produces “crew-cut” aggregates with an ample variety of morphologies, including spheres, cylindrical micelles (rods), bicontinuous structures, lamellae, vesicles, large compound micelles (LCM), large compound vesicles (LCV), tubules, and ‘onion’ and ‘eggshell’ structures.

Overall, more than 20 possible morphologies have been identified, including some that are thermodynamically induced and others that are formed under kinetic control (Figure 1.15).^{43, 44, 45}

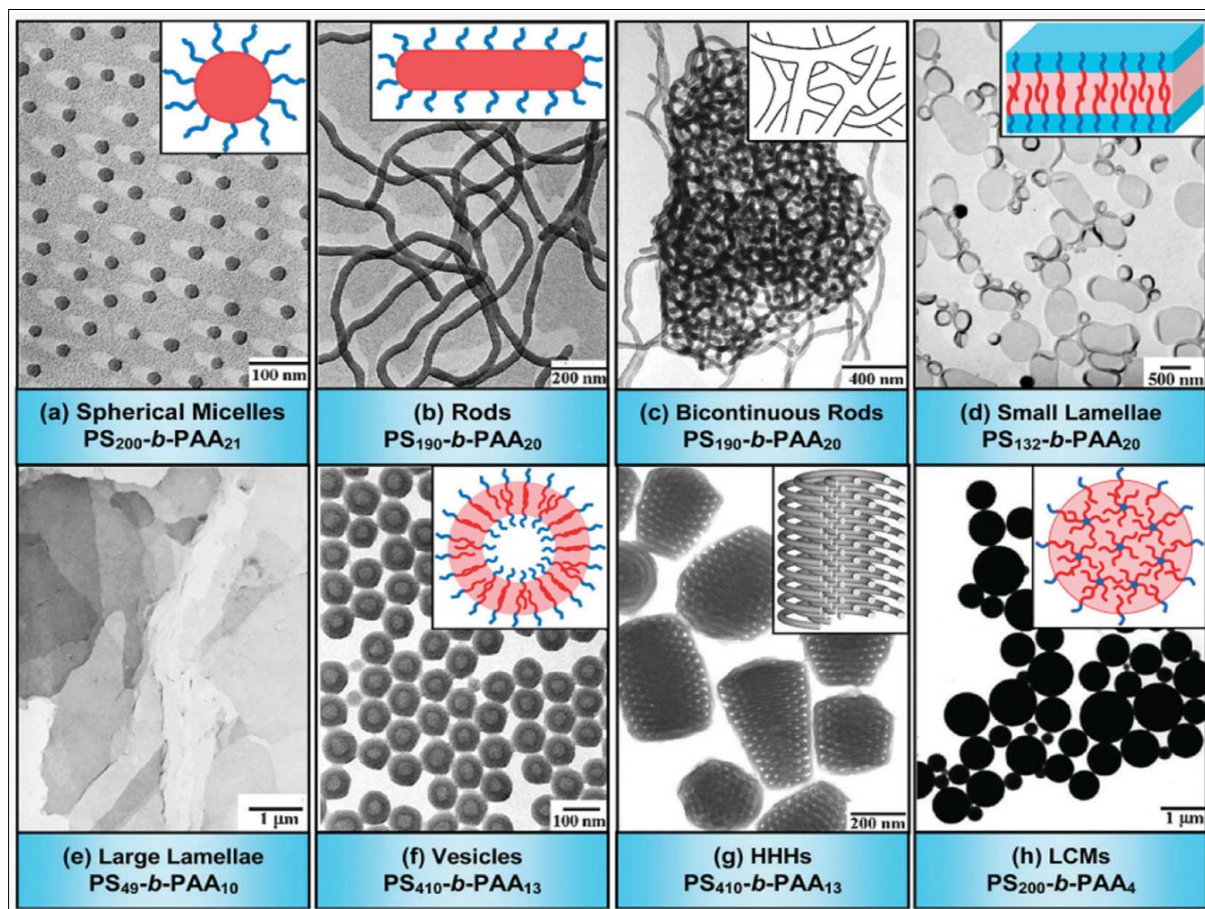


Figure 1.15. Transmission electron microscopy (TEM) micrographs and schematic drawings that match to various morphologies formed by amphiphilic PS_m - b - PAA_n copolymers.⁴³

Note: m and n denote the degrees of polymerization of PS and PAA, respectively. In the schematic diagrams, red represents hydrophobic PS parts, while blue denotes hydrophilic PAA segments. HHH: hexagonal packed hollow hoops; LCMs = large compound micelles, in which inverse micelles consist of a PAA core surrounded by PS coronal chains. Generally, the hydrophilic segments (e.g. coronas) of the crew-cut aggregates cannot be seen in TEM images if they are not stained.⁴⁴

1.6 References

1. Moghimi, SM; Hunter, AC; Murray, J.C; Nanomedicine: current status and future prospects. *FASEB J*, Mar **2005**; 19, 3:311-30.
2. Bartelmees, J. and Giordani, S.; Carbon nano-onions (multi-layer fullerenes): chemistry and applications. *J. Nanotechnol.* **2014**, 5, 1980–1998.
3. Feynman R.; *Engineering and Science* February, **1960**, 23, 5, 22- 36.
4. Roco, M.C.; Bainbridge, W.S.; Societal implications of nanosciences and nanotechnology: Maximizing human benefit. *Journal of Nanoparticles Research.* **2005**, 7: 1-13.
5. Nordmann, A.; *Converging technologies: shaping the future of European societies.* Brussels: European Commission; **2004**.
6. Zonneveld, L.; *Reshaping the human condition: exploring human enhancement.* The Hague: Rethebau Institute; **2008**.
7. Kjolberg, K.; Strand, R.; Delgado, G.C.; Wickson, F.; Models of governance for converging technologies. *Technology Analysis & Strategic Management*, **2008**, 20, 83.
8. Grieneisen, M.L.; The proliferation of nano journals. *Nature Nanotechnology*, November **2010**, 5, 825.
9. Dang, Y.; Chen, Y.; and Roco, M.C.; Trend in worldwide nanotechnology patent applications: 1991 to 2008. *Journal of Nanoparticles Research*, **2010**, 12, 3, 687-706.
10. The Nanobiotechnology Market for Drug Discovery, Drug Delivery, Diagnostics and Others: Global Industry Perspective, Comprehensive Analysis and Forecast, 2015–2021?. Zion Market Research Analysis, ID: 3782349, April **2016**.
11. Webster, T.J.; Nanomedicine: what's in a definition? *Int J Nanomedicine.* **2006**; 1 (2):115-6.
12. Brower, V.; Is nanotechnology ready for primetime? *J Natl Cancer Inst*, **2006**, 98, 9-11.
13. Ferrari, M.; Cancer nanotechnology: opportunities and challenges. *Nat Rev Cancer* **2005**, 5, 161-171.
14. Saldivar-Guerra, E.; Vivaldo-Lima, E.; “Introduction to Polymers and Polymer Type”.
15. Handbook of Polymer Synthesis, Characterization, and Processing (**2013**):1.
16. Prokop, A; and Davidson, J.M.; Nanovehicular Intracellular Delivery Systems. *J Pharm Sci*, **2008**, 97, 3518-3590.
17. Muller, R.H.; Colloidal Carriers for Controlled Drug Delivery and Targeting: Modification, Characterization, and in Vivo Distribution. Wissenschaftliche Verlagsgesellschaft, Stuttgart, Germany, and CRC Press, Boca Raton, FL, **1991**.
18. Lasic, D.D.; and Martin, F.; *Stealth Liposomes*, CRC Press, Boca Raton, **1995**.
19. Cohen, S.; Bernstein, H.; *Microparticulate Systems for the Delivery of Proteins and Vaccines*, Marcel Dekker, New York, **1996**.
20. Torchilin, V.P.; Trubetskoy, V.S.; Which polymers can make nanoparticulate drug carriers long-circulating? *Adv Drug Deliv Rev*, **1995**, 16, 141-155.
21. Torchilin, V.P.; How do polymers prolong circulation time of liposomes? *J Liposome Res*, **1996**, 6, 1, 99-116.
22. Duncan R. Polymer-drug conjugates. In Handbook of Anticancer Drug Development, Editors Budman DR, Calvert AH & Rowinsky EK. Philadelphia, USA: Lippincott, Williams & Wilkins. Edn 1, 2003: 239-260.
23. Rawat, M.; Singh, D.; Saraf, S.; Saraf, S.; Nanocarriers: promising vehicle for bioactive drugs. *Biol Pharm Bull*, **2006**, 29, 9, 1790-1798.
24. Chorny, M.; Cohen-Sacks, I.; Fishbein, H.D.; Danenberg, H.D.; Golomb, G.; Biodegradable nanoparticles as drug delivery systems for parenteral administration. *Tissue Engineering and Novel Delivery Systems*, **2004**, 393-422.

25. Lu, W.; Sun, Q.; Wan, J.; She, Z.; Jiang, X.G.; Cationic Albumin–Conjugated Pegylated Nanoparticles Allow Gene Delivery into Brain Tumors via Intravenous Administration. *Cancer Res*, **2006**, 66, 24, 11878-11887.
26. Mitra, A., Nan, A.; Line, B.R.; Ghandehari, H.; Nanocarriers for nuclear imaging and radiotherapy of cancer. *Curr Pharm Des*. **2006**, 12, 36:47294749.
27. Zeng, F.; Liu, J.; Synthesis and Characterization of Biodegradable Poly(ethylene glycol)-*block*-poly(5-benzyloxy-trimethylene carbonate) Copolymers for Drug Delivery. *Biomacromolecules*, **2004**, 5, 5: 1810-1817.
28. Torchilin, V.P.; Lipid-Core Micelles for Targeted Drug Delivery. *Curr Drug Deliv*, **2005**, 2, 4: 319-327.
29. Bailey, F. E.; Koleske, J. V.; Poly(ethylene oxide). *Academic Press*, 1976.
30. Krsko, P.; Libera, M.; Biointeractive hydrogels. *Materials Today*, 2005, 8: 36-44.
31. Working, P. K.; Newman, M. S.; Johnson, J. et al., Safety of Poly(ethylene glycol) and Poly(ethylene glycol) Derivatives. *ACS Symposium Series*, **1997**, 680,45-57.
32. Barthel, M. J.; Schacher, F. H.; Schubert, U. S.; Solution self-assembly of poly(ethylene oxide)-*block*-poly(furfuryl glycidyl ether)-*block*-poly(allyl glycidyl ether) based triblock terpolymers: a field-flow fractionation study. *Polym. Chem.* **2014**, 5, 2647–2662.
33. Hartmann, M. H.; *Biopolymers from Renewable Resources*, 1998, 367–411.
34. Garlotta, D.; J; A literature Review of Poly(Lactid Acid). *Polym Environ*, **2002**, 9, 61–84.
35. Lunt, J.; Large-scale production, properties, and commercial applications of polylactic acid polymers. *Polym. Degrad. Stab.* **1998**, 59, 145-152.
36. Gupta, A. P.; Kumar, V.; New emerging trends in synthetic biodegradable polymers – Polylactide: A critique. *European Polymer Journal*, **2007**, 43, 10: 4053-4074.
37. Drumright, R. E.; Gruber, P. R.; Henton, D. E.; Polylactid Acid Technology. *Adv. Mater.* **2000**, 12, 1841.
38. Kelley, E.G.; et al. Stimuli-responsive copolymer solution and surface assemblies for biomedical applications. *Chem Soc Rev*, **2013**,42, 7057-7071.
39. Smart, T.; Lomas, H.; Massignani, M.; Flores-Merino, M.V.; Perez, L.R.; and Battaglia, G.; Block copolymer nanostructures. *Nanotoday*. **2008**, vol 3 (3-4), 38-46.
40. Forster, S.; Plantenberg, T.; *Angewandte Chemie*, International Edition 41, 688, **2002**. 66.
41. Bates, F.S. and Fredrickson, G.H.; Block copolymers-designer soft materials. *Physics Today*, **1999**, 52, 32-38.
42. Bates, F.S; Polymer-polymer phase behavior. *Science*, 1991,251, 898-905.
43. Mai, Y. Y.; and Eisenberg A., Self-assembly of block copolymers. *Chem. Soc. Rev.*, **2012**, 41,18: 5969–598.
44. Cameron, N.S., Corbierre, M.K. and Eisenberg, A.; Asymmetric amphiphilic block copolymers in solution: a morphological wonderland. *Can.J. Chem.*, **1999**,77,8, 1311-1326.
45. Israelachvili Mitchell, D.; and Ninham, B.; Theory of self-assembly of hydrocarbon amphiphiles into micelles and bilayers. *J. Chem*, **1976**, 1525–1568.

CHAPTER 2

SYNTHESIS OF mPEO₁₁₃-b-PLA_x COPOLYMERS BY RING-OPENING POLYMERISATION

2.1 Experimental Section

2.1.1 Materials

Tetrahydrofuran CHROMASOLV ® Plus (THF, 99.9%), ethyl acetate, toluene anhydrous (99.9%), chloroform (CDCl₃ deuterate, 99.9%), dichloromethane anhydrous (99%) 2-propanol, ethanol (99%) and benzoic acid were purchased from Sigma Aldrich and used as received. Milli-Q water was obtained by systems Direct-Q5 (Millipore). Poly(ethylene oxide) monomethyl ether with $\bar{M}_w=5000$ g/mol (mPEO₁₁₃, Sigma Aldrich) was precipitated twice from ethanol, dried by azeotropic distillation from toluene, and stored in a dry nitrogen atmosphere. Racemic lactide (*rac*-Lac, Sigma Aldrich) was recrystallised four times from ethyl acetate. 1,8-Diazabicyclo[5.4.0]undec-7-ene (DBU, Sigma Aldrich, 98%) was distilled from CaH₂ under reduced pressure.

2.1.2 Synthetic Methods

The main step in the PLA synthesis via ring-opening polymerisation (ROP) consists in the anionic attack to the carbonyl on lactide, which generates a transesterification reaction (Figure 2.1) ¹. A catalyst is necessary to initiate the polymerisation. The most widely used catalyst at an industrial level is the tin (II) bis (2-ethylhexanoate), also called tin octanoate, (Sn (Oct) 2); it is accepted as a food additive and approved by the FDA¹⁻⁶.

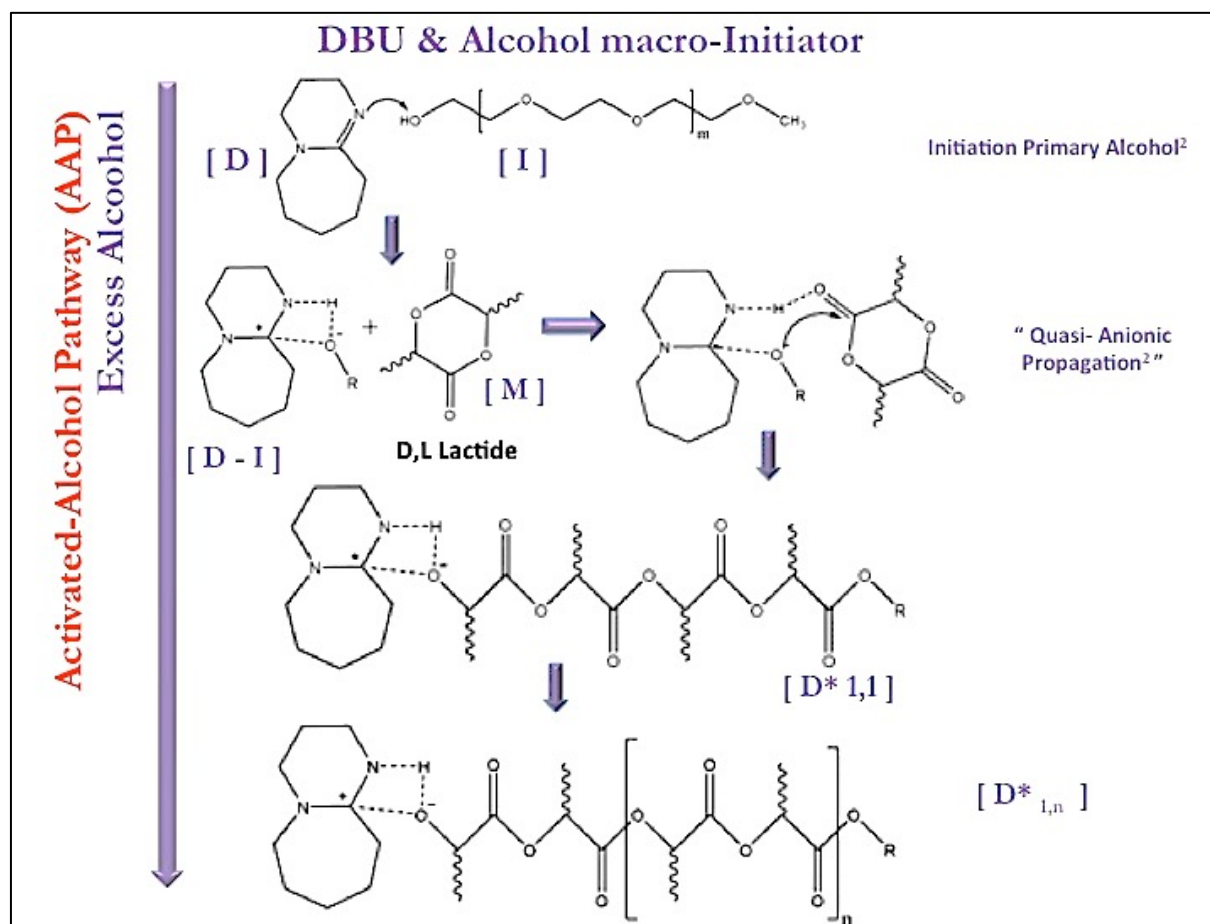


Figure 2.1. General mechanism of ROP polymerisation catalysed by DBU¹ (D), initiator (I), and monomer (M)¹.

Whereas Sn(Oct)₂ remains the most commonly used catalyst for the alcohol-initiated ROP of lactide and other cyclic esters, transesterification reactions may take place that lead to wider molecular weight distributions and poor control on chain end groups. Although FDA-approved, metal contamination of the final product by residual catalyst can be problematic for drug delivery applications.

In order to avoid any problems of poor biocompatibility or allergenicity⁴, the ROP synthesis of the poly (lactic acid block) on a block of poly (ethylene oxide) was instead catalysed by DBU. This catalyst is a non-toxic,⁸ metal-free superbases that allows for remarkable control of molecular weight and molecular weight distributions of different polyesters in mild reaction conditions.⁹⁻¹¹

With the more reactive monomers such as lactide, this catalysis is able to synthesise polymers at molecular weights of the order of 10,000 g/mol in 1 hour at room

temperature. In case one wishes to polymerise less reactive esters, such as ϵ -caprolactone, to speed up the reaction, it is possible to associate with the superbase a suitably functionalised thiourea, which also activates the monomer.¹¹

For the synthesis of the PLA block, the methodology described by Qian et al.⁷ has been followed. All block copolymers were prepared using methyl-terminated poly(ethylene oxide) with a molecular weight of 5000 g/mol as initiator. This molecular weight was chosen because mainly mPEO5000 or mPEO2000 are used in the literature to form nanoparticles for drug delivery.¹²⁻¹⁶ The polymer has two different terminal groups: methoxy on one end, and OH on the other.

The choice to have only one terminal with an -OH group ensures the growth of the PLA block on one end only.

All reactions were carried out at room temperature under N₂ atmosphere, using dry solvents and reagents. Using PEO₁₁₃-b-PLA₃₉₆ as an example, 0.500 g (10⁻⁴ mol) of dried mPEO₁₁₃ was dissolved in a Schlenk flask in 1.5 mL of anhydrous DCM. A solution of *rac*-lactide (2.880 g, 2·10⁻² mol) in DCM (2.0 M) was prepared separately and added to the flask. Lastly, DBU (10⁻⁴ mol, 0.0152 g, 15 μ l) was added to the reaction vessel. When different degrees of polymerisation of the PLA block were targeted, the ratio of *rac*-lactide to mPEO₁₁₃ was varied accordingly. The resulting solution was allowed to react for 1 hour under magnetic stirring, then quenched by adding 0.028 g (2.5·10⁻⁴ mol) of solid benzoic acid. The resulting polymer was precipitated three times into excess 2-propanol to remove any unreacted species and the DBU/benzoic acid salt. The product was then dried under vacuum overnight and stored in sealed screw-capped vials under N₂ at 4 °C.

The degree of polymerisation and the number-average molecular weight of the PLA block was determined by ¹H-NMR from comparison of the PLA methine (δ = 5.10–5.28 ppm) and methyl (δ = 1.40–1.60 ppm) signals and the mPEO₁₁₃ methylene (δ = 3.46–3.80 ppm) signal.

2.1.3 NMR spectroscopy (NMR)

Nuclear magnetic resonance (NMR) spectroscopy is a powerful analytical technique to obtain detailed information about the molecular structure of the compounds by measuring the emission of electromagnetic radiation in molecules immersed in a strong magnetic field. The emission takes place by means of particular atoms with active spin nuclei (in our case ¹H). The instrument used for the ¹H-NMR analysis is a Bruker AVANCE 500. The spectra were analysed with Mestre-C software. Nuclear magnetic resonance analysis also determines both the tacticity of the polymer formed and the presence of comonomers and their distribution. In particular, since the length of the PEO block is predetermined, it is possible to estimate the average weight of the PLA block by comparing the signal intensity associated with the two blocks.

2.1.4 Gel Permeation Chromatography (GPC)

Gel permeation chromatography (GPC) is a technique that uses specialised columns to distinguish polymers, natural macromolecules and nanoparticles on the basis of the steric interaction of the sample with the chromatographic columns. This technique allows an estimate of the molecular weight and polydispersity index (PDI) of a polymer sample. The method of analysis is based on the construction of the calibration curves of the elution time against the weight of controlled polymer standards. If the standards are structurally similar to the polymers used, then the elution time of the polymers can be used to determine the molecular weight with an accuracy of $\pm 5\%$. Due to their amphiphilic nature, block copolymers are difficult to properly compare with calibration curves.⁷ Thus, methods based on NMR are preferred for the calculation of the relative block length, whereas GPC provides reliable data on the block copolymer weight distribution (PDI).

2.1.5 Differential Scanning Calorimetry (DSC)

Differential scanning calorimetry (DSC) is one of the thermo-analytical techniques that allows the detection of the phase transitions that occur in a material along a range of user-selected temperatures (Figure 2.2)¹⁷. It is a powerful technique for obtaining the thermo-analytical parameters of biomolecules and nanomaterials¹⁸⁻²³.

Some of the main thermal properties of the polymeric materials measurable through DSC are the following:

- 1) glass transition temperature (T_g),
- 2) crystallisation temperature (T_c),
- 3) melting temperature (T_m).

It is also possible to detect non-reversible processes such as polymerisation reactions or the thermal decomposition of the samples.

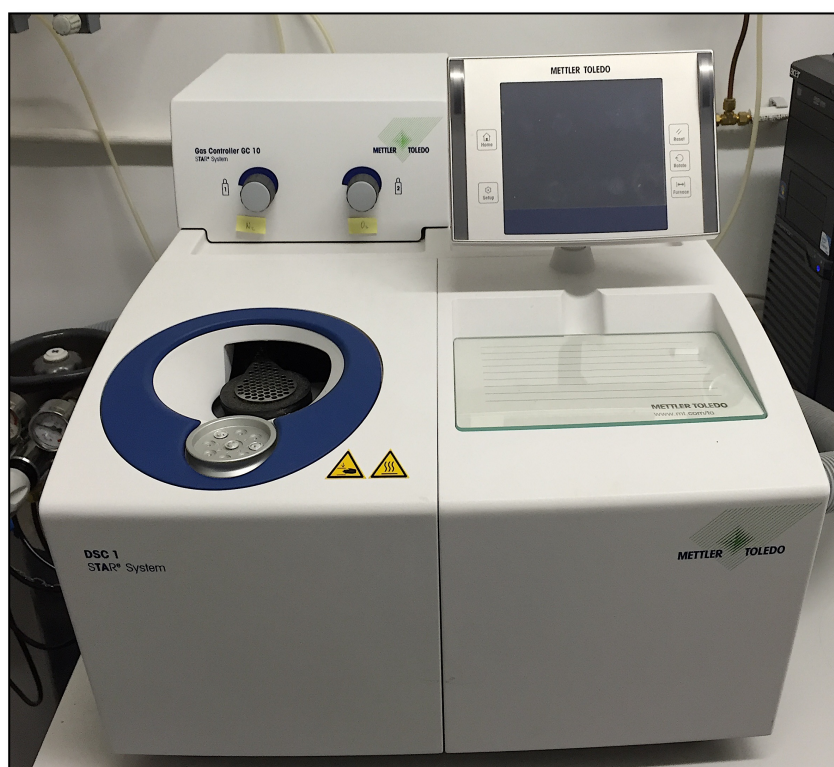


Figure 2.2. Differential Scanning Calorimetry (DSC).

Differential scanning calorimetry measures the heat flow between the crucible containing the sample and an empty reference crucible, given a certain speed of heating or cooling. The thermal behaviour of the PEO₁₁₃-b-PLA_x was analysed using a DSC1 (Mettler Toledo Instrument). Approximately 7–10 mg of sample was accurately weighed into a 30- μ L hermetic aluminium pan and sealed. A temperature range of 0 °C to 150 °C was scanned using a heating rate of 20 °C/min. Indium was used as the standard reference material to calibrate the temperature and energy scale of the apparatus.

2.2 Results and Discussion

Monohydroxyl-terminated mPEO has been extensively used to induce the ring-opening of different lactones in the presence of DBU to yield linear diblock copolymers with biocompatibility and biodegradability properties suitable for biomedical applications.²⁴⁻²⁸ A set of mPEO₁₁₃-b-PLA_x copolymers with different compositions was obtained by reacting dry mPEO₁₁₃ and *rac*-Lac in anhydrous DCM in the presence of DBU at room temperature.

Despite often being considered non-nucleophilic due to steric hindrance,⁷ DBU is known to be able to react with the cyclic ester bonds of lactide¹ and to compete with alcohols for ring-opening initiation when the [DBU]:[R-OH] ratio is high. To prevent the formation of DBU-initiated PLA homopolymeric blocks, a fixed [DBU]:[mPEO₁₁₃] ratio of 1 was maintained throughout all polymerisations. The PLA block length was modulated by varying the monomer feed and conducting all reactions up to 100% conversion. The GPC measurements are then used to determine the polydispersity index of the chains and whether the polymer is formed from one or more populations. The shape of the curve is in fact determined by the interaction of the polymer with the chromatographic column and is therefore intrinsically correct this is in contrast to the calculated numerical values, which depend on the performed calibration. Every sample exhibited a monomodal GPC curve (Figure 2.3) with narrow polydispersity (DPI <1.24), in accordance with exclusive ROP initiation by mPEO₁₁₃ (Table 2.1).

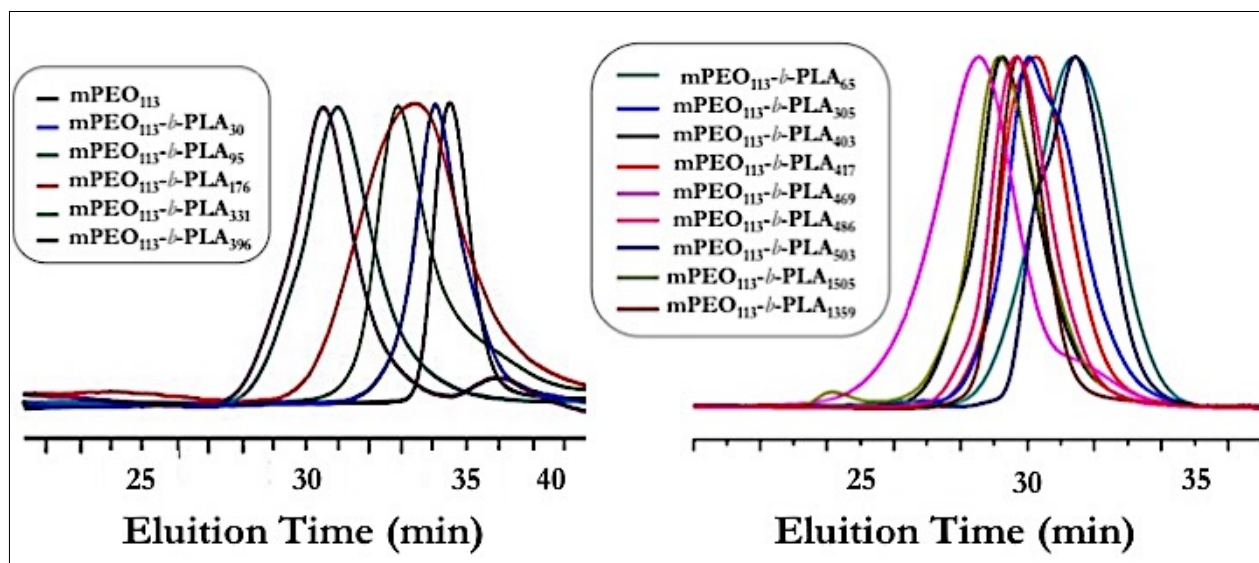


Figure 2.3. GPC chromatograms of mPEO and a selection of mPEO₁₁₃-b-PLA_x samples.

Sample	Mn (g/mol)	Mw (g/mol)	PDI
mPEO ₁₁₃	7000	7400	1.05
mPEO ₁₁₃ -b-PLA ₃₀	7500	8500	1.14
mPEO ₁₁₃ -b-PLA ₆₅	13600	17300	1.27
mPEO ₁₁₃ -b-PLA ₉₅	9300	12600	1.35
mPEO ₁₁₃ -b-PLA ₁₇₆	8800	12700	1.44
mPEO ₁₁₃ -b-PLA ₃₀₅	21000	23800	1.13
mPEO ₁₁₃ -b-PLA ₃₃₁	25200	33300	1.32
mPEO ₁₁₃ -b-PLA ₃₉₆	26100	36200	1.39
mPEO ₁₁₃ -b-PLA ₄₀₃	29000	33000	1.14
mPEO ₁₁₃ -b-PLA ₄₁₇	22600	25000	1.11
mPEO ₁₁₃ -b-PLA ₄₆₉	54300	66700	1.23
mPEO ₁₁₃ -b-PLA ₄₈₆	26400	29000	1.10
mPEO ₁₁₃ -b-PLA ₅₀₃	22000	25000	1.14
mPEO ₁₁₃ -b-PLA ₁₃₅₉	31000	34200	1.10
mPEO ₁₁₃ -b-PLA ₁₅₀₅	35300	43500	1.23

Table 2.1. Number average molecular weight (Mn), weight average molecular weight (Mw), and polydispersity index (PDI) measured by CPC on mPEO and a selection of mPEO₁₁₃-b-PLA_x samples, showing values below 1.5.

The Mn and Mw values presented in Table 2.1 are based on a calibration with polystyrene standards. Since the actual interaction of the polymer with the chromatographic column depends on the nature of the polymer itself, the values can be overestimated or underestimated. For example, it is reported in the literature that a PEO₁₁₃ has a polystyrene-equivalent number average molecular weight of 7600 g/mol, a value comparable to that obtained by us. The addition of the PLA block further modifies the interaction of the polymer with the GPC matrix in a measure that depends on the relative weight of the PLA block itself, thus rendering any conversion between elution time and molecular weight very complex.

The degree of polymerisation and number-average molecular weight of the PLA block was determined by comparing the integrated intensity of ¹H-NMR resonances univocally associated to each of the two blocks. In particular, PLA methylene ($\delta = 5.10\text{--}5.28$ ppm) and methyl ($\delta = 1.40\text{--}1.60$ ppm) signals were compared with the mPEO₁₁₃ methylene ($\delta = 3.46\text{--}3.80$ ppm) signal.

The number average molecular weight of PEO₁₁₃-b-PLA_x was calculated from ¹H-NMR after purification by comparing integrals d and b (Figure 2.4) according to Equation (1):

$$\bar{M}_n = m_{LA} \cdot \frac{I_d}{I_b} \cdot (4N_{EO}) + M_{PEO}, \quad (1)$$

where m_{LA} is the molecular weight of the LA repeating unit (72 g/mol), N_{EO} is the number of ethylene oxide repeating units in mPEO₁₁₃, and M_{PEO} is the molecular weight of mPEO₁₁₃ (5000 g/mol) (Table 2.2). PEO volume fraction, f_{PEO} , varies from 0.05 to 0.52.

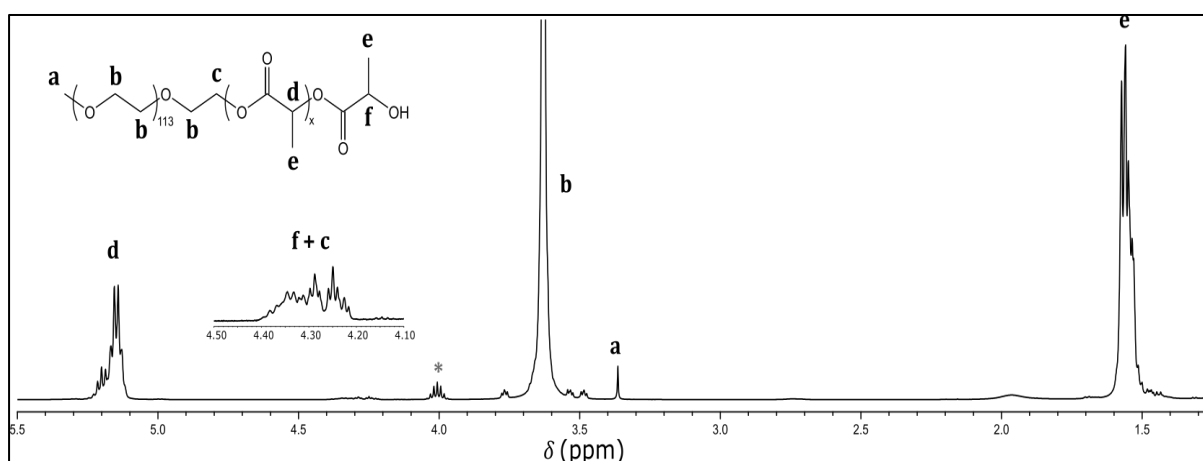


Figure 2.4. Representative ¹H-NMR spectrum of PEO₁₁₃-b-PLA_x (CDCl₃, 500 MHz).

Sample	n_{EO}	m_{LA}	N	f_{PEO}	f_{PLA}	M_n^{NMR} (g/mol)
mPEO ₁₁₃ -b-PLA ₃₀	113	30	-	-	-	-
mPEO ₁₁₃ -b-PLA ₆₅	113	65	178	0.52	0.48	9650
mPEO ₁₁₃ -b-PLA ₉₅	113	95	-	-	-	-
mPEO ₁₁₃ -b-PLA ₁₇₆	113	176	-	-	-	-
mPEO ₁₁₃ -b-PLA ₃₀₅	113	305	-	0.19	0.81	26932
mPEO ₁₁₃ -b-PLA ₃₃₁	113	331	-	-	-	-
mPEO ₁₁₃ -b-PLA ₃₉₆	113	396	-	-	-	-
mPEO ₁₁₃ -b-PLA ₄₀₃	113	403	516	0.15	0.85	33988
mPEO ₁₁₃ -b-PLA ₄₁₇	113	417	530	0.15	0.85	34996
mPEO ₁₁₃ -b-PLA ₄₆₉	113	469	582	0.13	0.87	38740
mPEO ₁₁₃ -b-PLA ₄₈₆	113	486	599	0.13	0.87	39964
mPEO ₁₁₃ -b-PLA ₅₀₃	113	503	616	0.12	0.88	41188
mPEO ₁₁₃ -b-PLA ₁₃₅₉	113	1359.2	1472.2	0.05	0.95	102834
mPEO ₁₁₃ -b-PLA ₁₅₀₅	113	1505.24	1618.24	0.05	0.95	133349

Table 2.2. Reaction parameters for polymerisations carried out, and yield obtained by ¹H-NMR of the purified polymer.

m_{LA} : number of repeating PLA unit calculated from ¹H-NMR spectra

f_{PEO} : calculated using $\rho_{PEO} = 1.21 \text{ g/cm}^3$ and $\rho_{PLA} = 1.25 \text{ g/cm}^3$.²

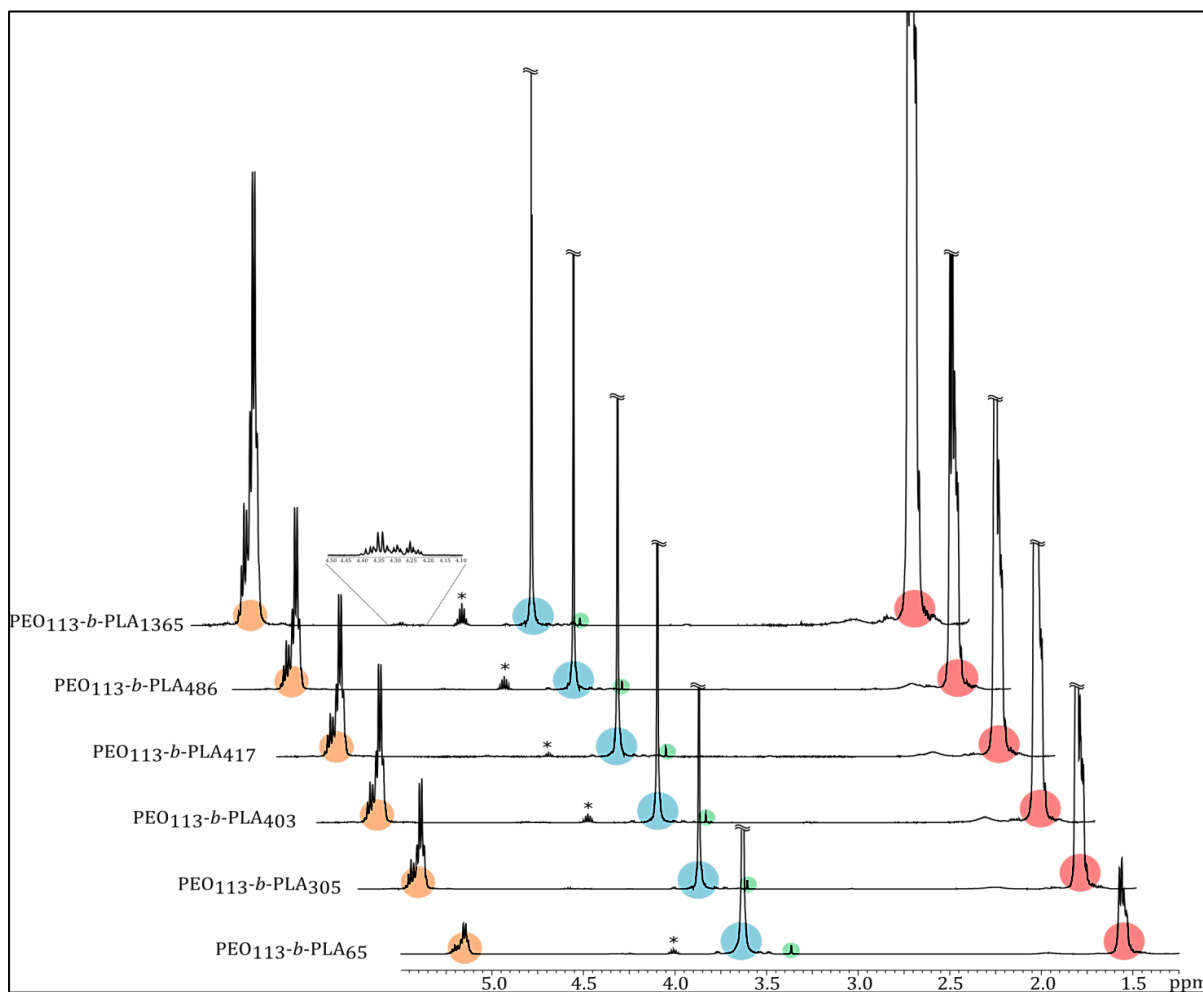


Figure 2.5. Comparison of ¹H-NMR spectra of mPEO₁₁₃-b-PLA_x in CDCl₃.

Figure 2.5 shows a comparison of the ¹H-NMR spectra of mPEO₁₁₃-b-PLA_x samples in CDCl₃.

All copolymers were also characterised by thermal analysis. The DSC cycle consists of three parts: a first heating ramp from 0 °C to 150 °C, a cooling from 150 °C to -100 °C, and a second heating ramp ranging from -100 °C to 150 °C. All ramps were carried out at a speed of 20 °C/min, a value that allows the identification of the glass transitions present (Figure 2.6).

During the first heating ramp, endothermic traces of irregular shape are often observed below 100 °C, which is attributable to the evaporation of solvent (isopropanol). In some samples, there is an intense melting peak around 50 °C attributable to the crystalline fraction of the mPEO block, which in the bulk forms crystalline domains similar to pure PEO.

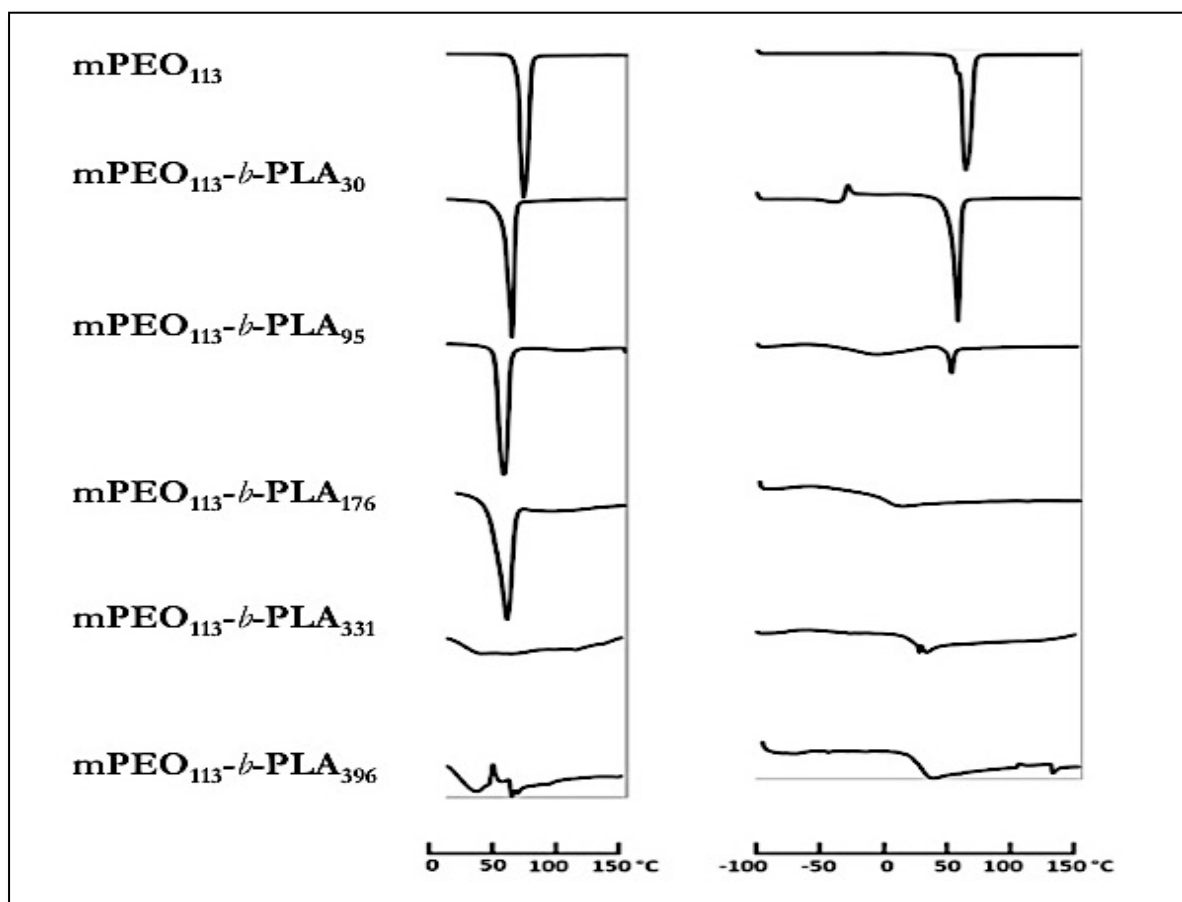


Figure 2.6. DSC curves of mPEO₁₁₃ and mPEO₁₁₃-b-PLA_x samples: (left) first heating ramp from 0 °C to 150 °C, (right) second heating ramp from -100 °C to 150 °C.

Comparing the enthalpies of fusion, normalised on the mass in the first heating ramp, they are in all cases comparable to that of mPEO homopolymer. In the second heating ramp, it is possible to observe that the melting peak decreases and finally vanishes as the PLA fraction increases. Moreover, a single glass transition is detected, gradually shifting from -48 °C to 27 °C as the PLA block molecular weight increases. Analysing the enthalpy values of the fusion in the second heating ramp, the amount of crystallinity in PEO can again be calculated. Chart 1 indicates that be observed as a function of the percentage by weight of the mPEO.

The copolymers characterised by an fPEO < 0.25 did not display melting peaks attributable to the mPEO block in neither the second nor the first heating ramp, which indicates that the long chains of totally amorphous PLA inhibit the crystallisation of the mPEO (Chart 1). For fPEO > 0.25 in the first heating ramp the melting peak remains

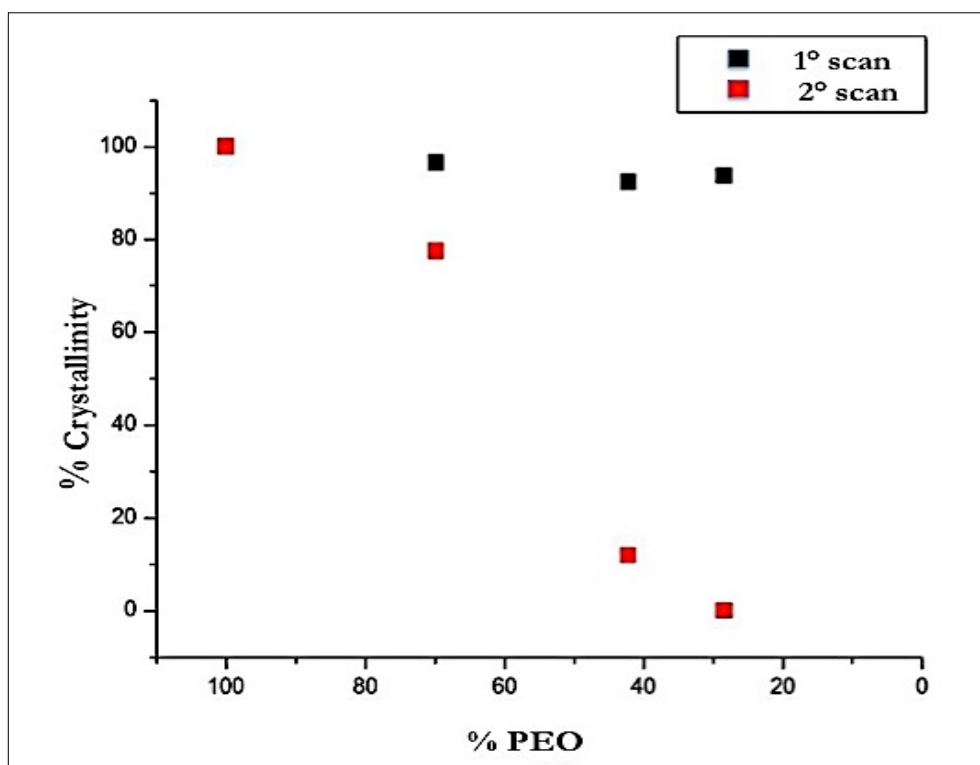


Chart 1. In black the degree of crystallinity percentage in the first heating ramp, while in red shows the degree of crystallinity in the heating ramp.

almost constant, indicating a good phase separation between the two blocks, while the decrease of the degree of crystallinity of the mPEO observable in the second heating ramp indicates the presence of a miscibility, at least partial, between the two blocks in the melt.

This result can be explained by considering the history of the sample: during the first heating ramp, we observe the thermal behaviour of the polymer coming directly from the purification step, which consists in the precipitation from isopropanol, a selective solvent for the mPEO block.

The self-assembly induced by the amphiphilicity of the system leads to the formation of mPEO domains separate from those of the PLA. This structuring is partially retained even after the removal of the solvent. In the third scan, the polymer was instead maintained for several minutes at temperatures much higher than the glass transition temperature of the PLA block, the mPEO block, and the melting temperature; the high

mobility of the chains means that as they cool, they are disposed in a way that requires the least energy possible; that is, when mixed, they inhibit phase separation and consequently also inhibit the crystallinity of the mPEO. The presence of a single T_g indicates miscibility of the two blocks; however, to determine its degree, the experimental values were compared with the theoretical values calculated using the Fox equation for binary blends, where total miscibility is assumed. As T_g limit values, one uses -61 °C for the PEO block⁹, while for the PLA, one calculates a theoretical value using the equation of Fox-Flory for homopolymers, which is then introduced into the equation for the blend. The equations used are the following:

$$T_g = T_{g1\infty} - \frac{k}{M_n} \quad (4)$$

$$\frac{1}{T_g} = \frac{w_1}{T_{g1}} + \frac{w_2}{T_{g2}} \quad (5)$$

Chart 2 shows T_g values calculated (black series) and experimental (red series) in function of the PLA fraction of the copolymer. As can be seen from the graph, the T_g of the analysed samples follow the linear trend of the Fox equation; however, the values are shifted higher by about 10 °C compared to the theoretical equation. This behavior indicates that the two blocks are only partially mixed together; in some portions of the material there is still phase separation. This conclusion is also confirmed by the trend of crystallisation peaks that should not be there if the two blocks were completely miscible.

The DSC analysis showed that the copolymer has a single T_g to values lower than those expected for a PLA homopolymer with the same molecular weight (Figure 2.7). In addition, the crystallisation of the PEO is inhibited when its weight fraction becomes less than 40%, indicating an at least partial miscibility of the two blocks in the bulk.

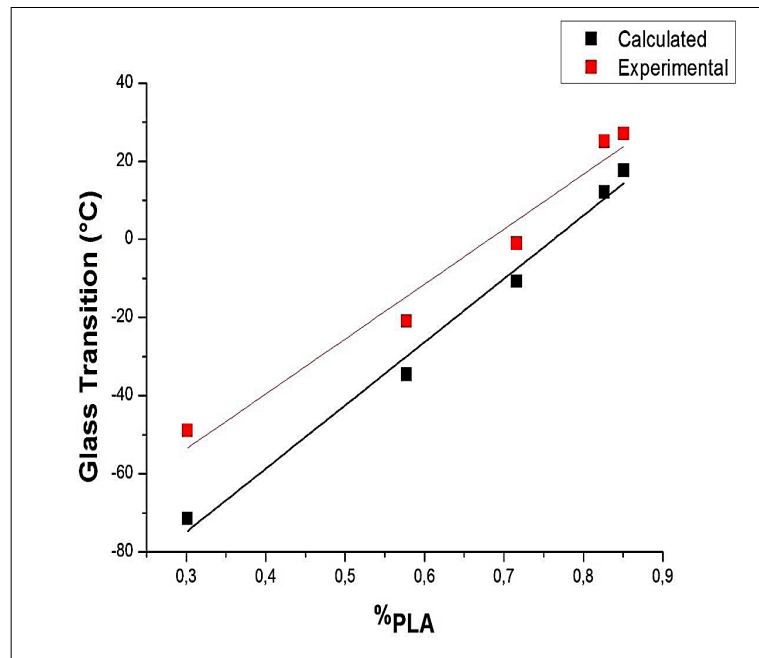


Chart 2. Comparison of the transition temperatures calculated with the Fox-Flory equation (black) and glass transition temperatures measured by DSC (red).³⁰

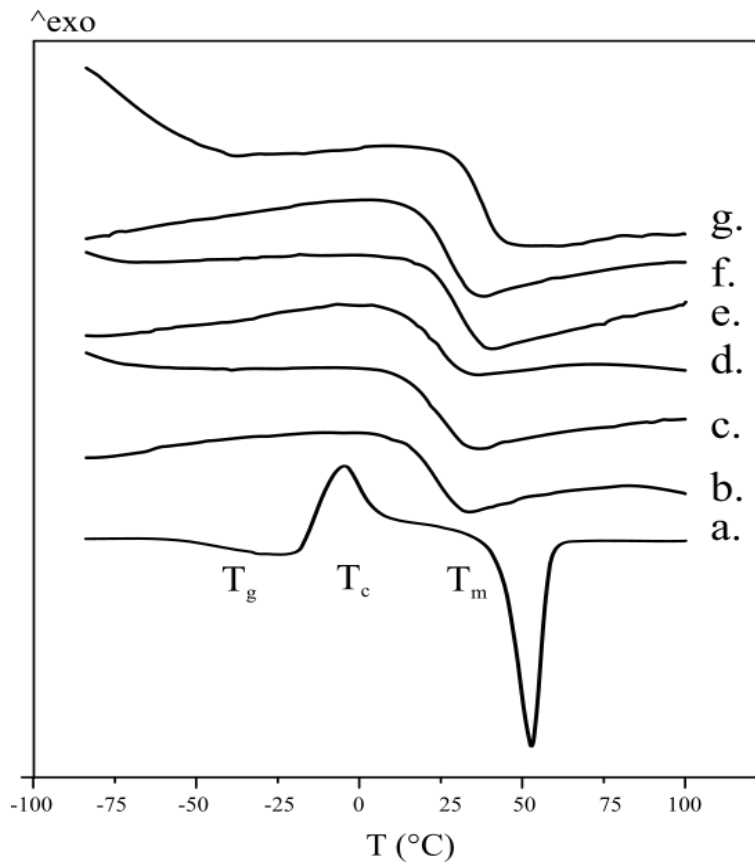


Figure 2.7. DSC curves of PEO-b-PLA samples. (a) mPEO₁₁₃-b-PLA₆₅, (b) mPEO₁₁₃-b-PLA₃₀₅, (c) mPEO₁₁₃-b-PLA₄₀₃, (d) mPEO₁₁₃-b-PLA₄₁₇, (e) mPEO₁₁₃-b-PLA₄₆₉, (f) mPEO₁₁₃-b-PLA₄₈₆, (g) mPEO₁₁₃-b-PLA₁₃₅₉.

2.3 Chapter Summary

In this chapter we have investigated the synthesis of lactide based polymers via ROP by DBU, an organic catalyst that has been shown to be not-toxic¹⁷ and therefore useful in synthesising polymers that are used in the branch of nanomedicine. It was possible to optimise the reaction parameters to obtain a quantitative yield of low polydispersity (1.08).

The synthesised polymers were then characterised by DSC to study the thermal behaviour. A partial miscibility was observed between the two blocks, demonstrated by both the gradual disappearance of the peak attributed to the fusion of the PEO and by the displacement of the glass transition temperature in a range of about 60 °C.

All samples were characterised by GPC, NMR and DSC.

Every sample exhibited a monomodal GPC curve with narrow polydispersity in accordance with exclusive ROP initiation by mPEO₁₁₃.

2.4 References

1. Sherck, N.J.; Kim, H.C.; Won, Y-Y.; Elucidating a Unified Mechanistic Scheme for the DBU-Catalyzed Ring-Opening Polymerization of Lactide to Poly(lactic acid). *Macromolecules*, **2016**, 49 (13), 4699-4713.
2. Dove, A.P. ; Organic Catalysis for Ring-Opening Polymerization. *ACS Macro Lett.* , **2012**, 1 (12), 1409-1412.
3. Culkin, D. A.; Jeong W. H. ; Csihony, S.; Gomez, E. D.; Balsara, N. R.; Hedrick, J. L.; Waymouth, R. M.; Zwitterionic polymerization of lactide to cyclic poly(lactide) by using N-heterocyclic carbene organocatalysts. *Angew. Chem., Int.* **2007**, Ed.46, 2627e2630.
4. Majerska, K.; Duda, A.; Penczek, S.; Kinetics and mechanism of cyclic esters polymerisation initiated with tin(II) octoate, 4. Influence of proton trapping agents on the kinetics of ϵ -caprolactone and L,L-dilactide polymerisation. *Rapid Commun.* **2000**, 21, 1327-1332.
5. S. Penczek, A. Duda, A. Kowalski, J. Libiszowski, K. Majerska, T. Biela, *Macromol. Symp.* **2000**, 15761-70.
6. Jérôme, C.; Lecomte, P. ; Recent advances in the synthesis of aliphatic polyesters by ring-opening polymerization. *Advanced Drug Delivery Reviews.* **2008**, vol. 60, pp. 1056-1076.
7. Qian, H.; Wohl, A.R.; Crow, J.T; Macosko, C.W.; Hoye, T.R.; A Strategy for Control of "Random" Copolymerization of Lactide and Glycolide: Application to Synthesis of PEG-b-PLGA Block Polymers Having Narrow Dispersity. *Macromolecules*, **2011**, 44, 18, 7132–7140.
8. Nachtergaeel, A.; Coulembier, O.; Dubois, P.; Helvenstein, M.; Duez, P.; Blankert, B.; Mespouille L., Organocatalysis Paradigm Revisited: Are Metal-Free Catalysts Really Harmless? *Biomacromolecules* **2015**, 16, (2), 507-514.
9. Coady, D.J.; Fukushima, K.; Horn, H.W.; Rice, J.E.; Hedrick J.L.; Catalytic insights into acid/base conjugates: highly selective bifunctional catalysts for the ring-opening polymerization of lactide. *Chem. Commun.* **2011**, 47, (11), 3105-3107.
10. Brown, H. A.; De Crisci, A. G. ; Hedrick, J. L.; Waymouth, R. M.; Amidine-Mediated Zwitterionic Polymerization of Lactide. *ACS Macro Lett.* **2012**, 1, (9), 1113-1115.
11. Lohmeijer, B.G.G.; Pratt, R. C.; Leibfarth, F.; Logan, J.W. ; Long, D.A.; Dove, A. P.; Nederberg, F. ; Choi, J.; Wade, C. ; Waymouth, R.M. and Hedrick, J. L.; Guanidine and amidine organo-catalysts for ring-opening polymerization of cyclic esters. *Macromolecules*, **2006**, 39, (25), 8574–8583.
12. Hagan, S. A.; Coombes, A. G. A.; Garnett, M. C.; Dunn, S. E.; Davies, M. C.; Illum, L.; and Davis S. S.; Polylactide-Poly(ethylene glycol) Copolymers as Drug Delivery Systems. 1. Characterization of Water Dispersible Micelle-Forming Systems. *Langmuir* 1996, 12, 2153-2161.
13. Riley, T.; Stolnik, S.; Heald, C. R.; Xiong, C. D.; Garnett, M. C.; Illum, L.; and Davis S. S.; Physicochemical Evaluation of Nanoparticles Assembled from Poly(lactic acid)-Poly(ethylene glycol) (PLA-PEG) Block Copolymers as Drug Delivery Vehicles. *Langmuir* **2001**, 17, 3168-3174.
14. Diou, O.; Greco, S.; Beltran, T.; Lairez, D.; Authelin, J.R.; Bazile D.; A method to Quantify the Affinity of Cabazitaxel for PLA-PEG Nanoparticles and Investigate the Influence of the Nano-Assembly Structure on the Drug/Particle Association. *Pharm Res.* 2015, 32 (10): 3188-3200.
15. Laredj-Bouezg, F.; Marie-Alexandrine Bolzinger, M.A.; J; Pelletier, J.; Valour, J.P; Rovère, M.R; Smatti, B.; Chevalier Y.; Skin delivery by block copolymer nanoparticles (block copolymer micelles). *International Journal of Pharmaceutics.* 2015, 30, 496 (2): 1034-46.

16. de Castro, C.E.; Bonvent, J.J.; da Silva F.L.; Giacomelli F.C.; Influence of Structural Features on the Cellular Uptake Behavior of Non-Targeted Polyester-Based Nanocarriers. *Macromol Biosci.* **2016**; 16 (11): 1643-1652.
17. Kodre, K.V. ; Attarde S.R.; Yendhe, P.R.; Patil, R.Y.; Barge, V.U.; Differential Scanning Calorimetry: A Review. *RRJPA.* **2014**, 3, 3, 11-22.
18. Gill, P; Moghadam, T.T. ; Ranijbar, B.; Differential Scanning Calorimetry Technique: Application in Biology and Nanoscience. *Journal of Biomolecular Technique.* **2010**, 21,4, 167-193.
19. Ranjbar, B.; Protasevich, I.I.; Shulga, A.A.; et al. *Mol Biol (Moscow).* **1997**;31:413-419.
20. Mikulecky, P.J. ; Feig, A.L.; Heat capacity change associated with nucleic acid folding. *Biopolymers* **2006**; 82:38–58.
21. Shah, S.; Kakumanu, V.; Bansal A.K. ; Analytical techniques for quantification of amorphous/crystalline phases in pharmaceutical solids. *J Pharm Sci* **2006**;95:1641-1665.
22. Varma, A.J. ; Deshpande, S.V.; Kennedy, J.F.; Metal complexation by chitosan and its derivatives: a review. *Carbohydr Polym* **2004**;55: 77-93.
23. Yao, H. ; Kagoshima, Y.; Kitamura, S.; Isohashi, T.; Ozawa, Y.; Kimura, K.; Superstructures of mesoscopic monomolecular sheets of thiocyanine J aggregates in solution. *Langmuir* **2003**;19:8882-8887.
24. Dong, Y. C.; Feng, S.S.; Methoxy poly(ethylene glycol)-poly(lactide) (MPEG-PLA) nanoparticles for controlled delivery of anticancer drugs. *Biomaterials* **2004**, 25, (14), 2843-2849.
25. Deng, C.; Rong, G.Z.; Tian, H.Y.; Tang, Z.H.; Chen, X.S; Jing, X.B.; Synthesis and characterization of poly(ethylene glycol)-b-poly (L-lactide)-b-poly(L-glutamic acid) triblock copolymer. *Polymer* **2005**, 46, (3), 653-659.
26. Savic, R.; Azzam, T.; Eisenberg, A.; Maysinger, D.; Assessment of the Integrity of Poly(caprolactone)-b-poly(ethylene oxide) Micelles under Biological Conditions: A Fluorogenic-Based Approach. *Langmuir* **2006**, 22, (8), 3570-3578.
27. Gagliardi, M.; Di Michele, F.; Mazzolai, B.; Bifone, A.; Chemical synthesis of a biodegradable PEGylated copolymer from ε-caprolactone and γ-valerolactone: evaluation of reaction and functional properties. *J. Polym. Res.* **2015**, 22:17.
28. Chognot, D.; Six, J.L.; Leonard, M.; Bonneaux, F.; Vigneron, C.; Dellacherie, E.; *J. Colloid Interface Sci.* **2003**, 268, (2), 441-447.
29. Rzayev, J. ; Hillmyer, M. A.; Nanochannel Array Plastics with Tailored Surface Chemistry. *Journal of the American Chemical Society.* **2005**, 127, (38), 13373-13379.
30. Jamshidi, K. ; Hyon, S. H.; and Ikada, Y.; Thermal characterization of polylactides. *Polymer*, **1988**, (29), 12, 2229-2234.

CHAPTER 3

SELF-ASSEMBLY OF AMPHIPHILIC BLOCK COPOLYMERS FROM GOOD SOLVENTS

3. 1 Experimental Section

3.1.1 Materials

Dimethylformamide (DMF), acetone, tetrahydrofuran (THF) and 1,4-dioxane were purchased from Sigma–Aldrich (Milano, Italy), and a dialysis bag (3500 MW cut off) from Spectrum Laboratories, Inc. (Rancho Dominguez, USA).

3.1.2 Nanoparticle fabrication

After a great variety of PLA chains of different lengths were polymerised (PEO₁₁₃-b-PLA_x- with x ranging from 30 to 1359), the polymeric nanoparticles (NP) were prepared by nanoprecipitation of PEO₁₁₃-b-PLA_x block copolymers. The NPs were assembled from different organic solvents: dimethylformamide (DMF), acetone, tetrahydrofuran (THF) and dioxane.

Due to the molecular weight of the polymers used, the process of aggregate formation is strongly determined by the kinetics. To ensure common starting conditions, a gradual solvent switching approach, or nanoprecipitation, has been chosen (Figure 3.1).

In particular, 15 mg of polymer were completely dissolved in 0.75 ml of acetone, DMF, dioxane or THF in a vial with a pierceable screw-cap. Filtered Milli-Q water was added dropwise by a syringe pump at a fixed rate of 4 ml/hr until the final volume of 3.75 ml was reached (Figure 3.2).

The apparatus used for the self-assembly of the NP is represented in Figure 3.3.

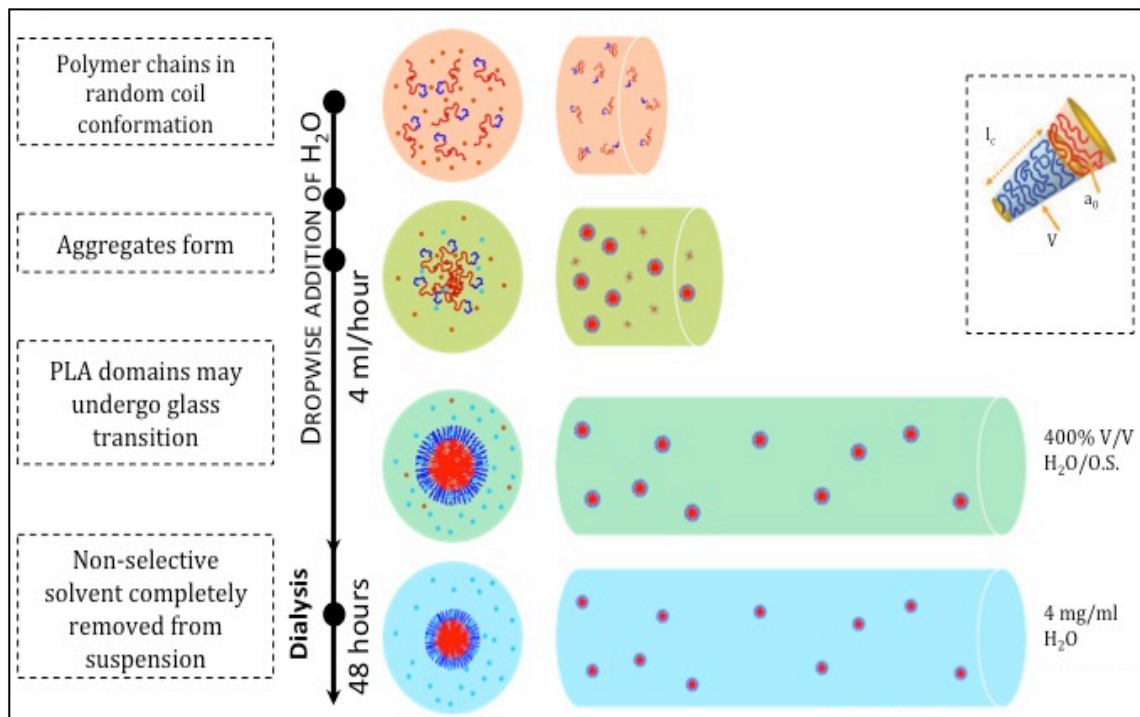


Figure 3.1. Schematic representation of the nanoprecipitation process.

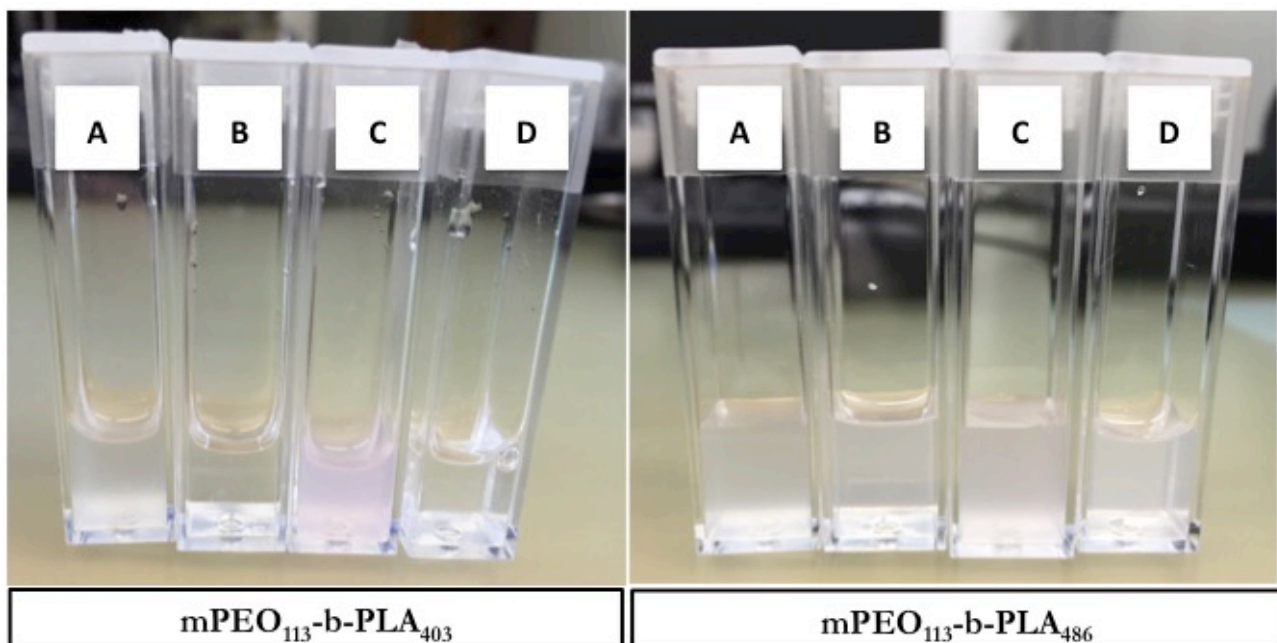


Figure 3.2. Photographs of cuvettes containing water dispersions of mPEO₁₁₃-b-PLA₄₀₃ (left image) and mPEO₁₁₃-b-PLA₄₈₆ (right image) assembled from different solvents (A=DMF, B=acetone, C=THF and D= dioxane) and dialysed for 48 hours. The opalescent appearance of several dispersions is due to light scattering caused by nanoparticles larger than 50 nm.



Figure 3.3. Self-assembly apparatus.

During the nanoprecipitation process, polymer chains migrate within the mobile phase and organise into aggregates with an internal compartmentalisation by virtue of their opposite affinity with the surrounding solvent. It is expected, therefore, that parameters such as the capacity of solvation, viscosity of the solvent, and the degree of immiscibility between the two blocks are able to greatly influence the assembly process. The Flory-Huggins theory considers the miscibility of polymers as based on the χ (chi) interaction parameter, which can be calculated from appropriate solubility parameters.

To predict the solubility of a solute (e.g. a polymer), Charles Hansen proposed a model that distinguishes three contributions:

δ_D : energy from dispersion forces between molecules;

δ_P : energy from dipolar intermolecular force between molecules;

δ_H : energy from hydrogen bonds between molecules.

Moreover, it is necessary to consider the contribution of solvent viscosity, η (eta), a property that regulates the mobility and evolution of macromolecules aggregates in solution.

Table 3.1 shows the Hansen solubility parameters of the solvents examined and of the PEO and PLA polymers, together with the solvent viscosity η (eta).

	δ_D [Mpa] ^{1/2}	δ_P [Mpa] ^{1/2}	δ_H [Mpa] ^{1/2}	δ_T [Mpa] ^{1/2}	η [cP]
H₂O	15.6	16.0	42.3	47.8	1.0
DMF	17.4	13.7	11.3	24.9	0.92
ACETONE	15.5	10.4	7	19.9	0.36
THF	16.8	5.7	8	19.5	0.55
DIOXANE	19	1.8	7.4	20.5	1.37
PEO	17	10.7	8.9	22.0	-
PLA	17.5	9.5	7.3	21.2	-
POLYMER-SOLVENT INTERACTION PARAMETER (χ_{P-S})					
	DMF	ACETONE	THF	DIOXANE	
PEO	0.120	0.094	0.212	0.840	
PLA	0.263	0.125	0.138	0.588	

Table 3.1. Hansen parameters of solubility and viscosity of the solvents examined and of the blocks of PEO and PLA, and values calculated for the interaction between polymers and solvents. Higher values correspond to lower solubility.

Based on these data, it is possible to estimate the interaction parameter χ between the polymer blocks (p) and the solvent (s):^{1,2}

$$\chi_{P-S} = \left(\frac{V_m}{RT} \right) \left[(\delta_D^s - \delta_D^p)^2 + 0.25(\delta_P^s - \delta_P^p)^2 + 0.25(\delta_H^s - \delta_H^p)^2 \right]$$

where δ_D , δ_p and δ_H are respectively the contributions of dispersion forces, dipolar interactions and hydrogen bonds, V_m is the molar volume of the solvent, T is the temperature and R is the gas constant. Compared to all other solvents used in our study, dioxane has lower solubility for both polymers but has higher viscosity. The other three solvents have high solubility and variable viscosity.³

The solubility parameters of PEO and PLA are very similar, and the literature, as well as our DSC experiments, reports that they are at least partially miscible in the bulk.⁴ Therefore, it is expected that the separation into distinct microphases of the corresponding block copolymers is not total.

Moreover, the high compatibility between solvents and polymer, and the fact that solvent could be trapped kinetically as a result of NP formation, poses the issue of the presence of residual solvent in the NPs. Thus, after assembly all dispersions were dialysed (MWCO = 15000 g/mol) against water for 48 hours to remove leftover organic solvents, then they were stored at 4 °C.

3.1.3 Dynamic Light Scattering

Dynamic light scattering (DLS) experiments were performed at 25 °C on a Malvern Zetasizer equipped with a continuous wave 1 mW He-Ne laser operating at 632.8 nm and an avalanche photodiode detector, Q.E. >50% at 633 nm, placed at 173° with respect to the incident beam.

Also known as photon correlation spectroscopy, DLS is a technique through which it is possible to determine the particle size of colloidal solutions. It is also used to study the behaviour of complex fluids, such as highly concentrated polymer solutions.

When photons are scattered many times before being revealed, it is very difficult to provide an accurate interpretation of the fluctuations of the scattered light. Therefore, it is advisable to prepare rather diluted samples so as to produce single-scattering situations. However, current instruments can suppress the channel of the multi-photon scattering in the DLS experiments by using a cross-correlation approach (CC).

The key parameters for the quantitative interpretation of the DLS output are the different autocorrelation functions. In particular, when one wants to calculate the hydrodynamic size, one needs to call into question both the autocorrelation function of the field $g^{(1)}(\tau)$ and the measured intensity autocorrelation function $g^{(2)}(\tau)$. The autocorrelation function of the g field (1) (τ) is determined from the measured g intensity autocorrelation function (2) (τ). The Siegert equation (2) links the two functions:

$$g^{(2)}(\tau - 1) = \beta |g^{(1)}(\tau)|^2$$

where β is an experimental factor of coherence, and $g^{(1)}(\tau)$ can be expressed as the integral along a single exponential decay:

$$g^{(1)}(\tau) = \int_0^{\infty} G(\Gamma) \exp(-\Gamma\tau) d\Gamma$$

where $G(\Gamma)$ is the distribution function of the decay, and Γ is the decay rate:

$$\Gamma = q^2 D$$

where q is the magnitude of diffusion vector and D is the diffusion coefficient.

The instrument used was a Malvern Zetasizer Nano S (Figure 3.4).



Figure 3.4. Malvern Zetasizer Nano S.

Nanoparticles were then purified by dialysis and analysed by DLS. In particular those assembled from copolymers $m\text{PEO}_{113}\text{-}b\text{-PLA}_{65}$; $m\text{PEO}_{113}\text{-}b\text{-PLA}_{305}$; $m\text{PEO}_{113}\text{-}b\text{-PLA}_{403}$; $m\text{PEO}_{113}\text{-}b\text{-PLA}_{417}$; $m\text{PEO}_{113}\text{-}b\text{-PLA}_{486}$ and $m\text{PEO}_{113}\text{-}b\text{-PLA}_{1359}$ with different selective solvents were subjected to a rigorous characterisation protocol (Figure 3.5). In this protocol, the DLS measurements were carried out following self-assembly and after dialysis (the time of dialysis varied between 24 and 72 hours depending on the solvent used). In addition, it was decided to evaluate the stability and aging of nanoparticles in solution by performing the daily measurements for 30 days consecutively.

The DLS measurements provide a measure of both the average hydrodynamic diameter (D_H) and its distribution.

Measurements of Zeta Potential (ZP or ζ), for all samples assembled, were performed at neutral pH. A survey of the structures formed from these systems was carried out by DLS of nanoparticle dispersions immediately after assembly.

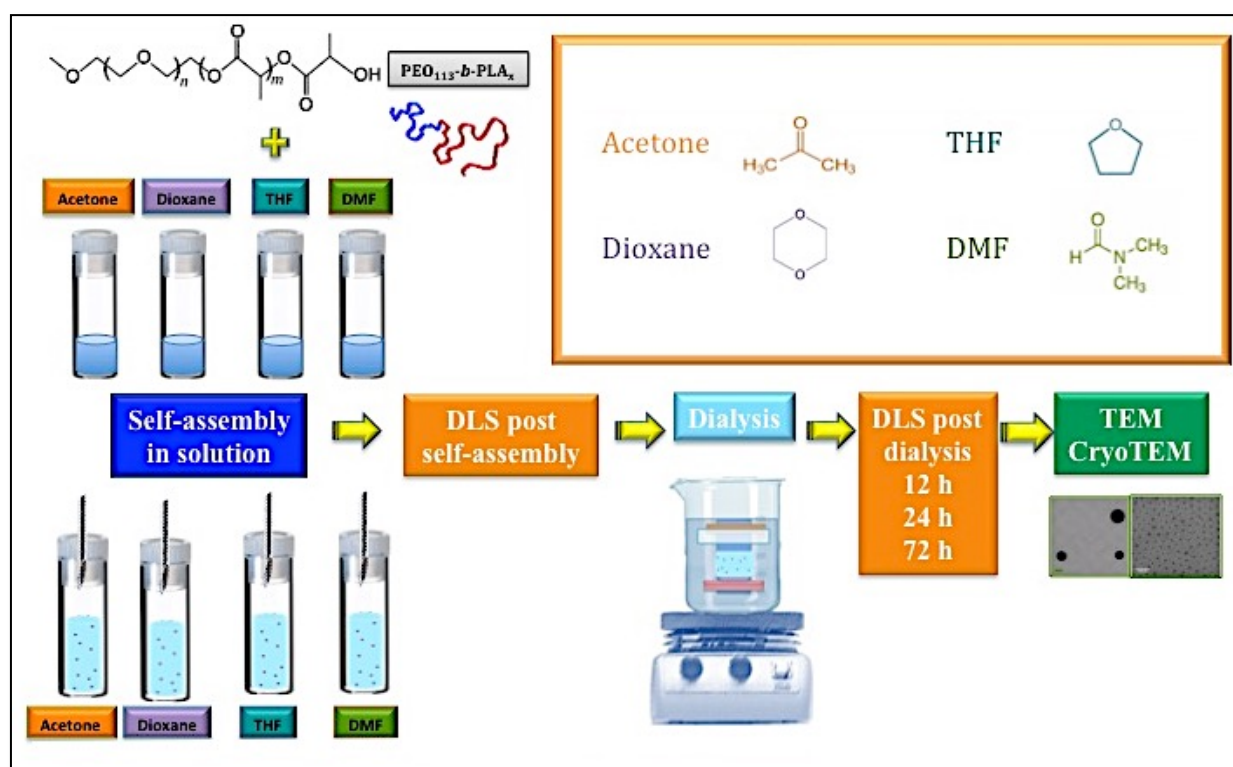


Figure 3.5. Schematic representation of the characterisation protocol used for the study of the sample: $mPEO_{113}-b-PLA_{65}$; $mPEO_{113}-b-PLA_{305}$; $mPEO_{113}-b-PLA_{403}$; $mPEO_{113}-b-PLA_{417}$; $mPEO_{113}-b-PLA_{486}$ and $mPEO_{113}-b-PLA_{1359}$ assembled from different organic solvents.

As reported in table 3.2 diameter of NPs ranged from 15 to 800 nm, with many of the polymers presenting different values as a function of the starting solvent. Moreover, ZP measurements on these NPs, at a temperature of 25 °C in deionized water (pH = 7), ranged between between -9.06 mV and -26.7 mV (Table 3.2). This suggests a good stability of the system also for applications in biomedical contexts. Data can be also visualized in figure 3.6, where two main trends emerge. As expected, the greatest NPs are obtained from polymers with a higher molecular weight; however, an increase in average size is also present to vary the solvent (in the order Acetone <Dioxane <THF <DMF). This increase can also be quite significant, up to a factor 2, and distributions tend to have a higher polydispersity, transiting from single monodisperse to polydisperse populations. However, in the choice of drug delivery devices, the nanoparticles with a bimodal distribution are not adequate, due to a big difference in the time of circulation, the biodistribution^{5,6,7} and the mechanism of entry into cells.^{3,8}

SAMPLES (PLA unit)	SOLVENTS			
	ACETONE	DIOXANE	THF	DMF
PLA ₃₀	-	-	-	Pk1= 236 PDI= 0.509 ZP=-15.3
PLA ₅₈	Pk1=381.7 PDI= 0.428 ZP=- 6.66	Pk1=183.1 PDI= 0.277 ZP=-25.3	Pk1=199.2 Pk2= 25.32 PDI= 0.415 ZP=-23.1	Pk1=254.5 PDI= 0.404 ZP=-20.2
PLA ₆₅	Pk1= 30.44 Pk1=562.4 PDI= 0.435 ZP= -20.5	Pk1=28.83 Pk2= 549.4 PDI= 0.309 ZP=- 15.7	Pk1= 51.69 Pk2= 932.3 PDI= 0.412 ZP= -24.3	Pk1=43.53 Pk2= 851.4 PDI= 0.631 ZP=-13.2
PLA ₉₅	-	-	-	Pk1=129 Pk2= 15 PDI= 0.916 ZP=-11.3
PLA ₁₇₆	-	-	-	Pk1= 69 PDI= 0.296 ZP=-13.6
PLA ₃₀₅	Pk1= 574.3 Pk2=30.02 PDI= 0.527 ZP= - 17.9	Pk1=32.89 PDI= 0.243 ZP= - 16.6	Pk1=74.77 PDI= 0.148 ZP=- 11.7	Pk1= 161.9 PDI= 0.339 ZP=- 14.3
PLA ₃₃₁	-	-	-	Pk1= 40 PDI= 0.068 ZP= -11
PLA ₃₉₆	-	-	-	Pk1= 97 PDI= 0.110 ZP= -13
PLA ₄₀₃	Pk1= 49.69 nm PDI= 0.242 ZP= - 21.5	Pk1=176 nm PDI= 0.377 ZP=-9.72	Pk1=50.29 nm Pk2= 38.3 nm PDI= 0.380 ZP=- 23.7	Pk1=85.62 nm Pk2= 469.5 nm PDI= 0.463 ZP=- 24.2
PLA ₄₁₇	Pk1=51.30 PDI= 0.076 ZP=- 15.4	Pk1=1205 Pk2= 130 PDI= 0.526 ZP=- 21.6	Pk1=343.9 Pk2= 42.26 PDI= 0.509 ZP=- 20.9	Pk1=124.3 Pk2= 808 PDI= 0.778 ZP=-26.7
PLA ₄₆₉	Pk1= 54.92 Pk2=609.7 PDI= 0.441 ZP= -17.3	Pk1=41.27 PDI= 0.161 ZP=-15.1	Pk1=205.7 Pk2= 1374 PDI= 0.652 ZP=-14.5	Pk1=1493 Pk2= 4592 PDI=0.574 ZP=- 9.23
PLA ₄₈₆	Pk1= 92.28 PDI= 0.191 ZP= -23.1	Pk1=101.2 PDI= 0.209 ZP=- 21.6	Pk1=1188 Pk2= 180 PDI= 0.434 ZP=- 25.6	Pk1= 899.7 Pk2= 112.6 PDI= 0.449 ZP=- 23.0
PLA ₅₀₃	Pk1= 99.57 PDI= 0.187 ZP= - 24.8	Pk1=415.3 Pk2 52.65 PDI= 0.283 ZP= - 17.2	Pk1= 2259 Pk2= 52.19 PDI= 1.000 ZP= - 9.4	Pk1= 108.0 Pk2= 469.8 PDI= 0.437 ZP= - 15.2
PLA ₁₅₀₅	Pk1=824.0 Pk2=149.3 PDI= 0.273 ZP=-22.1	-	-	-
PLA ₁₃₅₉	Pk1=613 Pk2= 152.5 PDI= 0.209 ZP=-21.4	Pk1=153.4 PDI=0.227 ZP=- 9.06	Pk1=802.8 Pk2= 42.37 PDI= 0.868 ZP=-15.2	Pk1=131.2 PDI= 0.158 ZP=-21.3

Table 3.2. Characterisation of PEO₁₁₃-b-PLA_x nanoparticles by DLS.

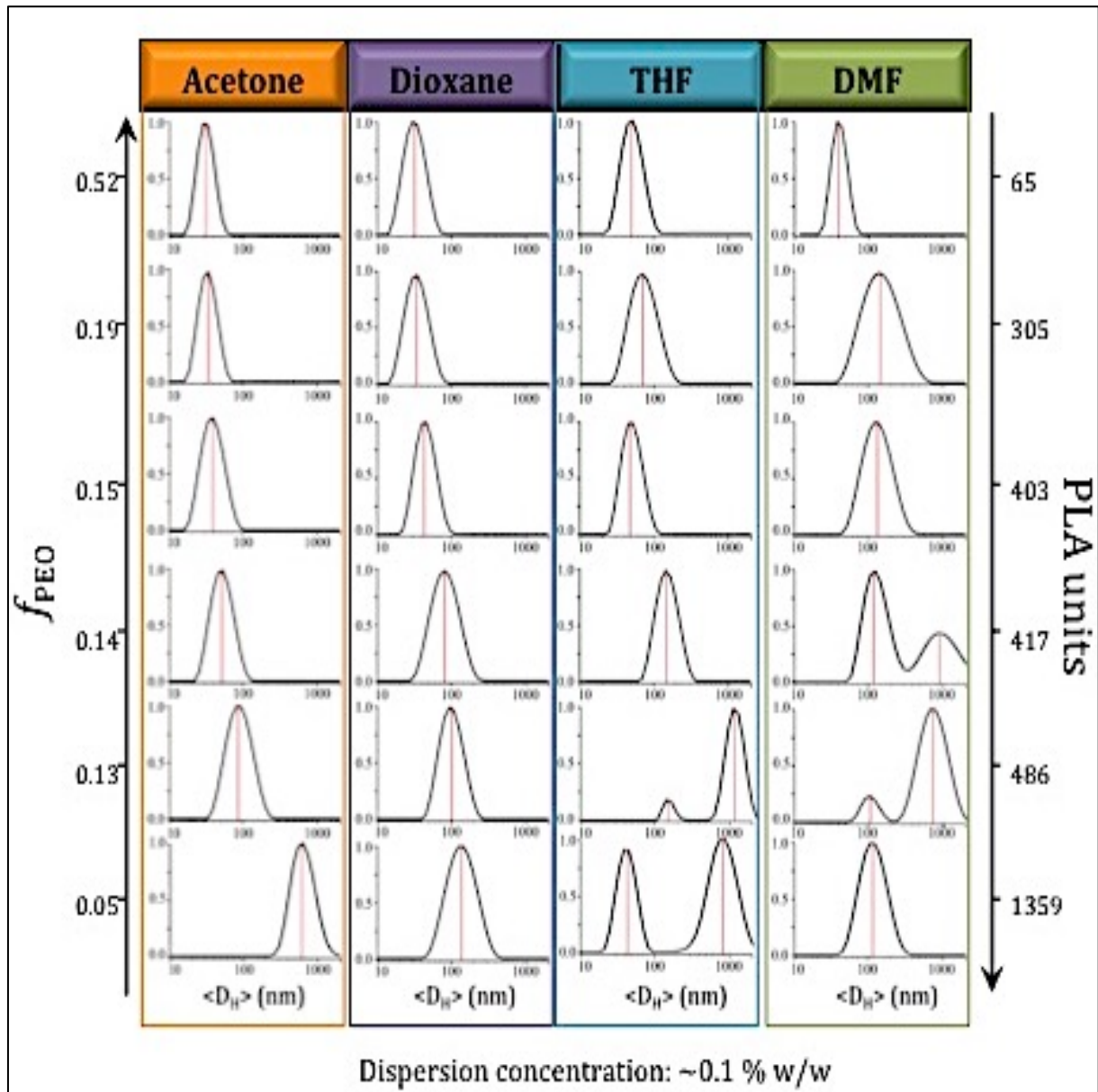


Figure 3.6. Intensity size distributions of the sample: mPEO₁₁₃-b-PLA₆₅; mPEO₁₁₃-b-PLA₃₀₅; mPEO₁₁₃-b-PLA₄₀₃; mPEO₁₁₃-b-PLA₄₁₇; mPEO₁₁₃-b-PLA₄₈₆ and mPEO₁₁₃-b-PLA₁₃₅₉ assembled from different organic solvents.

3.1.4 Transmission Electron Microscopy (TEM)

The transmission electron microscope is a very powerful tool for material science. A high energy beam of electrons is shone through a very thin sample, and the interactions between the electrons and the atoms can be used to observe features such as the crystal structure as well as features within the structure, such as dislocations and grain boundaries. The TEM operates on the same basic principles as the light microscope but uses electrons instead of light. Because the wavelength of electrons is much smaller than that of light, the optimal resolution attainable for TEM images is many orders of magnitude better than that from a light microscope. Thus, TEMs can reveal the finest details of internal structure, in some cases as small as individual atoms. The beam of electrons from the electron gun is focused into a small, thin, coherent beam by the use of the condenser lens. This beam is restricted by the condenser aperture, which excludes high angle electrons. The beam then strikes the specimen, and parts of it are transmitted depending upon its thickness and electron transparency. This transmitted portion is focused by the objective lens into an image on a phosphor screen or a charge-coupled device (CCD) camera. Optional objective apertures can be used to enhance the contrast by blocking out high-angle diffracted electrons. The image is then passed down the column through the intermediate and projector lenses and is enlarged all the way.

The image strikes the phosphor screen and light is generated, allowing the user to see the image. The darker areas of the image represent those areas of the sample that fewer electrons are transmitted through, while the lighter areas of the image represent those areas of the sample that more electrons were transmitted through.

As the electrons pass through the sample, they are scattered by the electrostatic potential set up by the constituent elements in the specimen. After passing through the specimen, they pass through the electromagnetic objective lens, which focuses all the electrons scattered from one point of the specimen into one point in the image plane.

A TEM specimen must be thin enough to transmit a sufficient number of electrons to form an image with minimum energy loss. Therefore, specimen preparation is an important aspect of the TEM analysis.

Given the limitations of the SEM, the morphology of the NP was evaluated by TEM using a JEOL JEM 1011 microscope at an accelerating voltage of 80 kV. For the analysis, after appropriate dilution in Milli-Q water, 7 μL of an aqueous micellar solution was dropped onto a glow-discharged carbon-coated copper grid. Figure 3.7 show a TEM micrograph of $\text{mPEO}_{113}\text{-}b\text{-PLA}_{486}$ from dioxane and $\text{mPEO}_{113}\text{-}b\text{-PLA}_{1359}$ from THF.

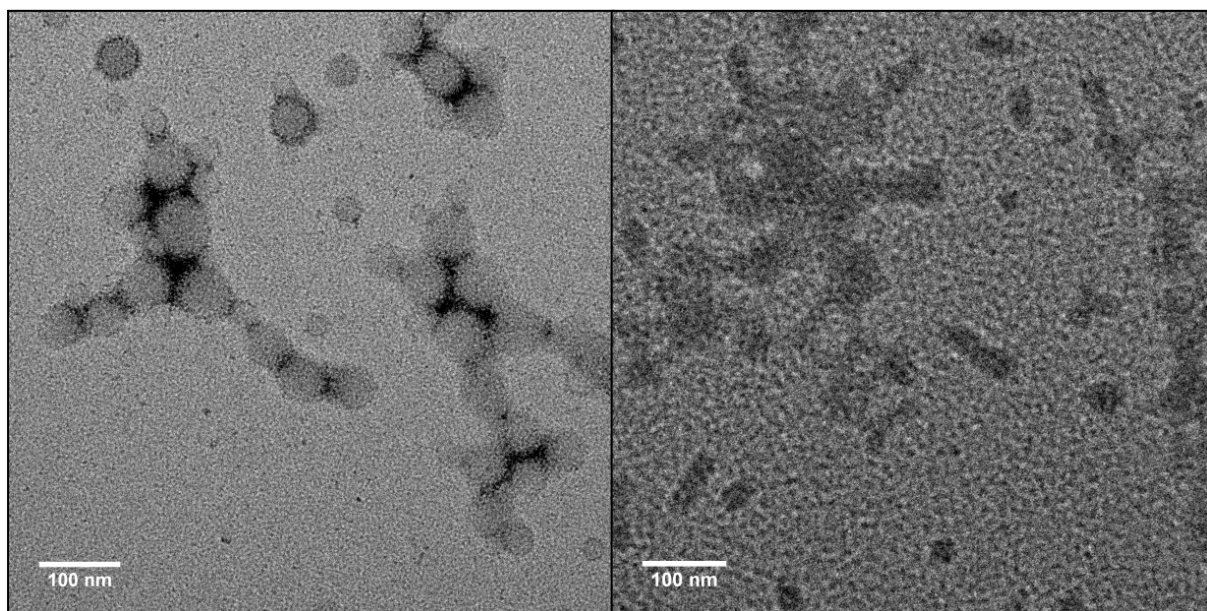


Figure 3.7. TEM micrographs of $\text{mPEO}_{113}\text{-}b\text{-PLA}_{486}$ from dioxane (left) and $\text{mPEO}_{113}\text{-}b\text{-PLA}_{1359}$ from THF (right).

3.1.5 TEM in cryogenic conditions (cryo-TEM)

Cryo-transmission electron microscopy (cryo-TEM) or cryo-electron microscopy (cryo-EM) is an ensemble of techniques allowing the observation of biological specimens in their native environment at cryogenic temperatures (-180°C for liquid nitrogen stages, -269°C for He).

In a TEM, an image is formed by directing a high-energy electron beam at a thin sample. A series of electromagnetic lenses collect the resulting elastically scattered electrons to form a magnified 2D image (projection) of the specimen, much like in a light microscope. The short wavelength of the electrons allows sub-nanometer resolution in these images. However, a fraction of the electrons will exchange energy with the sample (inelastic scattering) and destroy it very rapidly. Therefore, for high resolution imaging, the sample is only exposed to a very low electron dose (10–20 electrons \AA^{-2}), and only during image acquisition.

For observation in cryoEM, biological samples are preserved frozen-hydrated in their native state. This is achieved by rapidly plunging the sample, reduced to a very thin liquid film, into a liquid ethane bath. This operation can be computer-controlled through an automatic plunging apparatus such as the Vitrobot.

The resulting images are 2D, related to a projection of the potential in the biological object. Electron detectors can be photographic emulsions, CCD or CMOS cameras. A number of iterative mathematical 3D reconstruction schemes can then be applied to obtain a 3D model from these data and refine it to higher and higher resolution.

Samples of NP dispersions after dialysis were vitrified by applying a 3 μl aliquot to a previously glow-discharged 200-mesh holey and Quantifoil carbon grids (Ted Pella, USA). Grids were blotted and then plunged into liquid ethane using a FEI Vitrobot Mark IV (FEI Company, the Netherlands). The samples were imaged using a Tecnai G2F20 microscope (FEI Company, the Netherlands) equipped with a Schottky Field Emission electron source, a US1000 2kx2k Gatan CCD camera and operating at an

acceleration voltage of 200 kV. The cryo-tomographic (CET) series were collected tilting the vitrified sample over $\pm 60^\circ$, with a tilt step of 2° . Computation of tomogram was carried out with the IMOD⁹ software package. Segmentation and 3D visualization were done using the Amira package (FEI Visualization Science Group, Bordeaux). The cryo-TEM and CET imaging were performed under low dose conditions (60-80 electron/ \AA^2). The first selected sample (mPEO₁₁₃-b-PLA₄₈₆ - dioxane) had the size of about 100 nm and a polydispersity around 1.1. The cryoTEM, in this case, clearly showed the presence of circles constituted by a dark border with a thickness of about 21 nm and an hollow interior with the same brightness as the external background (Figure 3.8, A). This observation corresponds with the presence of polymersomes, whose production was one of the main goals of the present work. The presence of solvent pockets within the structure holds great promise for drug delivery but also explains why this shape could not be observed by standard TEM: in high vacuum condition, we expect the solvent to escape the structure destructively.

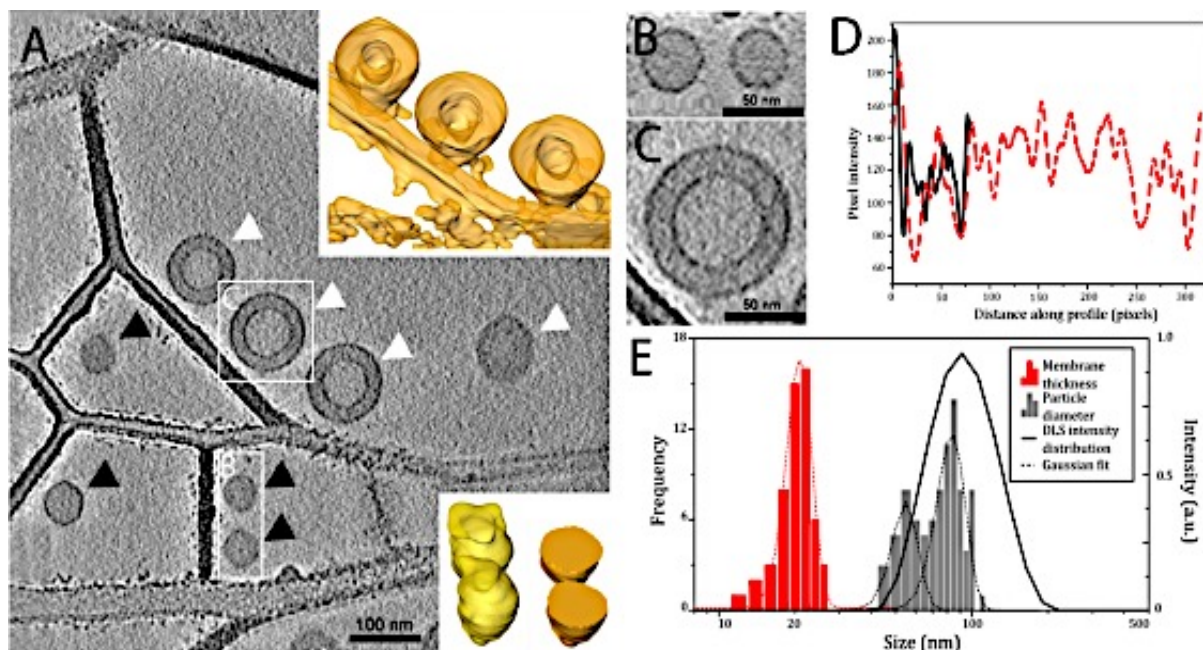


Figure 3.8. Nanoparticle morphology of PEO₁₁₃-b-PLA₄₈₆ assembled from dioxane as revealed by CET: (A), averaged tomographic slice showing micelles (black arrowheads) and polymersomes (white arrowheads). The insets show the 3D models of polymersomes (upper right) and micelles (bottom right). (B) high magnification of the boxed region in A (micelles). (C) high magnification of the boxed region in A (polymersomes). (D) Electron density (plotted as pixel light intensity) measured along the diameter of micelles (solid black line) and polymersomes (red dashed line). (E) Particle size distribution calculated by DLS (solid line) and CEM (grey histogram), and polymersome membrane thickness measured by CEM (red histogram).

The second sample examined, mPEO₁₁₃-b-PLA₁₃₅₉ assembled from THF, presents two populations in DLS characterisation: one below 50 nm and the other one above 500 nm. CryoTEM structures that appear in the image as dark spots with a diameter of around 30 nm are compatible with the first population. The second population, NPs formed by having more than 500 nm in size, was studied by TEM, which showed a morphological picture compatible with that of the composite micelles. The DSC data and TEM and cryoTEM micrographs of nanoparticles of mPEO₁₁₃-b-PLA₁₃₅₉ assembled from THF are reported in Figure 3.9.

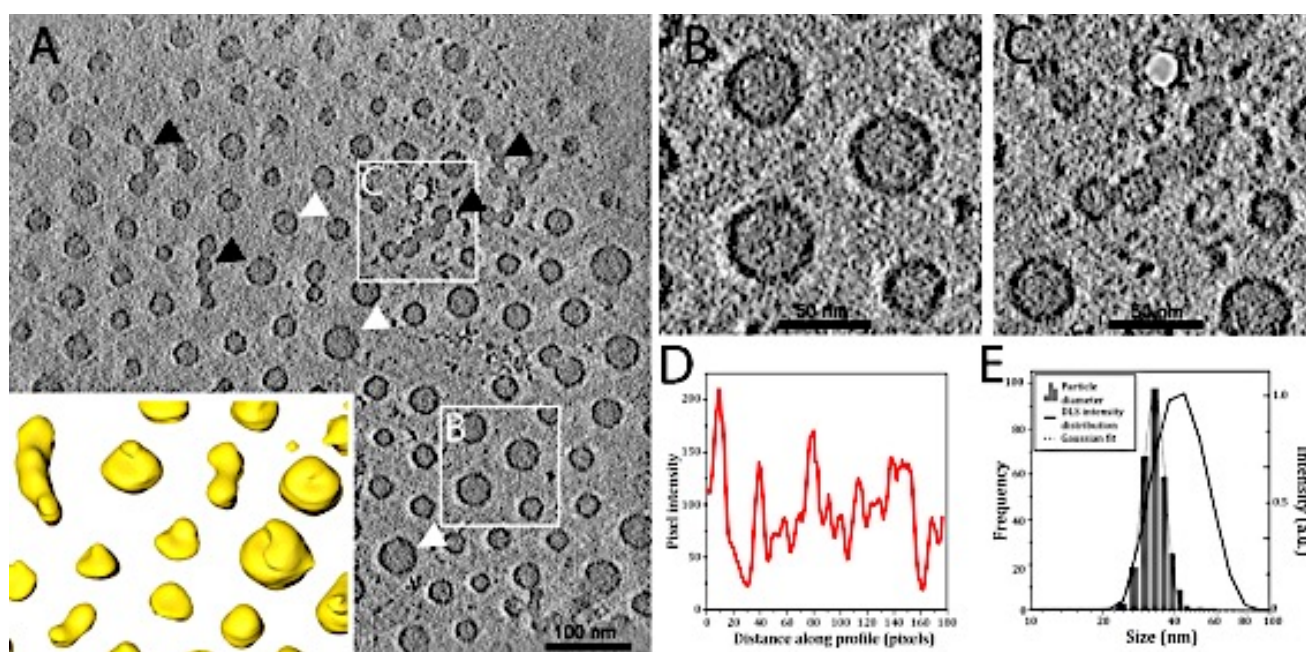


Figure 3.9. Nanoparticle morphology of PEO₁₁₃-b-PLA₁₃₅₉ assembled from THF as revealed by CEM (A). The inset shows the 3D models of single micelles and necklace-like aggregates. (B) High magnification of the boxed region in A (single micelles). (C) high magnification of the boxed region in A (necklace-like aggregates). (D) Electron density (plotted as pixel light intensity) measured along a micelle diameter. (E) Particle size distribution calculated by DLS (solid line) and CEM (histogram).

The same copolymer self-assembled from DMF confirms the existence of two types of objects, one with $\langle D_H \rangle = 219$ nm and the other with the same dimension of the large objects obtained from THF. In this case, CEM micrographs reveal the presence of large variety of shape and dimensions: in figure 3.9, single or partially fused micelles ranging

from 100 nm to 300 nm are visible. Electron density profiles (Figure 3.9, C) highlight uniformly dense objects that can be considered as large compound micelles (LCM). CET reported in figure 3.10, E and F reveal a further process of aggregation of the LCMs forming low symmetry objects of about 1000 nm. In this case the single LCM appear to be deformed assuming an ellipsoidal shape. This hierarchical self-assembly is quite common for triblock copolymers¹⁶ but rarely described for simple diblock copolymers.

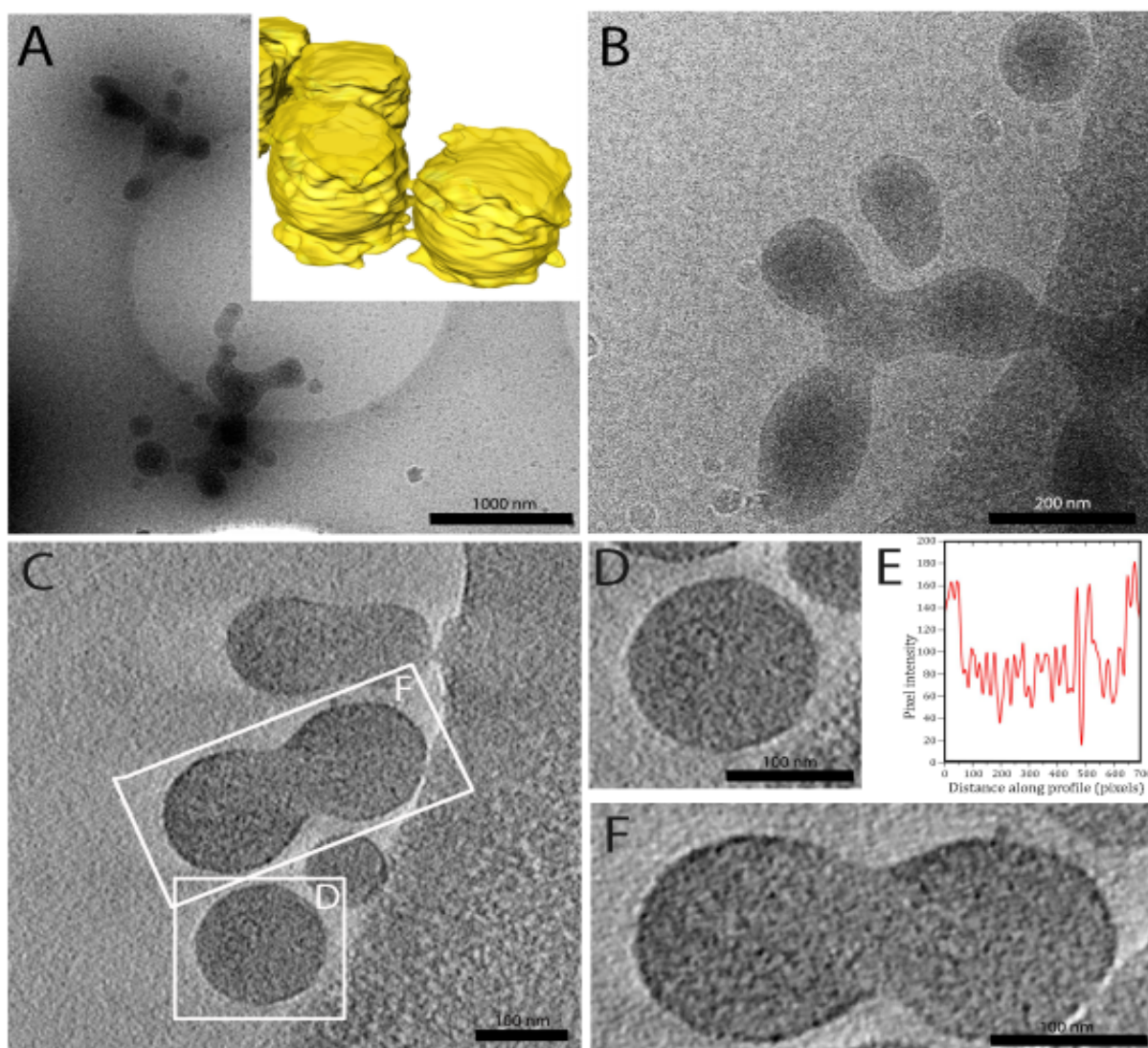


Figure 3.10. Nanoparticle morphology of PEO₁₁₃-*b*-PLA₁₃₅₉ assembled from DMF as revealed by cryo-EM and CET: (A) low magnification projection image showing micron-scale irregular aggregates. The inset shows the 3D model of large compound micelles. (B) projection image showing fused large compound micelles (LCM). (C) averaged tomographic slice through LCMs; (D) high magnification of the boxed region in C showing a single LCM. (E), Electron density (plotted as pixel light intensity) measured along the diameter of the single LCM. (F) high magnification of the boxed region in C showing fused LCMs.

3.2 Results and Discussion

The DLS characterisation study of mPEO₁₁₃-b-PLA_x samples provides a detailed picture of the self-assembly phenomenon in relation to the chemical nature of the solvents tested (DMF, acetone, THF and dioxane). It is apparent that non-selective solvents may be used to obtain different morphologies without varying the polymer composition. Furthermore, the simple measures of the self-assembled nanoparticles by DLS may provide, as a function of the preparation conditions, the first estimate of the type of structure formed by a given copolymer. The data obtained through the DLS revealed an increase in the size of NP and can be related to both the nature of the solvent and the molecular weight of the polymer. In particular, an increase of average size is also present to vary the solvent (in the order acetone <dioxane <THF <DMF). In the present study we have observed a strong correlation between the size of the NP and the molecular weight of the PLA block. These data are in agreement with those reported in the literature by Davis and colleagues, according to which the size of the PEO-b-PLA particles, prepared from acetone by nanoprecipitation, is modified by varying the molecular weight of the PLA block.^{5,7}

However, Wu et al. found no significant changes in the dimensions of the particles of PEO-b-PCL copolymers of different hydrophilic/hydrophobic balances and prepared with THF.¹¹ These conflicting data suggest the importance of the method of preparation.⁵

Furthermore, due to the complexity of the mechanisms regulating the self-assembly of amphiphilic block copolymers, it is necessary to maintain tight control of both the chemical (molecular weight, volume fraction of each block, interaction between the various blocks) and methodological (choice of co-solvent, temperature, pH) parameters in order to properly drive the final morphology of the nanoparticles.^{7,12,13}

The possibility of mastering the process of the self-assembly of amphiphilic block copolymers with different solvents can offer the great advantage of optimising the

choice of the ideal NPs for the delivery of drugs. For example, polymersomes, on account of their large internal volume, low permeability and the high tenability of their membrane, allow the drug encapsulation to be much more effective compared to other transport systems (e.g., liposomes, dendrimers, micelles, solid NPs).^{14,15}

The morphology characterization, obtained through cryoTEM revealed the structure of the first selected sample (mPEO₁₁₃-b-PLA₄₈₆ – dioxane) which had the size of about 100 nm and a polydispersity around 1.1. The cryoTEM, in this case, clearly showed the presence of polymersomes (Figure 3.11, left image), whose production was one of the main goals of the present work. The presence of solvent pockets within the structure holds great promise for drug delivery but also explains why this shape could not be observed by standard TEM: in high vacuum condition, we expect the solvent to escape the structure destructively.

The second sample examined (mPEO₁₁₃-b-PLA₁₃₅₉-THF), which resembles a crew cut,¹⁰ i.e. with a large predominance of the hydrophobic block, in DLS characterisation consists of two populations: one below 50 nm and the other above 500 nm (Figure 3.11, right image). The dark spots of approximately 30 nm in diameter that appear in the CryoTEM image are compatible with the first population. The NPs exhibit a dark core and a thin outer shell. The second population of NPs, formed by those of more than 500 nm in size, was also studied by TEM. The analysis demonstrated their morphological compatibility with that of the composite micelles, generated by a process of second-order hierarchical self-assembly. This process initially comprises the formation of particles of around 30 nm, the corona of which is too thin to stabilise the dispersion. The NPs of 30 nm aggregate, forming systems of 500-nm NPs, where there is a considerable decrease in the specific surface area. From the point of view of the relationship between kinetic assembly and formed structures, we can say that for the four best solvents, namely ACT, THF, DMF, and Dioxane, the viscosity is the key element: when the viscosity is high, the diffusion of the polymer chains in the mixture solvent is hindered, and thus larger and polydisperse particles form.

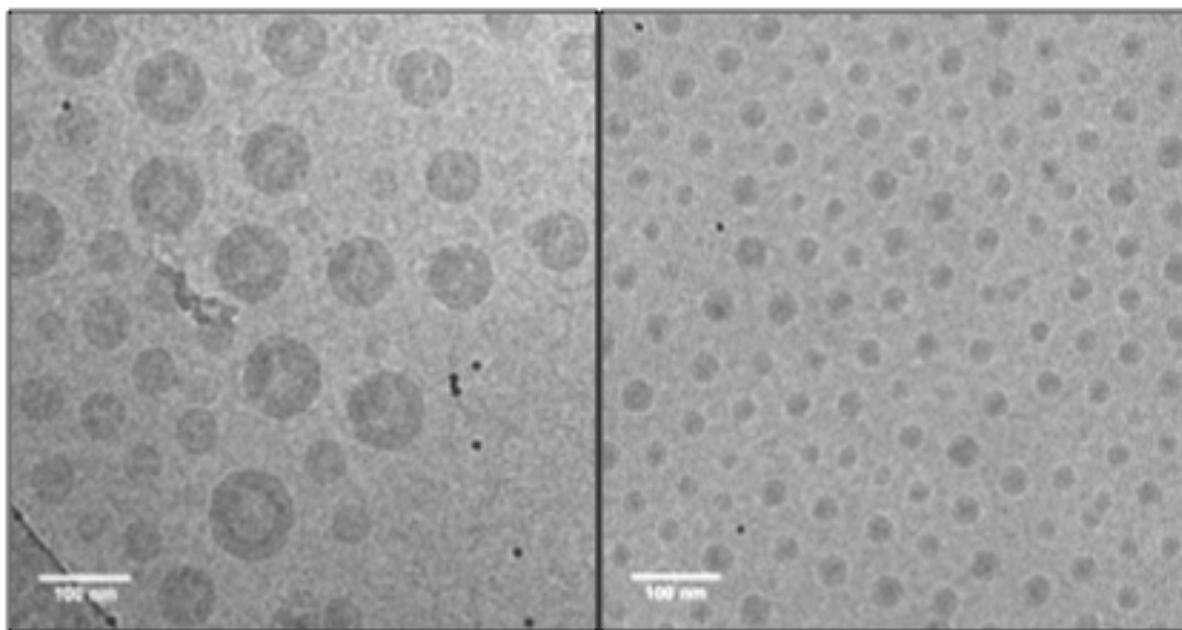


Figure 3.11 Micrographs cryoTEM nanoparticles. To the left, polymersomes obtained from the sample $m\text{PEO}_{113}\text{-b-PLA}_{486}$ assembled from dioxane. Right, core-corona micelles obtained from $m\text{PEO}_{113}\text{-b-PLA}_{1359}$ assembled from THF.

Finally, we tried to generalise the correlation between hydrodynamic radius and distribution (associated with PDI) of NP size for different solvents with the morphology by collecting all data in a “map”.

In each specific area of the map are represented the nanoparticles of different shapes, in particular simple micelles, polymersomes/hard nanoaggregates and finally the large compound micelles. The correlation between morphology, hydrodynamic radius and PDI of NP for different solvents is shown in the figure 3.12 in the top position. They assign different areas, on the basis of the literature and cryoTEM measures, to different types of structures (bottom image).

Creating a map dedicated to the $m\text{PEO}_{113}\text{-b-PLA}_x$ system has proven to be a useful tool for describing and representing this system in a synthetic and visual way, enabling understanding and organization of work. This map can be used to assess the result of assembly of similar polymers in other solvents, such as the acetone/acetonitrile mix described in chapter 5.

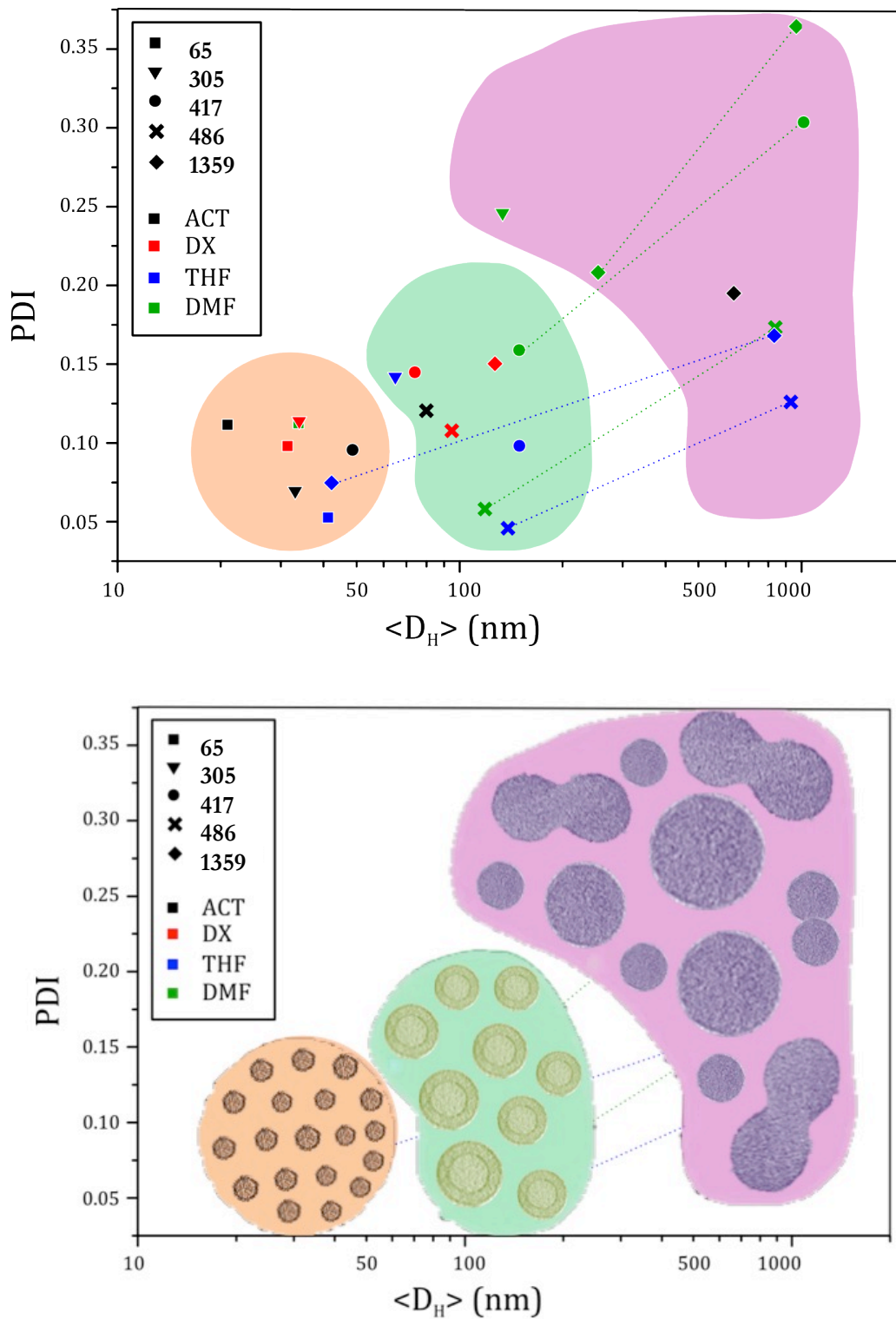


Figure 3.12. Correlation between morphology, hydrodynamic radius and PDI of NP for different solvents (top image). They assign different areas, on the basis of the literature and cryoTEM measures, to different types of structures (bottom image).

3.3 Chapter Summary

In Chapter 3, the data for the self-assembly, via slow nanoprecipitation in water from four organic solvents with different polarity and viscosity (DMF, acetone, THF, dioxane), were reported for the mPEO₁₁₃-b-PLA_x system. It is apparent that non-selective solvents may be used to obtain different morphologies without varying the polymer composition. As a function of the preparation conditions, the DLS characterisation forecasts the first estimate of the type of structure formed by a given copolymer. The data obtained through the DLS analysis revealed an increase in the size of NP and their morphology and can be related to both the nature of the solvent and the molecular weight of the polymer. In particular, an increase in average size was also present upon varying the solvent (in the order Acetone <Dioxane <THF <DMF).

Correlating all of the data obtained from both DLS characterisation (size and distribution) and TEM and cryoTEM (morphology), we have developed a map highlighting different areas in which the structures formed by the assembled NPs are concentrated.

The morphological map could provide highly valuable guidelines in the selection of 'smart nanoparticles' for the delivery of both hydrophilic and hydrophobic drugs.

Regarding the group assembled from acetone and forming small micelles (40–120 nm), they may possibly be used for delivering drugs through the blood brain barrier (BBB)¹⁷ while increasing the therapeutic efficacy and reducing collateral effects.¹⁸

Finally, polymer micelles satisfy the stringent requirements that guide the biomedical applications of nanoparticles (monodispersity, low cytotoxicity, biodegradability, prolonged circulation time in the bloodstream), in particular monodispersity and good stability.

3.4 References

1. Zhang, L.; and Eisenberg, A.; Multiple Morphologies of "Crew-Cut" Aggregates of Polystyrene-*b*-poly(acrylic acid) Block Copolymers. *Science*, **1995**, 23; 268 (5218): 1728-1731.
2. Hansen, C. M.; CRC Press, **2000**.
3. Brandrup, J.; Immergut, E.H.; Interscience Publishers, **1999**.
4. Cohn, D.; Hotovely-Salomon, A.; Biodegradable multiblock PEO/PLA thermoplastic elastomers: molecular design and properties. *Polymer*, **2005**, 46, 2068-2075.
5. Vangeyte P., Gautier S., Jérôme R., Colloids and Surfaces A: Physicochem. Eng. Aspects. **2004**, 242 203–211.
6. Cammas, S.; Suzuki, K.; Sone, C.; Sakurai, Y.; Kataoka, K.J.; *J. Controlled Release* **48**, **1997**, 157.
7. Allen, C.; Yu, Y.; Maysinger, D.; Eisenberg, A.; Polycaprolactone-*b*-poly(ethylene oxide) block copolymer micelles as a novel drug delivery vehicle for neurotrophic agents FK506 and L-685,818. *Bioconjugate Chem.* **1998**, 9, 5, 564-572.
8. Nagarajan, R.; Ganesh, K.J.; Block copolymer self-assembly in selective solvents: Spherical micelles with segregated cores. *J. Chem. Phys.* **1989**, 90, 5843.
9. Kremer, J.R.; Mastrorade, D.N.; McIntosh, J.R.; Computer visualization of three-dimensional image data using IMOD. *J Struct Biol*, **1996**, 116 (1), 71–76.
10. Zhang, L. and Adi Eisenberg A.; Multiple Morphologies and Characteristics of "Crew-Cut" Micelle-like Aggregates of Polystyrene-*b*-poly(acrylic acid) Diblock Copolymers in Aqueous Solutions. *J. Am. Chem. Soc.* **1996**, 118, 3168-3181
11. Zhao, Y.; Liang, H.; Wang, S.; Wu, C.; Self-Assembly of Poly(caprolactone-*b*-ethylene oxide-*b*-caprolactone) via a Microphase Inversion in Water. *J. Phys. Chem. B.*, **2001**, 105, 4: 848-851.
12. Yu, K.; Zhang, L.; Eisenberg, A.; Novel Morphologies of "Crew-Cut" Aggregates of Amphiphilic Diblock Copolymers in Dilute Solution. *Langmuir*, **1996**, 12, 25: 5980-5984.
13. Cameron, N. S.; Corbierre, M. K.; Eisenberg, A.; Asymmetric amphiphilic block copolymers in solution: a morphological wonderland, *Can J Chem*, **1999**, 77, 8: 1311-1326.
14. Bermudez, H.; Brannan, A. K.; Hammer, D. A.; Bates, F. S.; Discher, D. E.; Molecular Weight Dependence of Polymersome Membrane Structure, Elasticity, and Stability. *Macromolecules*, **2002**, 35, 21: 8203-8208.
15. Discher, B. M.; Won, Y. Y.; Ege, D. S.; Lee, J. C. M.; Bates, F. S.; Discher, D. E.; Hammer, D. A.; Polymersomes: Tough vesicles made from diblock copolymers. *Science* **1999**, 284, 5417: 1143-1146.
16. Groschel, A. H.; Schacher, F. H.; Schmalz, H.; Borisov, O. V.; Zhulina, E. B.; Walther, A.; Muller, A. H. E., Precise hierarchical self-assembly of multicompartiment micelles. *Nature Communications* **2012**, 3.
17. Gregori, M.; Bertani, D.; Cazzaniga, E.; Orlando, A.; Mauri, M.; Bianchi, A.; Re, F.; Sesana, S.; Minniti, S.; Francolini, M.; Nardo, L.; Salerno, D.; Mantegazza, F.; Masserini, M.; Simonutti, R.; Investigation of Functionalized Poly(N,N-dimethylacrylamide)-block-polystyrene Nanoparticles As Novel Drug Delivery System to Overcome the Blood-Brain Barrier In Vitro. *Macromol. Biosci.*, **2015**, 15, 12: 1687-1697.
18. Riehemann, K.; Schneider, S. W.; Luger, T. A.; Godin, B.; Ferrari, M.; Fuchs, H.; Nanomedicine: challenge and perspectives. *Angew. Chem. Int.*, **2009**, 48, 5: 872-897.

CHAPTER 4

SELF-ASSEMBLY OF AMPHIPHILIC BLOCK COPOLYMERS FROM A MIXTURE OF GOOD SOLVENTS

4.1 Experimental Section

4.1.1 Materials

Acetone, Acetonitrile, Coumarin 6 (C6) and Sepharose CL-4B were purchased from Sigma–Aldrich (Milano, Italy) and a dialysis bag (3500 MW cut off) from Spectrum Laboratories, Inc. (Rancho Dominguez, USA).

4.1.2 Preparation of C6-NPs for crossing the blood brain barrier

After being synthesised, assembled and characterised a library of m-PEO₁₁₃-b-PLA_x, some samples were selected for overcoming the blood-brain barrier (BBB). The BBB is a highly selective barrier, since it has the function of protecting a noble organ such as the brain by pathogenic noxae of different sorts. Therefore, the ideal nanocarriers must meet extremely stringent criteria. The most important prerequisites are non-toxicity, biodegradability and biocompatibility. Application also requires chemical stability in blood (non aggregation), avoidance of the mononuclear phagocyte system (MPS) and the capability to cross the BBB for brain delivery (receptor-mediated transcytosis across brain capillary endothelial cells); amenableness to small molecules, peptides, protein, or nucleic acids (Figure 1.4); scalable and cost-effective manufacturing process^{1,2}.

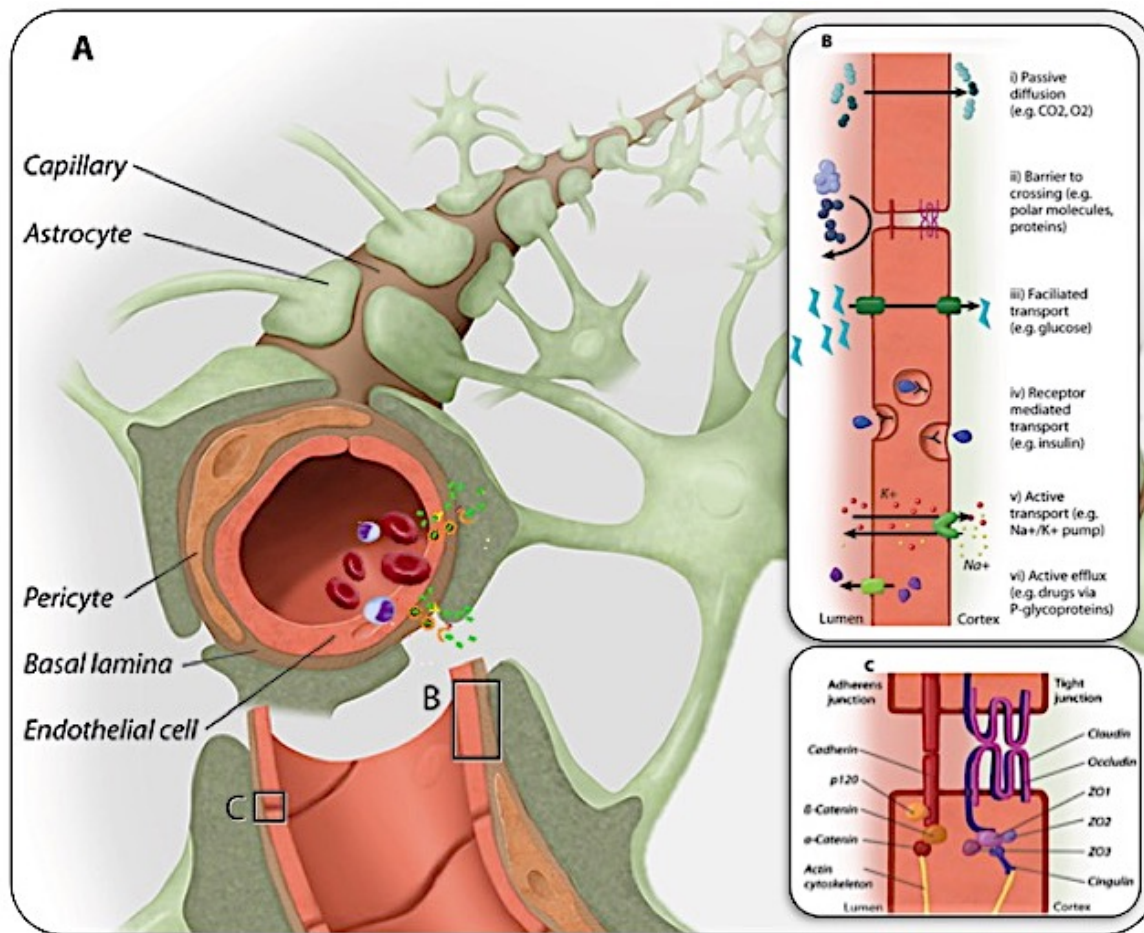


Figure 4.1. Targeted therapy across the blood-brain barrier.³

The loadinf tests were conducted using the coumarin 6 [3-(1,3-benzothiazol-2-yl)-7-(diethylamino) chromen-2-one] as a drug model. Among the various assembled nanoparticles, the preference was given to the micelles of small size (40–130 nm) obtained from the assembly of copolymers with intermediate PLA block length (m-PEO₁₁₃-b-PLA₄₀₈ and m-PEO₁₁₃-b-PLA₄₈₆) from acetone. New assemblies were therefore carried out to load the C6 (Figure 4.2). Since the NPs are intended for the biological system, the phosphate-buffered saline (PBS) at pH 7.4 was used instead of MQ water in the assembly. The C6-loaded NPs were prepared by adding C6 (0.2 wt%) to the polymer solution before the self-assembly.

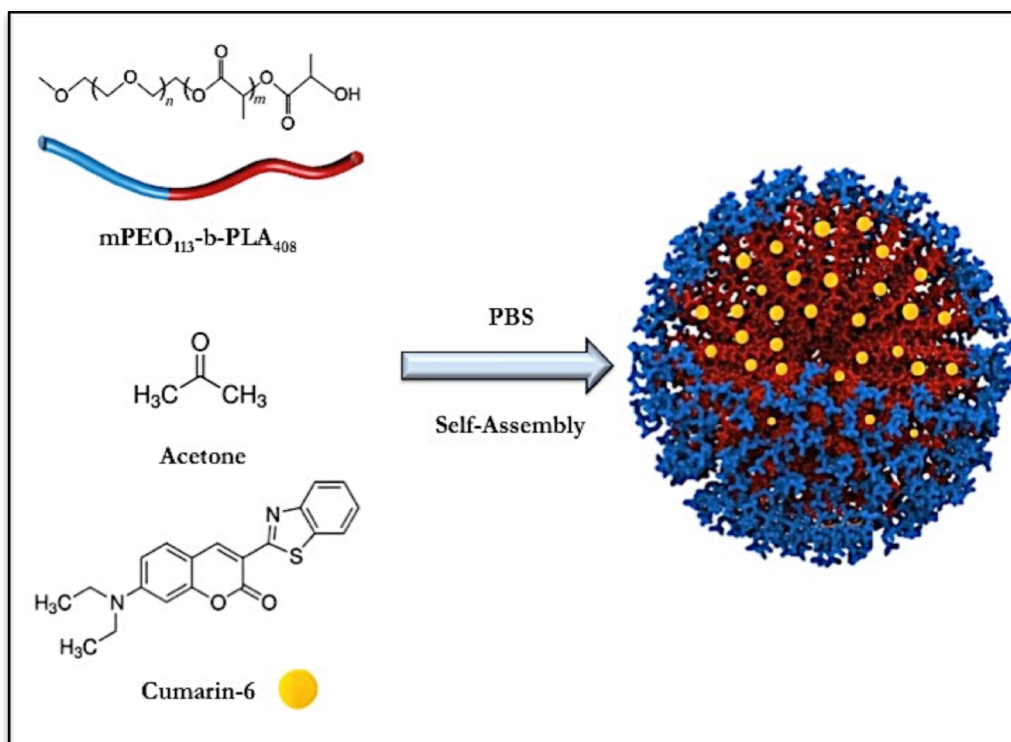


Figure 4.2. Schematic representation of the C6-NP preparation: The solution of Coumarin 6 dissolved in acetone was added to mPEO₁₁₃-b-PLA₄₀₈ before the self-assembly. C6 resides in the hydrophobic core of NP (red).

In particular, 15mg of m-PEO₁₁₃-b-PLA₄₀₈ and m-PEO₁₁₃-b-PLA₄₈₆ were dissolved in 0.75 ml of acetone with C6 (at different concentrations: 100, 200, 500 µg/mL) and using the technique of nanoprecipitation, the solution of PBS was added dropwise at the speed of 4 ml/h. The obtained nanodispersions were subjected to dialysis with PBS for 24 hours. The samples were purified by gel filtration through a Sepharose CL-4B column (25×1 cm) (Figure 4.3). All C6 NP preparations were characterised in terms of size, ζ-potential, polydispersity index, and stability by DLS (Table 4.1). In particular, experiments were performed at 25 °C in PBS and pH 7.40 with a sample concentration of 100mg mL⁻¹ on a Malvern Zetasizer Instrument. Zeta potential was measured at 25 °C in PBS (150 mM NaCl) and pH 7.40, with a sample concentration of 100mg mL⁻¹ and using a Malvern Zetasizer Instrument (and using the standard Smoluchowsky theory).



Figure 4.3. Procedure of gel filtration through a Sepharose CL-4B column.

In the table 4.1 it is possible to note how the C6 micelles fillers have a diameter slightly greater than of the naked micelles; this is probably due to the presence of drug molecules within the micellar core. However, in both cases the particles are quite small in size, so that they can be used for all routes of administration, including the parenteral route. In addition, the nanometric dimensions are a positive characteristic for such systems because they allow the extension of their stay in the bloodstream, escaping the process of phagocytosis by the reticuloendothelial system (RES).

SAMPLES DESCRIPTION	NP DIAMETER (nm)	PdI	ZP (mV)
mPEO ₁₁₃ -b-PLA ₄₀₃	99.7 nm	0.005	-2,83
mPEO ₁₁₃ -b-PLA ₄₀₃ (C6-100)	105.3 nm	0.005	-2,85
mPEO ₁₁₃ -b-PLA ₄₀₃ (C6-200)	102.9 nm	0.142	-3.94
mPEO ₁₁₃ -b-PLA ₄₀₃ (C6- 500)	126.3 nm	0.131	-3.06
mPEO ₁₁₃ -b-PLA ₄₈₆ (C6-200)	121.7 nm	0.005	-4.32

Table 4.1. Mean diameter, polydispersity index (PdI) and zeta potential (ZP) obtained by the dynamic light scattering (DLS) of C6 NPs.

Measuring the amount of C6 encapsulated in micelles through the following method. After dialysis, C6-NP were disassembled by adding acetone (4 μ L of NP dissolved in 1 mL of acetone). After centrifugation at 4.000 rpm for 40 minutes, the concentration of coumarin-6 in the supernatant was detected by the fluorescence spectrophotometer (λ_{ex} =446 nm, λ_{em} =507 nm), and the total amount of encapsulated C6 was calculated. In order to obtain C6 concentration in the solution, fluorescence index (FI) were compared to a previously established calibration curve for C6, constructed with known amounts of C6: 20 ng, 40 ng and 80 ng (Figure 4.4). Spectra of C6 dissolved in acetone are reported in Figure 4.5.

Drug loading (DL%) was calculated by the following equation (1):

$$DL (\%) = \frac{C6 \text{ concentration in nanoparticles}}{\text{nanoparticles concentration in the same solution}} \times 100 \quad (1)$$

The drug loading estimated for the mPEO₁₁₃-b-PLA₄₀₃ (C6-200) is 20%, and for the mPEO₁₁₃-b-PLA₄₀₃ (C6- 500) it is 24%.

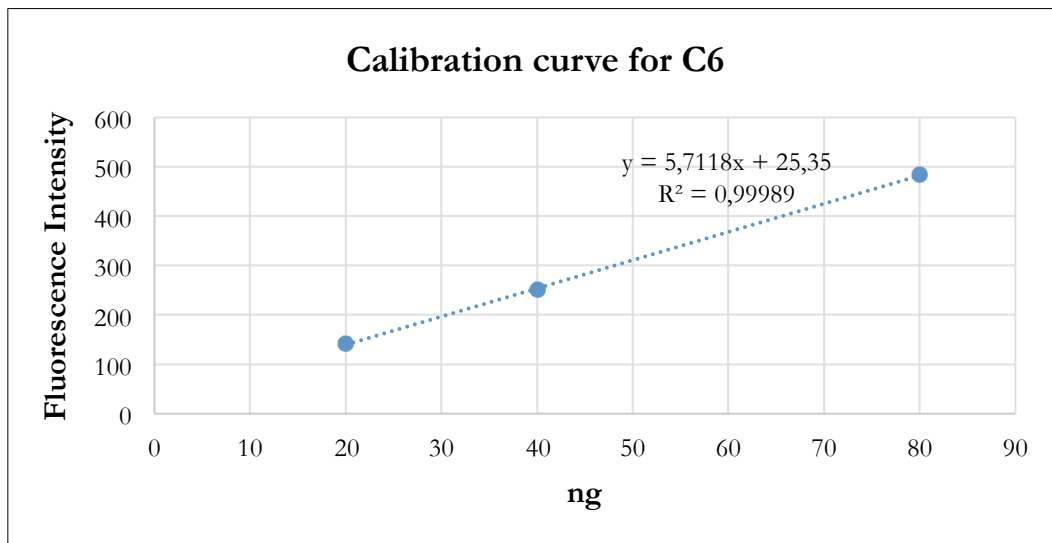


Figure 4.4. Calibration curve for C6.

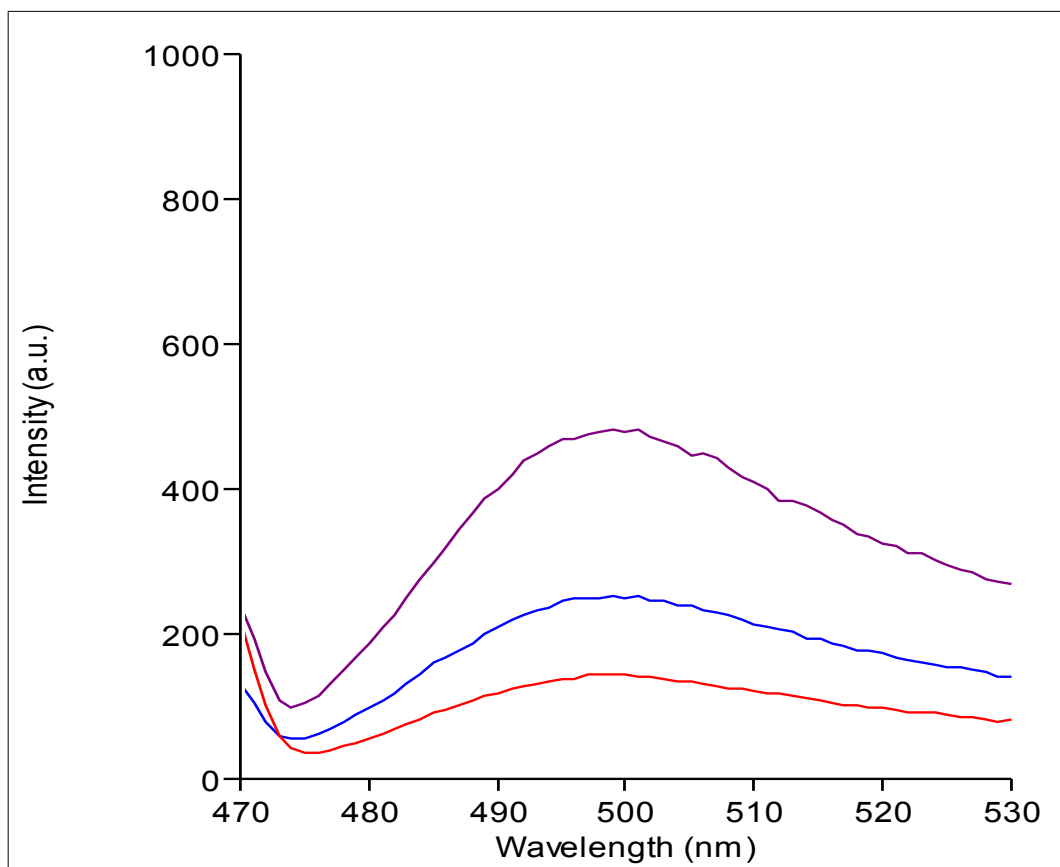


Figure 4.5. Absorption spectra of C6 acetone solutions used for calibration.

4.1.3 Self-assembly of amphiphilic block copolymers from a mixture of good solvents

Due to the hydrophobic nature of the C6, the first results were not satisfactory. The solvent acetone was not indicated to dissolve C6, and therefore it was not possible to load it in the best way. For this reason, it was decided to study the self-assembly of copolymers with a mixture of solvents. As stated previously, the nature of the solvent influences the morphology and the size of the NPs. Therefore, mixes of solvents were selected. An ideal mix had to be capable of insignificantly changing the size and morphology of the NPs and simultaneously optimising the loading of C6.

The most effective solvent for C6 is acetonitrile; therefore, it was decided to prepare three mixes with two solvents: acetone and acetonitrile (MIX A with a ratio of acetone:acetonitrile of 3:1, MIX B with a ratio of acetone:acetonitrile of 1:2, MIX C with a ratio of acetone:acetonitrile of 1:3). The samples (mPEO₁₁₃-b-PLA₅₀₃; mPEO₁₁₃-b-PLA₄₀₃; mPEO₁₁₃-b-PLA₄₈₆; mPEO₁₁₃-b-PLA₁₃₅₉) were assembled with the three mixes and subjected to DLS characterisation before and after dialysis.

The characterisation allowed the exclusion of the samples assembled with the mix C because the excess of acetonitrile did vary the size and shape of the NPs. Consequently, measurements of zeta potential were made on the samples assembled with the mixes A and B only.

All data on the characterisation of NPs in the mix A and mix are summarised in Table 4.2.

MIX SOLVENTS- DLS -size (nm)/PDI/ZP (mV)			
SAMPLES DESCRIPTION	SOLVENTS		
	ACETONE	MIX A	MIX B
mPEO ₁₁₃ -b-PLA ₄₀₃	Pk1= 46 nm PDI= 0.242 ZP=-9.72	Pk1= 62 nm PDI= 0.866 ZP= -4.2	Pk1= 50 nm PDI= 0.369 ZP= -8.4
mPEO ₁₁₃ -b-PLA ₄₈₆	Pk1= 85 nm PDI= 0.191 ZP= -23.1	Pk1= 76.26nm PDI= 0.127 ZP= -10.9	Pk1= 79.11 nm PDI= 0.255 ZP= -9.32
mPEO ₁₁₃ -b-PLA ₅₀₃	Pk1= 99.57 nm PDI= 0.187 ZP= - 24.8	Pk1= 58.63 nm PDI= 0.399 ZP= - 16.8	Pk1= 65.86 nm; PDI= 0.246 ZP= -19.2
mPEO ₁₁₃ -b-PLA ₁₃₅₉	Pk1= 774 nm PDI= 0.317 ZP= - 24.1	Pk1= 129 nm PDI= 0.153 ZP= - 18.2	Pk1= 119.4 nm PDI= 0.130 ZP= -21.4

Table 4.2. Mean diameter, polydispersity index (PDI) and zeta potential (ZP) obtained by the dynamic light scattering (DLS) of mPEO₁₁₃-b-PLA₄₀₃; mPEO₁₁₃-b-PLA₄₈₆; mPEO₁₁₃-b-PLA₅₀₃ and mPEO₁₁₃-b-PLA₁₃₅₉ assembled from acetone, mix A and mix B.

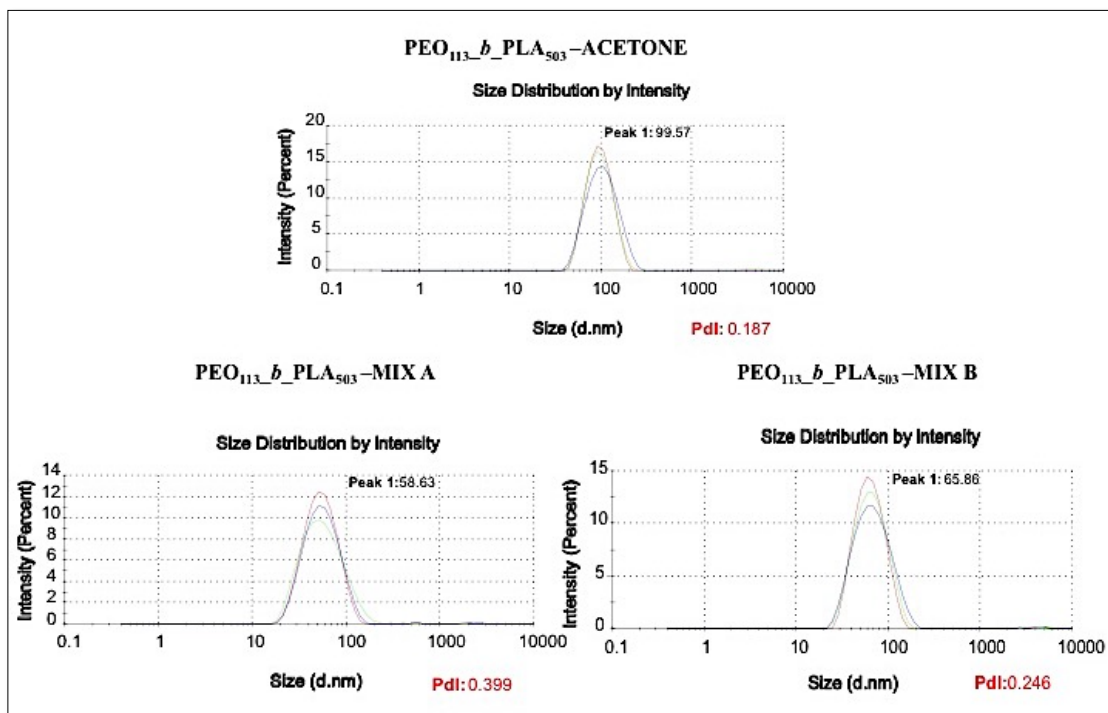


Figure 4.6. Comparison of the DLS measurement of mPEO₁₁₃-b-PLA₅₀₃ from acetone (at the top), mPEO₁₁₃-b-PLA₅₀₃ from mix A (on the left), and mPEO₁₁₃-b-PLA₅₀₃ from mix B (on the right).

4.2 Results and Discussion

Various parameters affect the efficiency of NP systemic circulation, BBB passage and cellular delivery. Numerous studies show a clear inverse correlation among NP size and BBB penetration.^{3,4,5,6,7} Most of the studies have been performed with spherical NPs with diameters between 50 nm to 100 nm. The shape of NPs also influences body distribution and cellular uptake.⁸ Zeta potential is another important parameter; it has been proven that NPs with high zeta potential (high positive charge) cause immediate toxicity to the BBB.⁹ Therefore, most of the NP formulations for brain delivery described in the literature have moderate (between -1 and -15 mV)^{10,11,12,13} or high negative zeta potentials (between -15 to -45 mV).^{8,14} Yet, some NP formulations with moderate (up to 15 mV) or high positive zeta potential (above 15 mV) are able to cross the BBB and in some cases are efficient brain delivery systems.^{15,16}

In order to facilitate BBB penetration, a number of ligands have been conjugated to NPs. Such molecules can be grouped into four different types⁴:

(1) ligands that mediate the adsorption from the bloodstream of proteins that in turn interact with BBB receptors or transporters (e.g. poly(sorbate 80) or Tween 80),^{4,17}

(2) ligands that have direct interaction per se with BBB transporters (e.g. transferrin peptides, transferrin proteins or antibodies against transferrin^{4, 12,18} and glucose transporter¹⁹), or receptors (e.g. insulin receptor).²⁰

(3) ligands that increase charge and hydrophobicity (e.g. amphiphilic peptides);^{4,21}

(4) ligands that improve blood circulation time (e.g., poly(ethylene glycol)(PEG).^{4,11}

In addition, both the number of ligands and their receptor affinity have an important impact on the transport of NPs across the BBB (avidity). Ligand density depends on both the NP surface area and the ligand size. Typically, the ligand affinity for its receptor is reduced when conjugated to NPs. NP avidity and selectivity increases when multiple targeting ligands are conjugated.²² However, NP avidity must be modulated for effective BBB transcytosis. High avidity impedes NPs bound to the receptor to be released into the brain parenchyma.

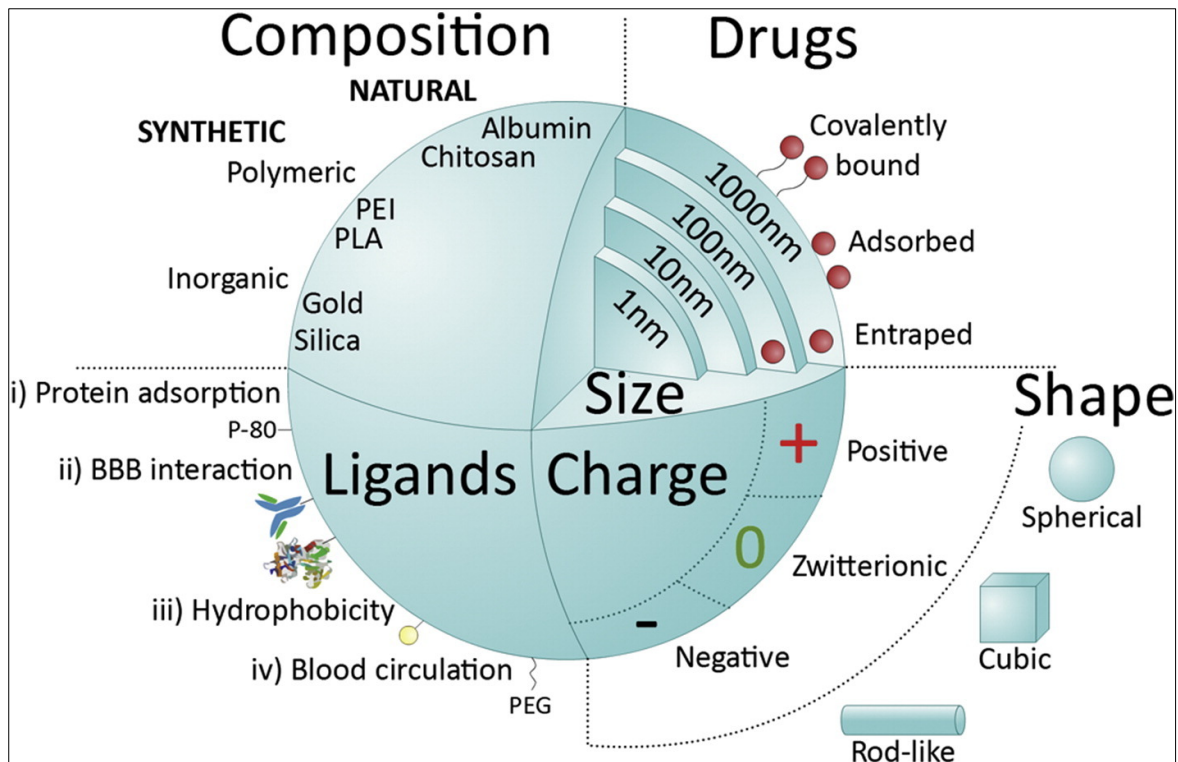


Figure 4.7. Main nanoparticle (NP) features influencing systemic delivery and blood brain barrier (BBB) passage, as discussed in ref. 4.

When NPs enter a physiological environment, there is a rapid adsorption of proteins from the bloodstream to the NP surface, forming a protein coating, called ‘protein corona’.^{23,24} The protein corona may alter the surface chemistry of the NPs along with its aggregation state. Very often it also accelerates blood clearance of the NPs through the reticuloendothelial system localised mostly in the spleen and liver,²⁵ which may both decrease the NP dose available for accumulation in the brain and induce inflammation. The most common way to overcome this issue is to use molecules with the capacity to minimise surface fouling in order to maintain the performance and safety of materials. In this sense, antifouling properties can be enhanced by using PEG-coated NPs, which present minimal surface charge, leading to lower NP opsonisation and lower reticuloendothelial system uptake.²⁶ Grafting NPs with PEG decreases protein adsorption and slows down the clearance of the nanomaterials.^{22,27} Moreover, due to its improved blood circulation time, PEGylated NPs accumulate more efficiently in the brain;^{22,28} for instance, polystyrene NPs (below 200 nm) coated with PEG (5 kDa; 9

PEG molecules per 100 nm²) are able to cross the BBB. Additionally, PLGA NPs (ca. 78 nm) coated with PEG are also able to rapidly penetrate rat brain tissue *ex vivo*, in contrast with uncoated NPs.²⁸ Yet, it is important to note that the best formulations administered intravenously deliver up to 5% of the initial dose effectively across the brain. NP brain delivery improvement might require systems that target and cross more efficiently not only the BBB but also systems that clear slowly from the bloodstream. Regarding this last issue, the charge and the morphology of the NP have a very important effect on the clearance. Neutral and zwitterionic NPs have a longer circulation time after intravenous administration, in contrast to negatively and positively charged NPs.²⁹ In addition, short-rod NPs are preferentially retained in the liver and present a rapid clearance rate, while long-rod NPs are caught in the spleen and have a lower clearance rate. If the surface is modified with PEG, retention increases in the lung for both formulations.¹³ According to the studies mentioned above, micelles selected for loading the C6 have a diameter and morphology compatible with the crossing of the BBB. Moreover, the negative values registered of ZP allow micelles to cross the BBB without damaging it. However, the small size of these systems do not allow the loading of appropriate quantities of C6. Furthermore, the hydrophobic nature of this substance represents another obstacle that can easily be overcome through the use of the ideal mixes of solvents both for the assembly and the drug loading. The characterisation studies carried out on the mixture of solvents selected have led to a specific choice of the mixes to be used. The best mixes were additionally tested for cytotoxicity.

4.3 Chapter Summary

Chapter 4 reported the studies on self-assembly with coumarin 6, used as a model drug. The studied nanoparticles were micelles of mPEO₁₁₃-b-PLA₄₀₈ and mPEO₁₁₃-b-PLA₄₈₆ assembled with a solution of acetone and C6. After the purification of the samples by dialysis, the C6 nanoparticles were characterised by DLS and ZP measurements. Furthermore, size exclusion chromatography (SEC) with columns was used to remove excess of free C6. Finally, nanoparticles were dissolved in acetone and analysed by fluorimeter to determine the amount of coumarin loaded into micelles. However, due to the apolar nature of coumarin 6, the use of acetone as a solvent is not indicated; it is unable to dissolve the drug completely and facilitate an effective loading. As opposed to acetone, the acetonitrile proved to be a good solvent for coumarin 6. As a result, assemblies were performed and aimed at maintaining the shape and the size of the micelles and at the dissolution of coumarin 6. Assemblies are made of samples (mPEO₁₁₃-b-PLA₄₀₃; mPEO₁₁₃-b-PLA₄₈₆; mPEO₁₁₃-b-PLA₅₀₃; mPEO₁₁₃-b-PLA₁₃₅₉) using the combination of acetone and acetonitrile solvent (mix A, mix B, mix C with acetone:acetonitrile ratios respectively 2:1, 1:1 and 1:2). The mix C, with excess acetonitrile, was excluded from the study because it changed the size of the nanoparticles. The samples assembled from the mixes A and B were studied by means of ZP. Measures and cytotoxicity tests will be discussed in Chapter 5.

4.4 References

1. Masserini, M; *Nanoparticles for Brain Drug Delivery*. Hindawi Publishing Corporation ISRN Biochemistry. Volume **2013**, pp. 1-18.
2. Lockman, P.R.; Mumper, R.J.; Khan, M.A.; Allen, D.D.; Nanoparticle Technology for Drug Delivery Across Blood-Brain Barrier. *Drug Development and Industrial Pharmacy*. **2002**, 28, 1, 1-13.
3. Ruozi, B.; Belletti, D.; Pederzoli, F.; Formi, F.; Vandelli, M.A.; Tosi, G.; Potential Use of Nanomedicine for Drug Delivery Across the Blood-Brain Barrier in Healthy and Diseased Brain. *CNS & Neurological Disorders-Drug Targets*. **2016**, 15, 9: 1079-1091.
4. Saraiva, C.; Catarina Praça, C.; Ferreira, R.A.; Santos, T.; Ferreira, L.; Bernardino, L.; Nanoparticle-mediated brain drug delivery: Overcoming blood–brain barrier to treat neurodegenerative diseases. *Journal of Controlled Release*. **2016**, 235, 34-47 .
5. Etame, A.B.; Smith, C.A.; Chan, W.C.; Rutka, J.T.; Design and potential application of PEGylated gold nanoparticles with size-dependent permeation through brain microvasculature. *Nanomedicine* **2011**, 7, 992–1000.
6. Hanada, S.; Fujioka, K.; Inoue, Y.; Kanaya, F.; Manome, Y.; Yamamoto, K.; Cell-based in vitro blood–brain barrier model can rapidly evaluate nanoparticles' brain permeability in association with particle size and surface modification. *Int. J. Mol. Sci.*, **2014**, 15: 1812-1825.
7. Sonavane, G.; Tomoda, K.; Makino, K.; Biodistribution of colloidal gold nanoparticles after intravenous administration: effect of particle size, *Colloids Surf. B Biointerfaces*, **2008**, 66: 274–280.
8. Decuzzi, P.; Godin, B.; Tanaka, T.; Lee, S.-Y.; Chiappini, C.; Liu, X; et al., Size and shape effects in the biodistribution of intravascularly injected particles, *J. Control. Release*. **2010**, 141: 320-327.
9. Lockman, P.R.; Koziara, J.M.; Mumper, R.J.; Allen, D.D.; Nanoparticle surface charges alter blood–brain barrier integrity and permeability, *J. Drug Target*. **2004**, 12: 635-641.
10. Bramini, M.; Ye, D.; Hallerbach, A.; Nic Raghnaill, M.; Salvati, A.; Aberg, C.; et al., Imaging approach to mechanistic study of nanoparticle interactions with the blood–brain barrier, *ACS Nano*. **2014**, 8: 4304-4312.
11. Choi, C.H.J.; Alabi, C.A.; Webster, P.; Davis, M.E.; Mechanism of active targeting in solid tumors with transferrin-containing gold nanoparticles. *Proc. Natl. Acad. Sci. U. S. A.* **2010**, 107: 1235-1240.
12. Wiley, D.T.; Webster, P.; Gale, A.; Davis, M.E.; Transcytosis and brain uptake of transferrin-containing nanoparticles by tuning avidity to transferrin receptor. *Proc. Natl. Acad. Sci. U. S. A.*, **2013**, 110: 8662-8667.
13. Huang, X.; Li, L.; Liu, T.; Hao, N.; Liu, H.; Chen, D.; et al., The shape effect of mesoporous silica nanoparticles on biodistribution, clearance, and biocompatibility in vivo, *ACS Nano*. **2011**, 5: 5390-5399,
14. Kreuter, J.; Hekmatara, T.; Dreis, S.; Vogel, T.; Gelperina, S.; Langer, K.; Covalent attachment of apolipoprotein A-I and apolipoprotein B-100 to albumin nanoparticles enables drug transport into the brain, *J. Control. Release*, **2007**, 118: 54-58.
15. Gao, X.; Qian, J.; Zheng, S.; Changyi, Y.; Zhang, J.; Ju, S.; et al.; Overcoming the blood– brain barrier for delivering drugs into the brain by using adenosine receptor nanoagonist, *ACS Nano* **2014**, 8: 3678-3689.
16. Jallouli, Y.; Paillard, A.; Chang, J.; Sevin, E.; Betbeder, D.; Influence of surface charge and inner composition of porous nanoparticles to cross blood–brain barrier in vitro, *Int. J. Pharm.* **2007**, 344: 103-109.
17. Petri, B.; Bootz, A.; Khalansky, A.; Hekmatara, T.; Müller, R.; Uhl, R., et al.; Chemotherapy of brain tumour using doxorubicin bound to surfactant-coated poly(butyl cyanoacrylate) nanoparticles: revisiting the role of surfactants. *J. Control. Release*, **2007**, 117: 51-58.
18. Ulbrich, K.; Knobloch, T.; Kreuter, J.; Targeting the insulin receptor: nanoparticles for drug delivery across the blood–brain barrier (BBB), *J. Drug Target*. **2011**, 19: 125–132.

19. Gromnicova, R.; Davies, H.A.; Sreekanthreddy, P.; Romero, I.A.; Lund, T.; Roitt, I.M.; et al.; Glucose-coated gold nanoparticles transfer across human brain endothelium and enter astrocytes in vitro. *PLoS One* **2013**, *8*, e81043.
20. Shilo, M.; Motiei, M.; Hana, P.; Popovtzer, R.; Transport of nanoparticles through the blood–brain barrier for imaging and therapeutic applications, *Nanoscale* **2014**, *6*: 2146-2152.
21. Guerrero, S.; Araya, E.; Fiedler, J.L.; Arias, J.I.; Adura, C.; Albericio, F.; et al., Improving the brain delivery of gold nanoparticles by conjugation with an amphipathic peptide, *Nanomedicine (Lond.)* **2010**, *5*: 897-913.
22. Martinez-Veracoechea, F.J.; Frenkel, D.; Designing super selectivity in multivalent nano-particle binding, *Proc. Natl. Acad. Sci. U. S. A.* **2011**, *108*: 10963-10968.
23. Walkey, C.D.; Olsen, J.B.; Guo, H.; Emili, A.; Chan, W.C.; Nanoparticle size and surface chemistry determine serum protein adsorption and macrophage uptake, *J. Am. Chem. Soc.* **2012**, *134*: 139–2147.
24. Doshi, N.; Prabhakarandian, B.; Rea-Ramsey, A.; Pant, K.; Sundaram, S.; Mitragotri, S.; Flow and adhesion of drug carriers in blood vessels depend on their shape: a study using model synthetic microvascular networks, *J. Control. Release.* **2010**, *146*: 196-200.
25. Goldsmith, M.; Abramovitz, L.; Peer, D.; Precision nanomedicine in neurodegenerative diseases, *ACS Nano* **2014**, *8*: 1958-1965.
26. Li, S.D.; Huang, L.; Nanoparticles evading the reticuloendothelial system: role of the supported bilayer. *Biochim. Biophys. Acta* **2009**, *1788*: 2259-2266.
27. Lee, S.Y.; Ferrari, M.; Decuzzi, P.; Shaping nano-/micro-particles for enhanced vascular interaction in laminar flows. *Nanotechnology* **2009**, *20*, 495101.
28. Nance, E.A.; Woodworth, G.F.; Sailor, K.A.; Shih, T.-Y.; Xu, Q.; Swaminathan, G.; et al.; A dense poly(ethylene glycol) coating improves penetration of large polymeric nanoparticles within brain tissue. *Sci. Transl. Med.* **2012**, *4*, 149ra119.
29. Arvizo, R.R.; Miranda, O.R.; Moyano, D.F.; Walden, C.A.; Giri, K.; Bhattacharya, R.; et al.; Modulating pharmacokinetics, tumor uptake and biodistribution by engineered nanoparticles, *PLoS One* **2011**, *6*, e24374.

CHAPTER 5

CYTOTOXICITY OF SELF-ASSEMBLED AMPHIPHILIC BLOCK COPOLYMERS NANOPARTICLES

5.1 Experimental Section

5.1.1 Materials

Human Umbilical Vein Endothelial Cells (HUVECs) were obtained from Lonza (Walkersville, MD); murine monocytic macrophage cell line RAW 264.7 were obtained from ATCC (LGC partner, Milan, Italy); EGM-2, SingleQuot kit were from Lonza (Walkersville, MD). All the stock solutions for cell cultures were from Euroclone (Milano, Italy). Immortalised hCMEC/D3 were provided by Institut National de la Santé et de la Recherche Medicale ([INSERM] Paris, France). Cytotoxicity Detection Kit (LDH) was from Roche (Switzerland). Amicon Ultra-15 centrifugal 10 K filter devices were from Millipore Corp (Bedford, USA). All other chemicals were of analytical grade and obtained from either Sigma–Aldrich or Merck.

5.1.2 Nanoparticles Fabrication

To perform cytotoxicity tests, all samples were re-assembled using the same procedure as described above.

In particular, each copolymer was dissolved in a common solvent for both blocks at a concentration of 20 mg/ml, and deionised and filtered water was added dropwise at a constant flow of 4 ml/h, at room temperature and under stirring, until a large excess with respect to the organic solvent was reached. The remaining organic solvent was removed at 48 h of dialysis against water. The complete removal of solvent is an important point both for the morphology of the particles and for the possible

application of the so obtained nanoparticles as drug delivery systems. Residual solvent can swell the hydrophobic regions and change the volume ratio between hydrophilic and hydrophobic parts, altering the final morphology of the particle. On the other hand, residual solvent can be also slowly released over time, providing a potential source of cytotoxicity.

5.1.3 Cell Cultures

The *in vitro* cytotoxicity allows the estimation of the acute physical harm that a particular compound causes in the cells. The mammalian cells grown *in vitro* on nutrient medium are brought into contact with the test compound or with the substances that the compound releases. If the viability of the cells is less of 80%, the compound or the test device is considered to be toxic.¹

5.1.4 Assessment of NP Cytotoxicity

The cytotoxicity assay was carried out using the brain microvascular endothelial cell line hCMEC/D3 (Figure 5.1). These cells represent one such model of the human BBB that can be easily grown and is amenable to cellular and molecular studies on pathological and drug transport mechanisms relevant to the central nervous system (CNS).^{2,3,4} The hCMEC/D3 cell line has been used to investigate nanoparticle transcytosis by various research groups, establishing it as a well-validated model.^{3,5,6,7}

The hCMEC/D3 cells were treated for 1 h and 24 h with different concentrations of NPmPEO₁₁₃b-PLA_x, specifically, 10, 100, or 500 µg/mL⁻¹.

5.1.5 MTT Assay

The MTT ([3-(4,5-dimethyliazol-2-yl)-2,5-diphenyltetrazolium bromide]) cell viability assay is a colorimetric assay that exploits the ability of mitochondrial dehydrogenases to split the tetrazole ring of the MTT molecule (tetrazolium salt) of yellow color to provide

a violet formazan salt (Figure 5.2). The amount of formazan produced is measured in a spectrophotometer, and it is proportional to the number of live cells. In particular, cells were treated with different concentrations (10, 100, or 50 $\mu\text{g}/\text{mL}^{-1}$) of NP for 1 h or 24 h and the cell viability was evaluated by MTT assay.¹ The MTT solution was added to the cells to a final concentration of 0.5 mg mL^{-1} , and the cells were incubated at 37 °C for 2 h. After incubation, ethanol was added to each well to dissolve the formed formazan crystals. Absorbance at 550 nm was measured with a microplate reader (Victor3 1420 multilabel counter, Perkin Elmer). Untreated cells were used as a negative control. Each sample was analysed at least in triplicate.

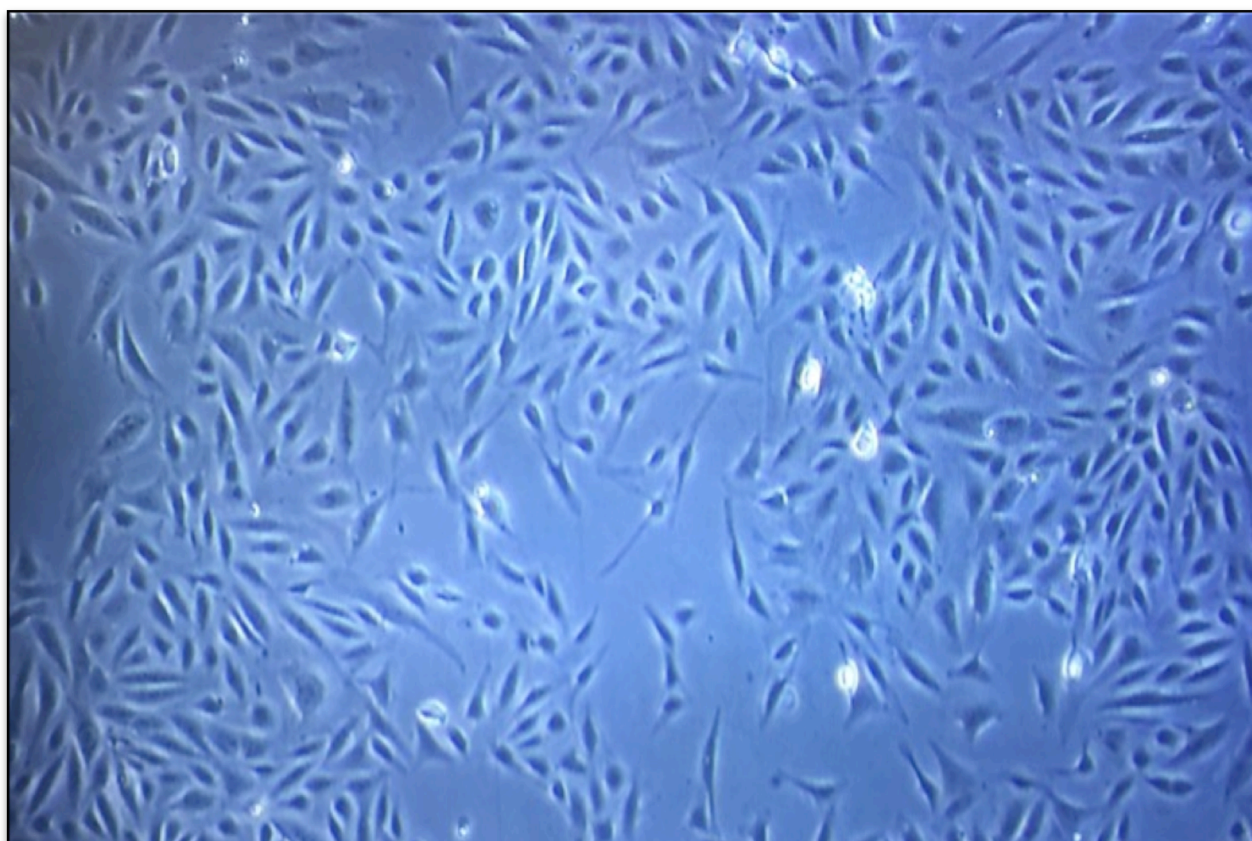


Figure 5.1. Human endothelial cells (hCMEC/D3) incubated with different NP concentrations (10, 100 and 500 $\mu\text{g}/\text{mL}^{-1}$) for 1 h or 24 h.

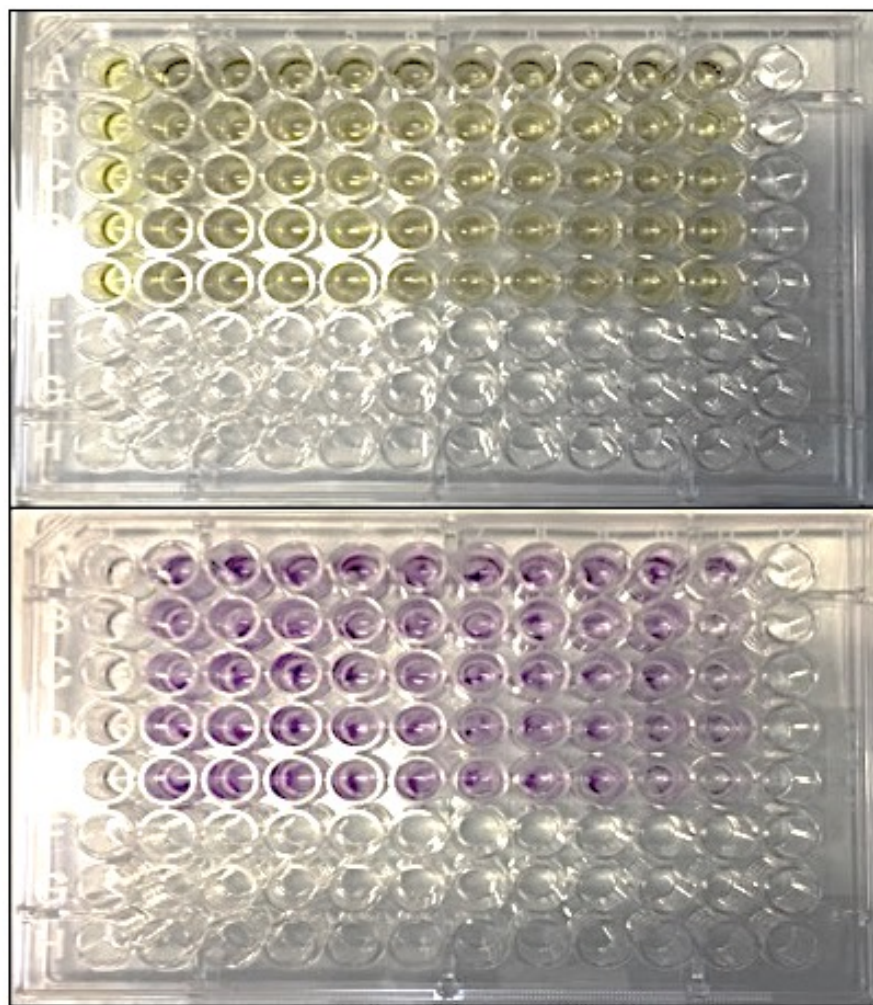


Figure 5.2. The MTT assay exploits the ability of mitochondrial dehydrogenases to split the tetrazole ring of the MTT (tetrazolium salt) molecule of yellow color to form a violet formazan salt.

5.2 Results and Discussion

The study of the cytotoxicity of nanoparticles is of fundamental importance in the choice of the nanocarriers to be used for a drug's delivery and intended for a biological system. Biological interactions and the toxic effects of NPs are significantly associated with their unique physiochemical properties.^{8,9,10}

The toxicity may depend on the details of polymer composition, NP size and surface.^{9,11} In the literature, toxicity of the entire formulation is often described; the findings on the unloaded nanoparticles are not reported. This ambiguity does not allow for a distinction between drug-associated toxicity and that associated with nanoparticles. Therefore, more attention in the present study should be paid to the toxicity of the 'empty' particles. This is particularly important for the understanding of chronic inflammatory reactions that may be caused by the accumulation of nanoparticles in different parts of the body.^{12,13} Therefore, we subjected the testing samples to cytotoxicity without drug loading. For the direct investigation of this subject, NP at three concentrations up to 500 mg mL⁻¹ were incubated with endothelial cells (HUVECs). The results of the MTT assay, which assess different aspects of cell toxicity, are shown in the following figures. The results are expressed as total cell viability compared to the control.

With regard to NP obtained from copolymers assembled in acetone, those with long chains of PLA (mPEO₁₁₃-b-PLA₁₃₅₉) were toxic (cell survival of 40% and 60% respectively) as compared to the control. In contrast, all of the NP obtained from short- and medium-chain-length copolymers (PLA₆₅, PLA₃₀₅, PLA₄₀₃, PLA₄₁₇ and PLA₄₈₆) assembled in acetone were not toxic (Figure 5.3). It was therefore decided to submit to the cytotoxicity assay the NP with medium-length chains (mPEO₁₁₃-b-PLA₄₈₆) assembled with different solvents: acetone, dioxane, DMF and THF (Figure 5.4). The data showed that only NP assembled in dioxane were cytotoxic (cell viability of 50%).

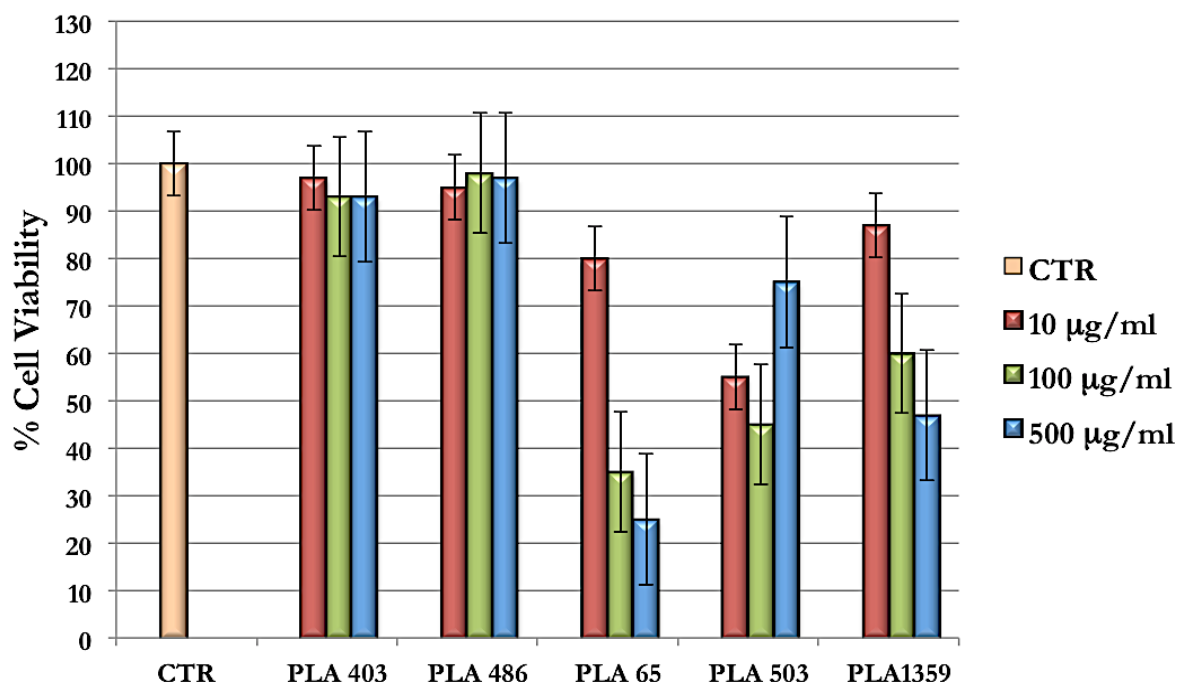


Figure 5.3. Comparison of cytotoxicity testing, at 24 h, of the NP (mPEO₁₁₃-b-PLA₆₅, mPEO₁₁₃-b-PLA₄₈₆, mPEO₁₁₃-b-PLA₄₀₃, mPEO₁₁₃-b-PLA₄₈₆, mPEO₁₁₃-b-PLA₅₀₃ and mPEO₁₁₃-b-PLA₁₃₅₉) from acetone. HUVECs were incubated with different concentrations (10/100/500 µg.mL⁻¹) of NP.

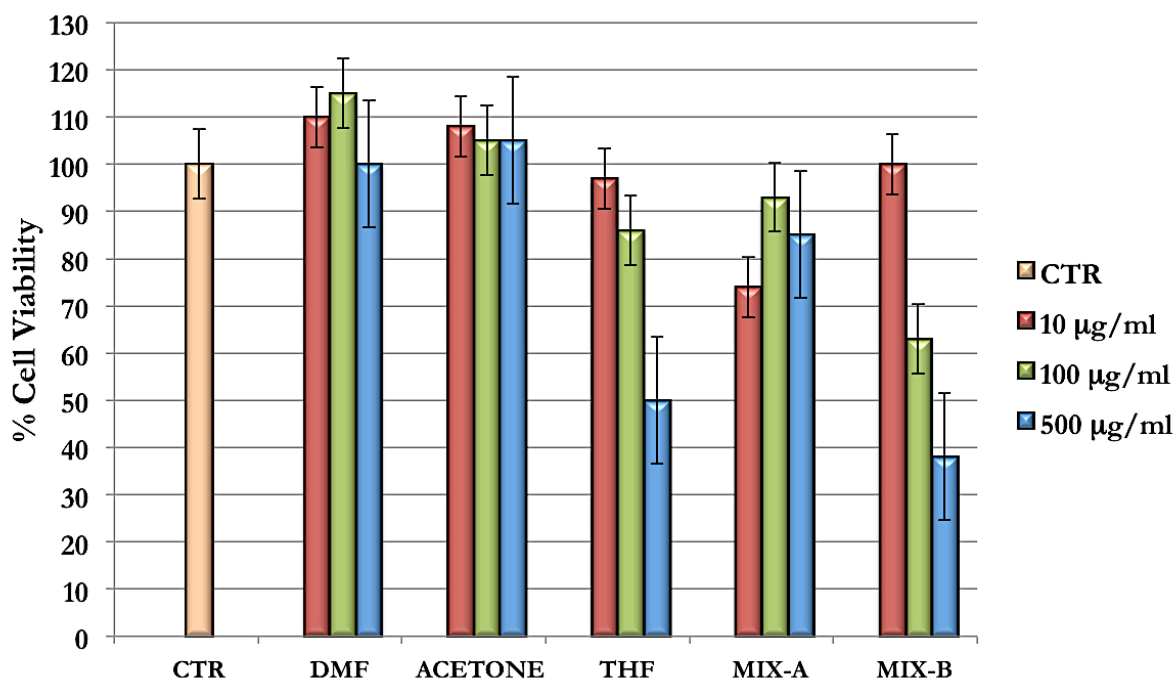


Figure 5.4. Cytotoxicity testing, at 24 h, of NP mPEO₁₁₃-b-PLA₄₈₆ assembled with DMF, acetone, THF, mix A and mix B. HUVECs were incubated with different concentrations (10/100/500 µg.mL⁻¹) of NP.

The NP with long-chain PLA (mPEO₁₁₃-b-PLA₁₃₅₉) assembled with different solvents were toxic especially at higher NP concentrations (500 µg.mL⁻¹), as shown in Figure 5.5.

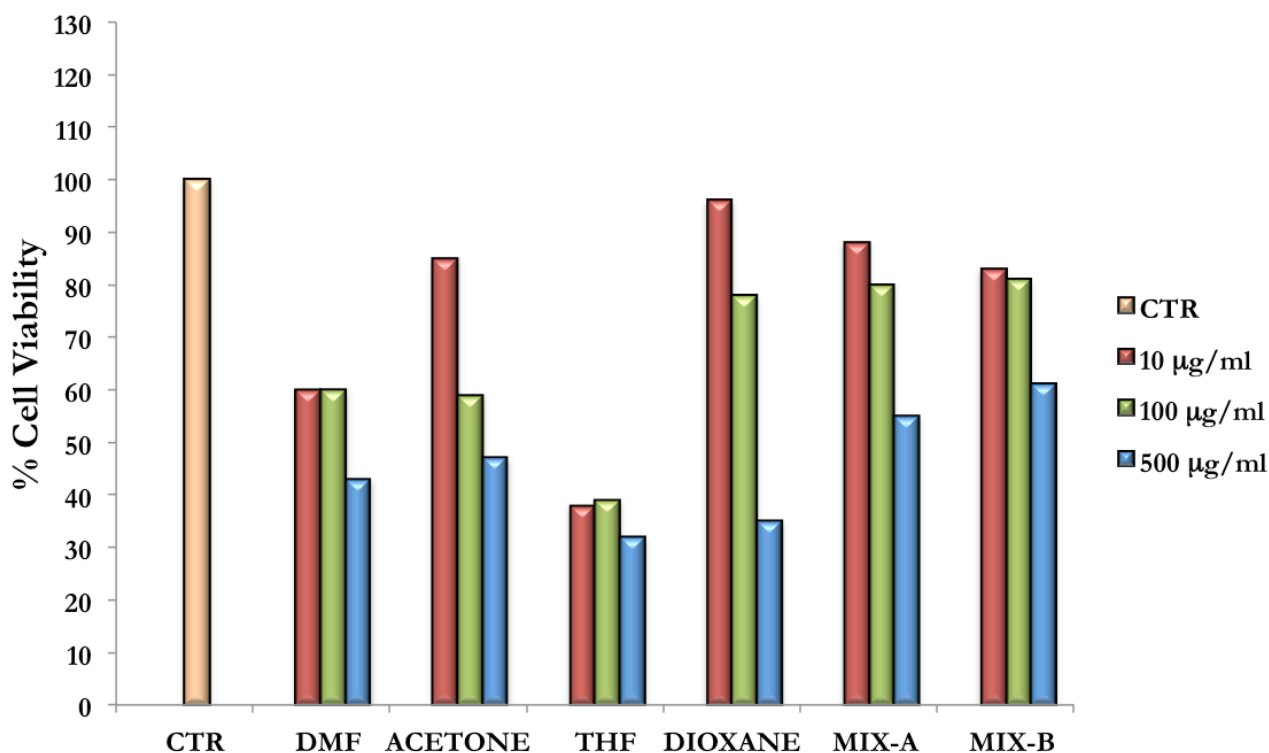


Figure 5.5. Cytotoxicity testing, at 24 h, of NP mPEO₁₁₃-b-PLA₁₃₅₉ assembled with DMF, acetone, THF, dioxane, mix A and mix B. HUVECs were incubated with different concentrations (10/100/500 µg.mL⁻¹) of NP.

All samples assembled in acetone, dioxane, THF and DMF (at low concentrations of NP after 24 h) were compared. In Figure 5.6, which refers to the results obtained at lower concentrations of NP (10 mg/ml), it is possible to note that only mPEO₁₁₃-b-PLA₄₈₆ in dioxane and mPEO₁₁₃-b-PLA₁₃₅₉ in THF and DMF are toxic to the cells (viability cell ≈ 50%).

Finally, mPEO₁₁₃-b-PLA₄₀₃, mPEO₁₁₃-b-PLA₄₈₆, mPEO₁₁₃-b-PLA₅₀₃ and mPEO₁₁₃-b-PLA₁₃₅₉ NPs assembled from acetone/acetonitrile mixtures were tested. Among these, the least toxic samples are mPEO₁₁₃-b-PLA₄₈₆ in mix A and mPEO₁₁₃-b-PLA₅₀₃ in mix B (Figure 5.7).

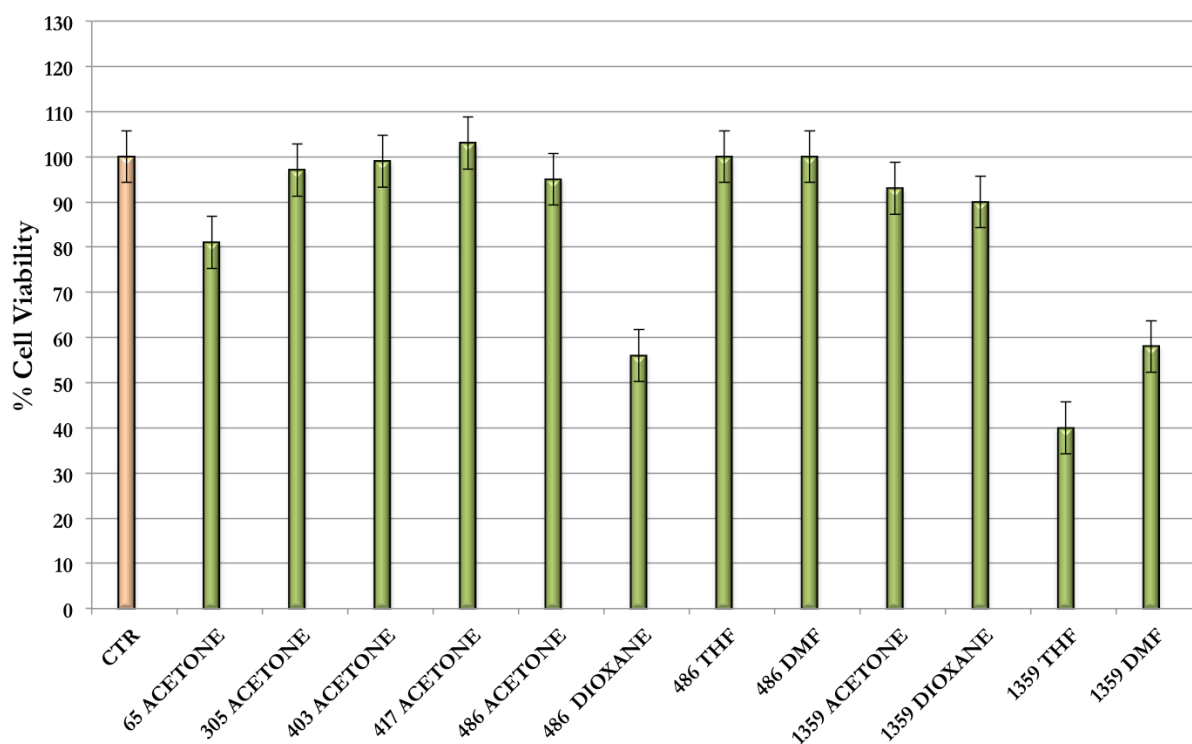


Figure 5.6. Comparison of all samples at lower concentrations of NP (10 mg/ml).

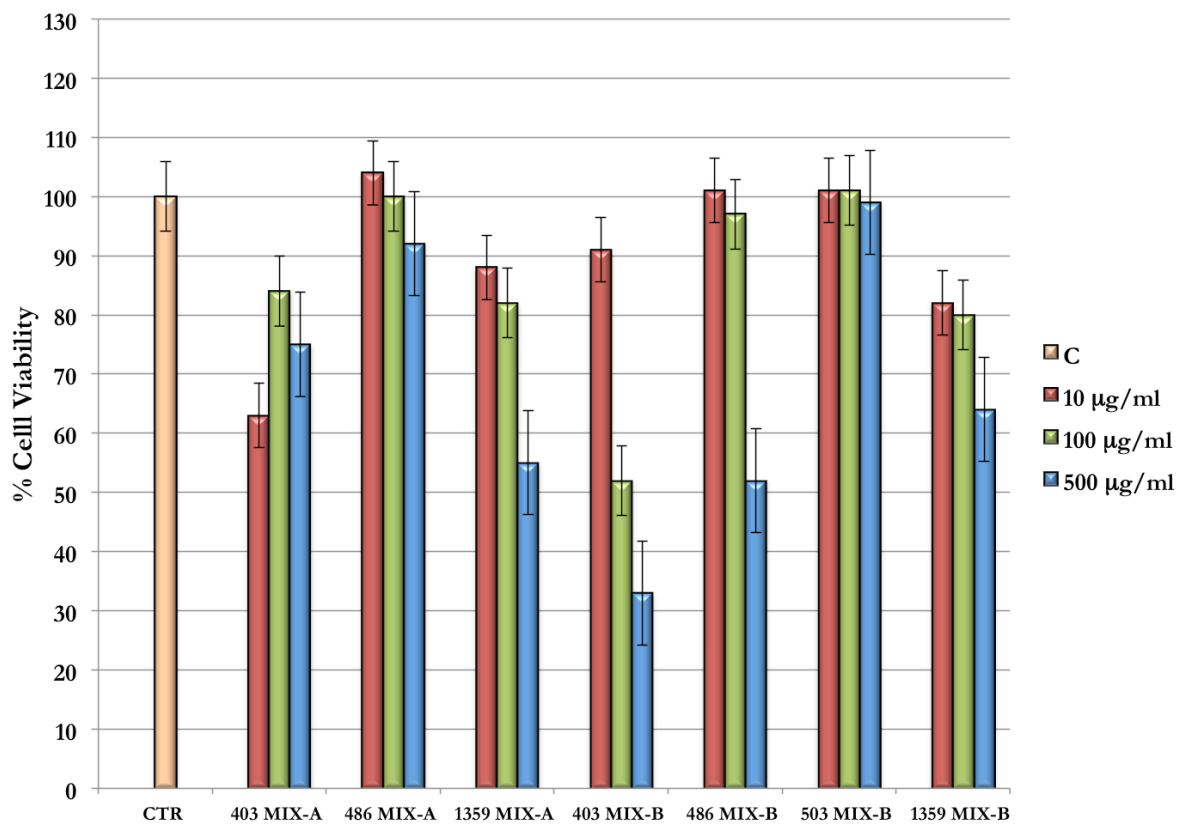


Figure 5.7. Comparison of cytotoxicity testing of the samples (mPEO₁₁₃-b-PLA₄₀₃, mPEO₁₁₃-b-PLA₄₈₆, mPEO₁₁₃-b-PLA₅₀₃ and mPEO₁₁₃-b-PLA₁₃₅₉) to various concentrations of NP (10/100/500 µg.mL⁻¹) at 24 h, assembled with the mix of solvents (mix A and mix B).

In the cytotoxicity study for NP, mPEO₁₁₃-b-PLA_x tests showed good results. Only some NP (e.g., NP mPEO₁₁₃-b-PLA₁₃₅₉ assembled in THF and DMF, and NP of mPEO₁₁₃-b-PLA₄₈₆ assembled in dioxane, which present a viability between 40% and 60%) are less tolerated by cells, although almost all present a cell viability greater than 80% at a concentration of 10 µg.mL⁻¹. In general, cytotoxicity increases by changing from low to high concentrations of NP. This affects all cell cultures and is probably motivated by a ‘choking effect’ due to the number of nanoparticles rather than chemical/biological toxicity. The NP of mPEO₁₁₃-b-PLA₄₈₆ in the mixes, and the NP of mPEO₁₁₃-b-PLA₅₀₃ in mix B are better tolerated and maintain a cell viability of 90% to 100% even at a concentration of 500 µg.mL⁻¹.

5.3 Chapter Summary

Chapter 5 provides a comprehensive picture of the cytotoxicity study on the polymeric nanoparticles NP-PEO₁₁₃-b-PLA_x. For the direct investigation of this subject, NP at three concentrations up to 500 mg mL⁻¹ were incubated with endothelial cells (HUVECs). The results of MTT and LDH assays, assessing different aspects of cell toxicity, were expressed as a reduction in cell viability compared to the control.

Results are extremely encouraging. Only NP of mPEO₁₁₃-b-PLA₁₃₅₉ assembled in THF and DMF, and NP of mPEO₁₁₃-b-PLA₄₈₆ assembled in dioxane, showed a viability between 40% and 60%; they are therefore less tolerated by cells. The remaining NP tested showed a higher cell viability, namely 80% at a concentration of 10 µg.mL⁻¹. However, if the concentration is increased to 100 µg.mL⁻¹ and 500 µg.mL⁻¹, cell cultures tend to suffer, probably from ‘suffocation’ due to internalization of multiple relatively large nanoparticles.

We compared also the cytotoxicity of the polymers assembled from mix A and mix B, which are solvent mixtures optimized for solubilisation of C6. The tests were aimed at selecting good candidates for the assembly of nanoparticles containing Paclitaxel or other molecules with low solubility in standard solvents. In fact, mPEO₁₁₃-b-PLA₄₈₆ NPs from mixes A and B (75.39 nm, PDI = 0.113) and mPEO₁₁₃-b-PLA₅₀₃ NPs from mix B (65.86 nm, PDI = 0.246) are well tolerated and maintain a cell viability of 90% to 100% even at a concentration of 500 µg mL⁻¹. The morphology of these nanoparticles can be identified, according to the morphological map, as small micelles.

Overall, our results suggest that such NP could serve as versatile nanovehicles for delivering hydrophobic drugs across the BBB, enhancing drug concentration at the BBB site and therefore increasing its brain bioavailability.

5.4 References

1. Orlando, A.; Re, F.; Sesana, S.; Rivolta, I.; Panariti, A.; Brambilla, D.; Nicolas, J.; Couvreur, P.; Andrieux, K.; Masserini, M.; Cazzaniga, E.; *Int. J. Nanomed.* **2013**, 8, 1335.
2. Cazzaniga, E.; Bulbarelli, A.; Lonati, E.; Orlando, A.; Re, F.; Gregori, M.; Masserini, M.; *Neurochem. Res.* **2011**, 36, 863.
3. Re, F.; Cambianica, I.; Sesana, S.; Salvati, E.; Cagnotto, A.; Salmona, M.; Couraud, P. O.; Moghimi, S. M.; Masserini, M.; Sancini, G.; *J. Biotechnol.* **2010**, 156, 341.
4. Weksler, B.B.; Subileau, E.A.; Perrière, N.; Charneau, P.; Holloway, K.; Leveque, M.; Tricoire-Leignel, H.; Nicotra, A.; Bourdoulous, S.; Turowski, P.; Male, D. K.; Roux, F.; Greenwood, J.; Romero, I. A.; Couraud, P. O.; Blood-brain barrier-specific properties of a human adult brain endothelial cell line. *The FASEB Journal* express article 10.1096/fj.04-3458fje. Published online September 1, **2005**.
5. Weksler, B.; Romero, IA; Couraud, P.O.; The hCMEC/D3 cell line as a model of the human blood brain barrier. *Fluids Barriers CNS.***2013** 26;10 (1): 16.
6. Markoutsas, E.; Pampalakis, G.; Niarakis, A.; Romero, I.A.; Weksler, B.; Couraud, P.O.; et al. Uptake and permeability studies of BBBtargeting immunoliposomes using the hCMEC/D3 cell line. *Eur J Pharm Biopharm.* **2011**;77(2):265–74. 1
7. Salvati, E; Re, F; Sesana, S; Cambianica, I.; Sancini, G.; Masserini, M.; et al. Liposomes functionalized to overcome the blood-brain barrier and to target amyloid-beta peptide: the chemical design affects the permeability across an in vitro model. *Int J Nanomedicine.* **2013**; 8: 1749–58.
8. Rae, T.; Tolerance of mouse macrophages in vitro to barium sulfate used in orthopedic bone cement. *J Biomed Mater Res.* **1977** Nov; 11(6):839-46,.
9. Bakand S.; Hayes, A.; Toxicological Consideration, Toxicity Assessment, and Risk Management of Inhaled Nanoparticles. *Int J Mol Sci.* **2016** Jun; 17 (6):929
10. Khalili Fard, J.; Jafari, S.; Eghbal, M.A.; A review of molecular mechanisms involved in toxicity of nanoparticles. *Adv. Pharm. Bull.* 2015; 5: 447– 454.
11. Donaldson, K.; Stone, V.; Gilmour, P.S.; Brown, D.M.; MacNee, W.; Ultrafine particles: Mechanisms of lung injury. *Philos. Trans. R. Soc. A.* **2000**; 358:2741–2749.
12. Gregori, M.; Bertani, D.; Cazzaniga, E.; Orlando, A.; Mauri, M.; Bianchi, A.; Re, F.; Sesana, S.; Minniti, S.; Francolini, M.; Cagnotto, A.; Salmona, M.; Nardo, L.; Salerno, D.; Mantegazza, F.; Masserini, M.; Simonutti, R.; Investigation of Functionalized Poly (N,N-dimethylacrylamide)-block-polystyrene Nanoparticles As Novel Drug Delivery System to Overcome the Blood–Brain Barrier In Vitro. *Macromol. Biosci.* **2015** Dec;15(12):1687-97.
13. De Jong, W.H.; Borm, P.J.A.; Drug delivery and nanoparticles: Application and hazard. *Int J Nanomedicine.* **2008**; 3(2)

CHAPTER 6

STUDY ON AGING OF mPEO₁₁₃-b-PLA_x SYSTEM

6.1 Experimental Section

6.1.1 Materials

Dimethylformamide (DMF), acetone, tetrahydrofuran (THF) and 1,4-dioxane were purchased from Sigma–Aldrich (Milano, Italy) and a dialysis bag (3500 MW cut off) from Spectrum Laboratories, Inc. (Rancho Dominguez, USA).

6.1.2 Aging of mPEO-b-PLA_x system

Almost all of the conventional plastics, such as PE, PP, PS and PVC, are resistant to microbial attack; in contrast, aliphatic polyesters such as PLA are readily degraded by microorganisms present in the environment.¹ According to ASTM D6400–04, a biodegradable plastic is ‘a plastic that degrades because of the action of naturally occurring microorganisms such as bacteria, fungi, and algae’, and a compostable plastic is ‘a plastic that undergoes degradation by biological processes during composting to yield carbon dioxide, water, inorganic compounds, and biomass at a rate consistent with other known compostable materials and leaves no visually distinguishable or toxic residues’.

The knowledge of the factors that determine the aging of mPEO₁₁₃-b-PLA_x copolymers, which are intended for drug delivery, is of great importance. Knowing the degradation times would prevent the inflammatory diseases caused by the accumulation of these substances in organs or vessels. The degradation of PLA was studied in animal and human bodies for use in medical applications such as surgical sutures, implants and drug delivery materials.²

In biological environments, PLA is initially degraded by hydrolysis, and the soluble oligomers formed are metabolised by cells. Upon disposal in the environment, PLA degradation is more challenging because PLA is largely resistant to attack by microorganisms in soil or sewage under ambient conditions.

There are some reports in the literature on bacterial degradation of PLA^{3,4,5} and some on degradation by a variety of enzymes, such as lysozyme.^{6,7} In particular *Bacillus sp. PG01* seems to be very effective in degrading PLA.¹

To try to delay the aging of the synthesised copolymers, all samples were stored in the fridge at a temperature of 4 °C and in nitrogen. The aging has been studied both for copolymers and for most of the assembled nanoparticles, using the main characterisation techniques according to the scheme illustrated in Figure 6.1.

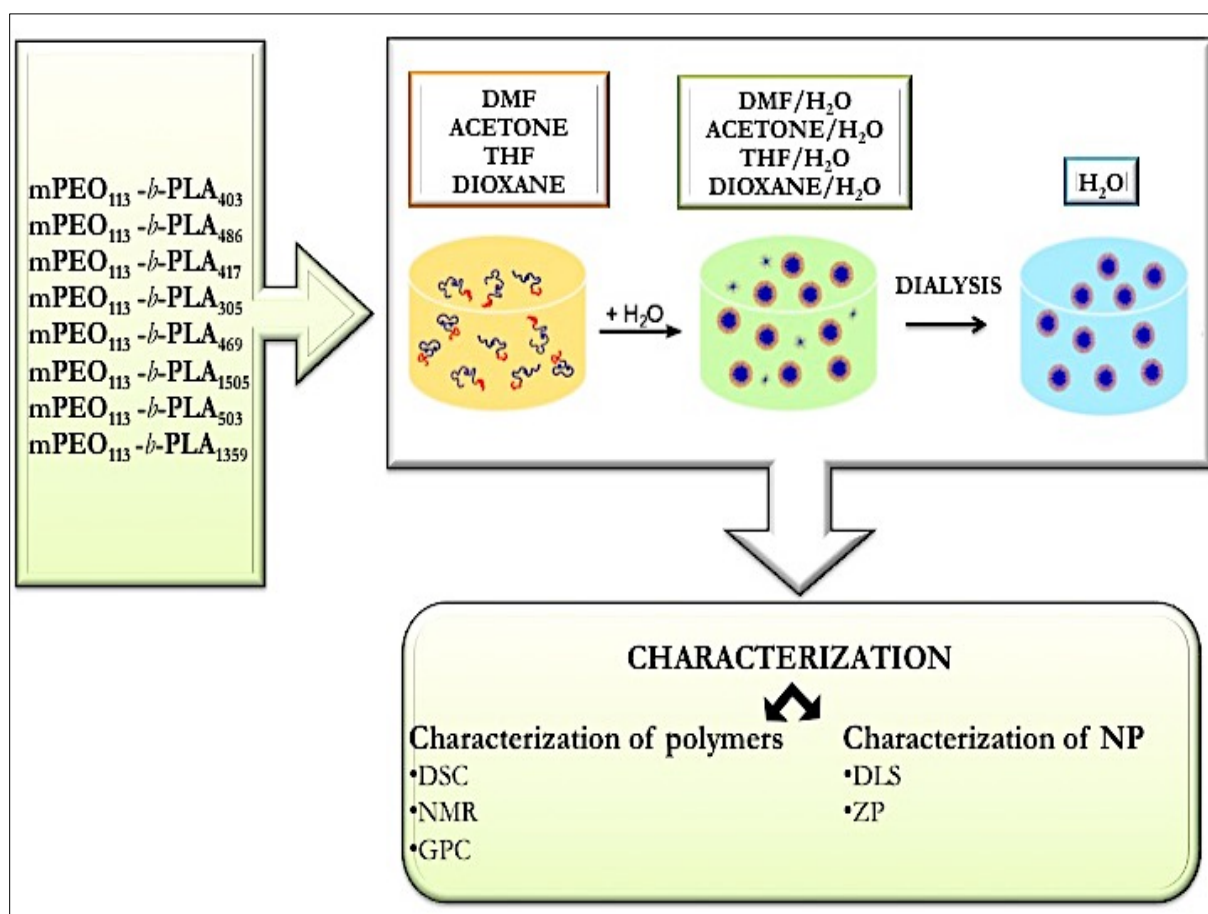


Figure 6.1. Schematic representation of the characterisation study of copolymers mPEO₁₁₃-b-PLA_x and NP mPEO₁₁₃-b-PLA_x intended for the drug delivery system.

6.1.3 Study on aging of the copolymers mPEO₁₁₃-b-PLA_x

In order to evaluate the aging of the synthesised polymers after one year, a characterisation was carried out by DSC, GPC and NMR on aliquots of polymers preserved in nitrogen atmosphere at 4 °C. DSC experiments were performed directly on the powdered polymer as recovered from the low T storage. In Table 6.1, we have reported the data relating to the comparison of the T_g values for copolymers analysed after one year.

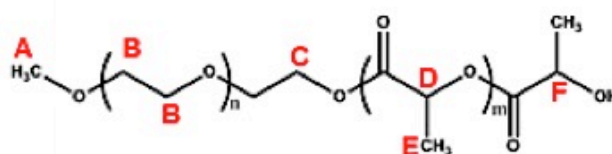
Sample	T _g (°C) 0 days	T _g (°C) 1 year
mPEO113 -b-PLA305	24	18.81
mPEO113-b-PLA403	21	29.4
mPEO113 -b-PLA417	19	31.78
mPEO113 -b-PLA486	27	32.74
mPEO113 -b-PLA469	30	36.44
mPEO113 -b-PLA503	-	31.83
mPEO113 -b-PLA1505	-	41.83
mPEO113 -b-PLA1359	38	44.72

Table 6.1. Comparison of T_g values at 0 days and 1 year.

An estimate of the molecular weight and polydispersity index of a polymer was obtained by GPC analysis. Table 6.2 shows a comparison of the data to the molecular weight (g/mol) and the PDI of newly synthesised copolymers and the same after one year. To obtain more information on the molecular structure of the polymers, after an interval of one year, all copolymers were subjected to NMR analysis. Table 6.3 shows a comparison of the results at 0 days and 1 year.

GPC CHARACTERIZATION						
SAMPLES	Mn (g/mol) 0 days	Mn (g/mol) 1 year	Mw (g/mol) 0 days	Mw (g/mol) 1 year	PDI 0 days	PDI 1 year
mPEO ₁₁₃ -b-PLA ₃₀₅	21044	20481	23824	26112	1.13	1.27
mPEO ₁₁₃ -b-PLA ₄₀₃	28818	45375	32967	56071	1.14	1.23
mPEO ₁₁₃ -b-PLA ₄₁₇	10113	23554	11033	27941	1.09	1.19
mPEO ₁₁₃ -b-PLA ₄₆₉	54255	51495	66752	73931	1.23	1.43
mPEO ₁₁₃ -b-PLA ₅₀₃	21913	15832	24901	18608	1.14	1.17
mPEO ₁₁₃ -b-PLA ₁₅₀₅	35313	30404	4397	40360	1.23	1.33
mPEO ₁₁₃ -b-PLA ₁₃₅₉	31076	29952	34214	33379	1.10	1.11

Table 6.2. Comparison of GPC data of all copolymers at 0 days and 1 year.



SAMPLES	NMR (COPOLYMER 0 DAYS)				NMR (COPOLYMER 1 YEAR)				SAMPLES
	A	C+F	D	E	A	C+F	D	E	
mPEO ₁₁₃ -b-PLA ₃₀₅	2.70	4.14	306.21	933.60	2.37	3.18	285.21	867.49	mPEO ₁₁₃ -b-PLA ₂₈₅
mPEO ₁₁₃ -b-PLA ₄₀₃	2.61	3.79	397.30	1208.78	2.72	2.69	418.08	1260.64	mPEO ₁₁₃ -b-PLA ₄₁₈
mPEO ₁₁₃ -b-PLA ₄₁₇	2.63	4.07	419.86	1267.93	2.80	4.23	418.55	1268.87	mPEO ₁₁₃ -b-PLA ₄₁₈
mPEO ₁₁₃ -b-PLA ₄₆₆	2.76	3.77	484.38	1493.14	2.93	4.48	478.88	1459.58	mPEO ₁₁₃ -b-PLA ₄₇₉
mPEO ₁₁₃ -b-PLA ₄₆₉	2.54	2.11	480.81	1465.05	2.66	2.16	472.48	1429.91	mPEO ₁₁₃ -b-PLA ₄₇₃
mPEO ₁₁₃ -b-PLA ₅₀₃	2.64	2.15	498.67	1424.20	2.48	3.32	468.12	1373	mPEO ₁₁₃ -b-PLA ₄₆₈
mPEO ₁₁₃ -b-PLA ₁₅₀₅	3.12	4.58	1479.02	4584.09	2.28	4.53	1466.05	4498.06	mPEO ₁₁₃ -b-PLA ₁₄₆₆
mPEO ₁₁₃ -b-PLA ₁₃₅₉	2.58	4.26	1314.18	3853.17	2.53	4.98	1314.07	3860.64	mPEO ₁₁₃ -b-PLA ₁₃₁₄

Table 6.3. Comparison of NMR data of all copolymers at 0 days and 1 year.

After characterising the polymers after an interval of one year, all samples are assembled again and characterised by means of DLS measurements.

The study of the dispersion of aging NP is shown in Figure 6.1. The data were then compared relating to the size of the NP, the polydispersity index (PDI), and measurements of ZP (Table 6.4). In the study of the characterisation of the first samples examined (with short-chain PLA, for example, the mPEO₁₁₃-b-PLA₃₀ sample), DLS characterisation and SEM were measured at 0 days and 97 days and showed a change both in size and morphology, as shown in Figures 6.2 and 6.3.

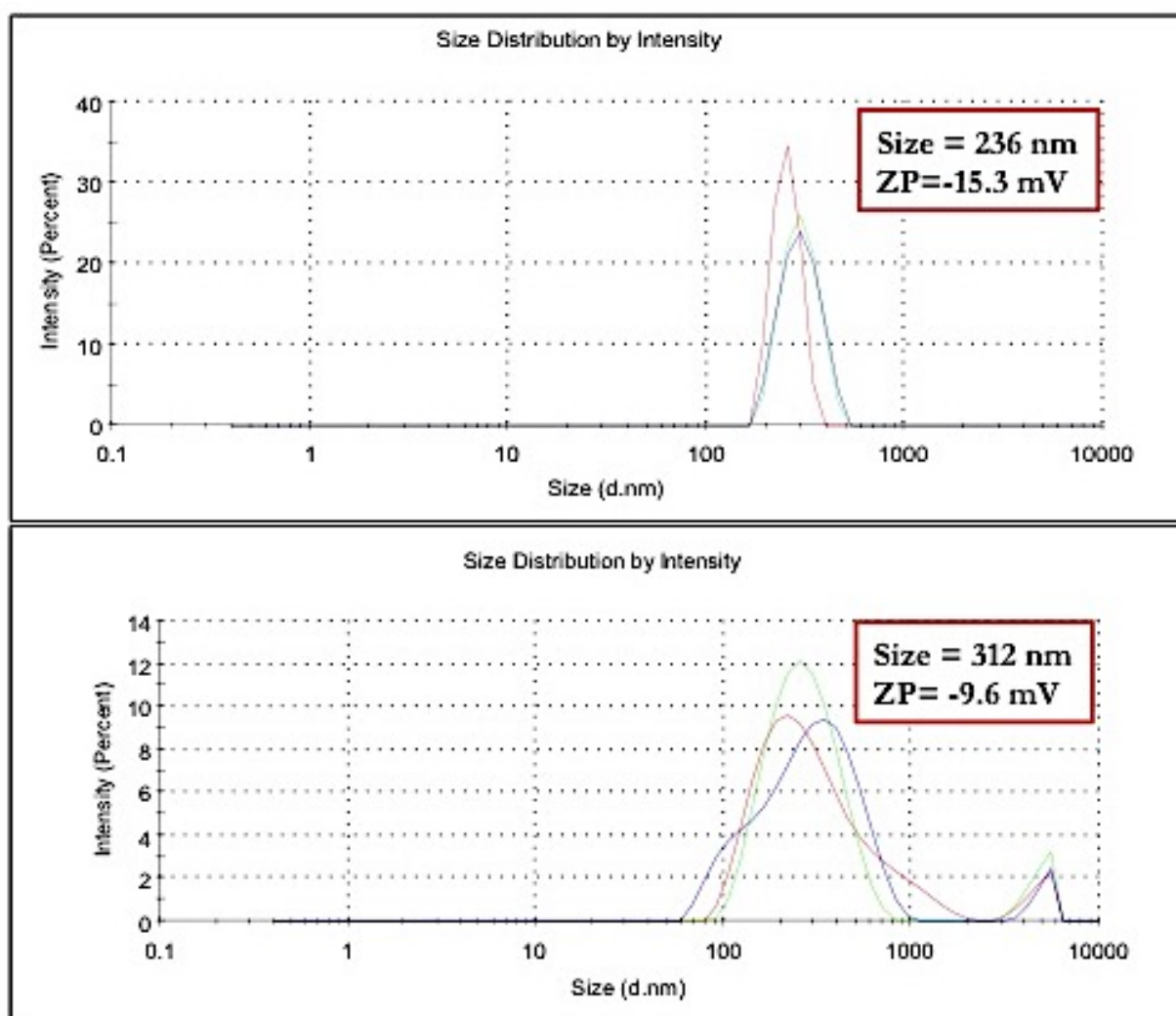


Figure 6.2. DLS characterisation of an mPEO₁₁₃-b-PLA₃₀ sample after 0 (above) and 97 days (below).

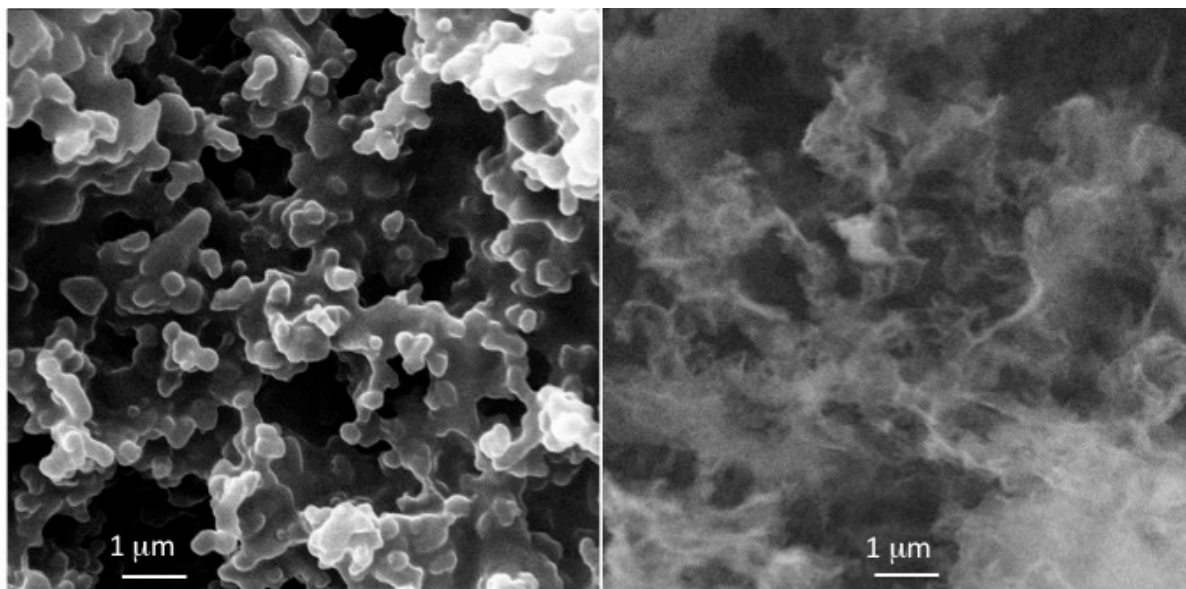


Figure 6.3. SEM images of an mPEO₁₁₃-b-PLA₃₀ sample analysed at 0 days (freshly prepared) and after storage at 0 °C for 97 days.

To try to estimate the aging of the NP with medium and long chains of PLA, DLS measurements were performed daily for the first 30 days and after one year.

In particular, Figure 6.4 shows the DLS measures at 0 and 30 days of mPEO₁₁₃-b-PLA₁₃₅₉ assembled from acetone and reported by intensity.

Figure 6.5 shows the DLS characterisation of mPEO₁₁₃-b-PLA₆₅, mPEO₁₁₃-b-PLA₃₀₅, mPEO₁₁₃-b-PLA₄₆₉ and mPEO₁₁₃-b-PLA₄₈₆ from acetone at various time intervals (0 and 1 year).

Figure 6.6 displays the DLS measures of mPEO₁₁₃-b-PLA₄₈₆ assembled from acetone and reported by intensity, at intervals of 0, 15, 29 days and 1 year.

Finally, measures of ZP on NP were assembled with fresh polymer and with that of a year. The comparison of the values obtained is shown in table 6.4.

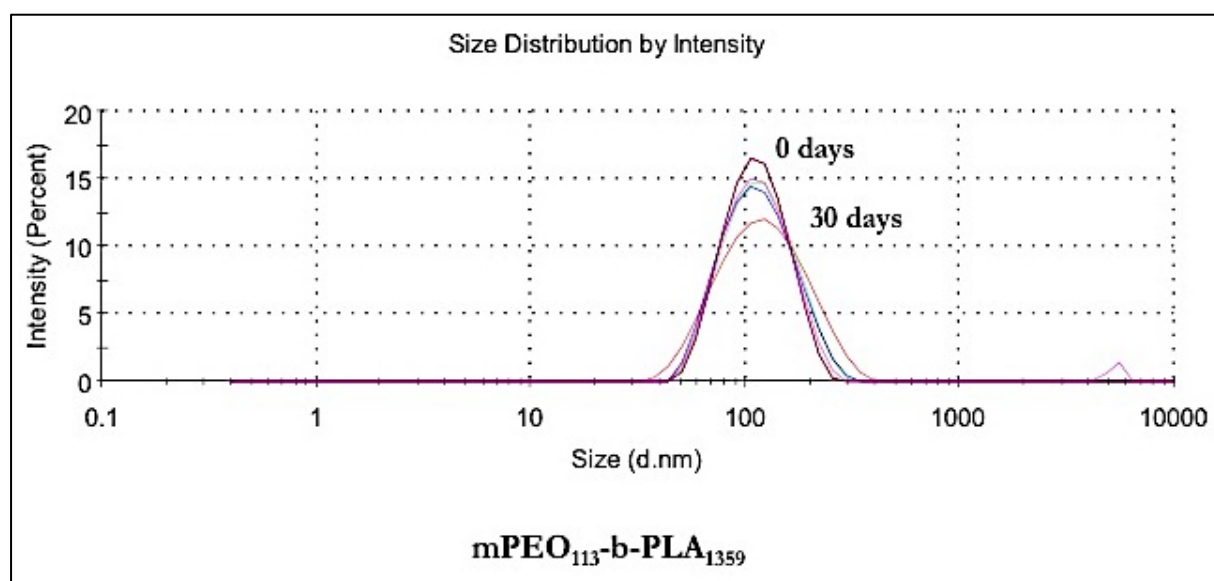


Figure 6.4. DLS characterisation of an mPEO₁₁₃-b-PLA₁₃₅₉ sample assembled in acetone, at various time intervals (0 and 30 days).

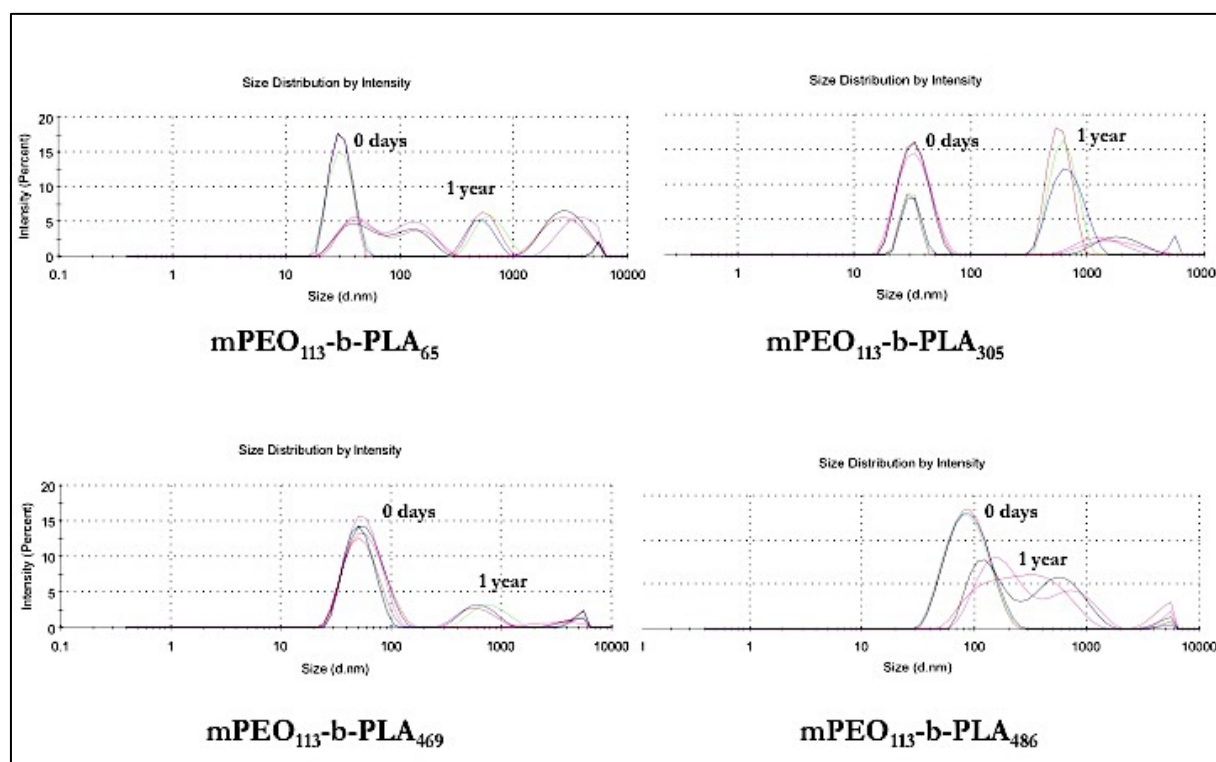


Figure 6.5. DLS characterisation of mPEO₁₁₃-b-PLA₆₅, mPEO₁₁₃-b-PLA₃₀₅, mPEO₁₁₃-b-PLA₄₆₉ and mPEO₁₁₃-b-PLA₄₈₆ from acetone, at various time intervals (0 and 1 year).

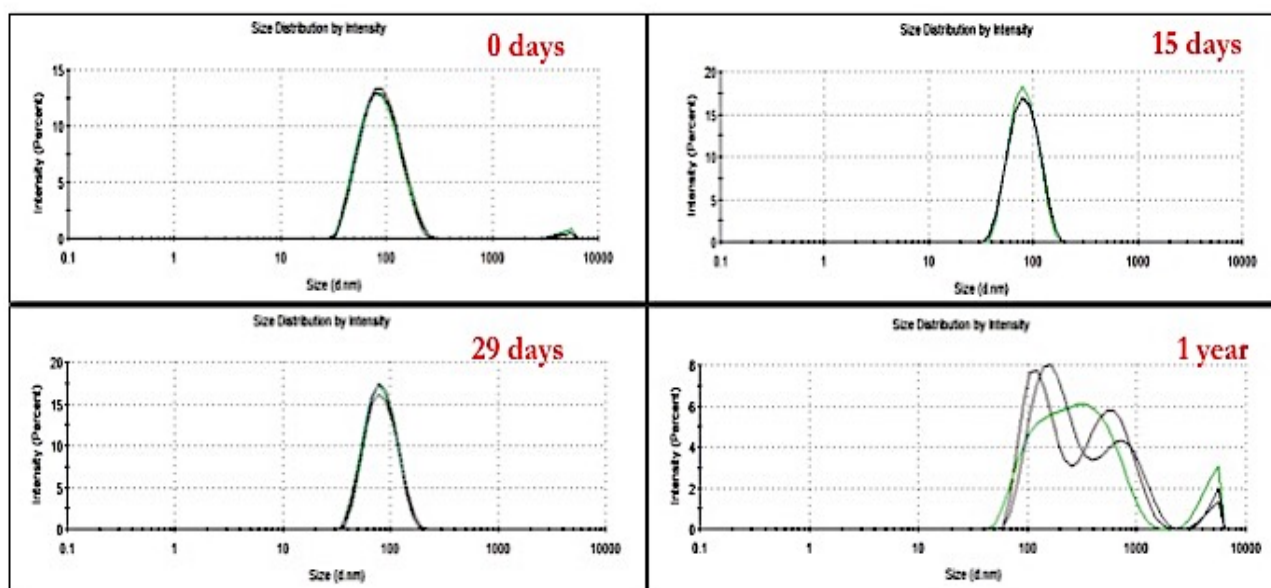


Figure 6.6. DLS characterisation of an mPEO₁₁₃-b-PLA₄₈₆ sample assembled in acetone, at various time intervals (0, 15, 29 days and 1 year).

SAMPLE	ZP (mV) OF COPOLYMERS ASSEMBLED WITH DIFFERENTS SOLVENTS (AGE COPOLYMERS = 0 DAYS)				ZP (mV) OF COPOLYMERS ASSEMBLED WITH DIFFERENTS SOLVENTS (AGE COPOLYMERS = 1 YEAR)			
	ACETONE	DIOXANE	THF	DMF	ACETONE	DIOXANE	THF	DMF
mPEO ₁₁₃ -b-PLA ₃₀₅	-21.6	-16.4	-15	-14.3	-17.1	-23.5	-24.1	-17.9
mPEO ₁₁₃ -b-PLA ₄₀₃	-22.1	-9.72	-22.9	-22.7	-14.2	-29.1	-25.5	-20
mPEO ₁₁₃ -b-PLA ₄₁₇	-19.1	-21.6	-25.6	-20.1	-21	-21.5	-24.4	-24.5
mPEO ₁₁₃ -b-PLA ₄₈₆	-19.1	-21.6	-25.6	-23	-29.4	-29	-30	-21.3
mPEO ₁₁₃ -b-PLA ₄₆₉	-17.3	15.1	14.5	-9.23	-28.1	-30.8	-9	-15.2
mPEO ₁₁₃ -b-PLA ₅₀₃	-24.8	-17.2	-9.4	-15.2	-20.9	-23.6	-19.6	-18.6
mPEO ₁₁₃ -b-PLA ₁₅₀₅	-22.1	18.2	-17.2	-10.7	-21.5	-21.5	-15.2	-15.2
mPEO ₁₁₃ -b-PLA ₁₃₅₉	-21.4	-9.06	-15.2	-21.3	-19.2	-24.4	-18.7	-15.8

Table 6.4 Comparison of the measures ZP samples assembled with fresh copolymer (age = 0 days) and those assembled with aged polymer (age = 1 year)

6.2 Results and Discussion

Among various families of biodegradable polymers, aliphatic polyesters hold a leading position: Hydrolytic and/or enzymatic chain cleavage yields hydroxy carboxylic acids, which in most cases are ultimately metabolised.

The key properties, for example, rate of degradation, tensile properties and surface chemical composition, can be optimised by copolymerisation or blending of homo- and/or copolymers. There are two principal ways by which polymer chains can be hydrolysed: passively by chemical hydrolysis or actively by enzymatic reaction. The latter is most important for naturally occurring polymers such as polysaccharides and poly(hydroxy alkanate)s, for example, polyhydroxybutyrate and polyhydroxy- valerate. Many synthetic aliphatic polyesters utilised in medical applications degrade mainly by pure hydrolysis.

There are several factors that influence the rate of degradation, including the type of chemical bond in the polymer backbone, hydrophilicity, molecular weight, crystallinity, copolymer composition, and the presence of low molecular weight compounds. Other concerns are related to polymers' loss of mechanical stability during degradation, which can be undesirable when it is too fast, or to the toxicity of high concentrations of degradation products. Many biodegradable polymers contain some kind of hydrolysable bonds. Polymers containing anhydride or ortho-ester bonds are the most reactive, possessing a fast rate of degradation; ester bonds degrade somewhat more slowly, and carbonates are almost totally resistant to hydrolysis. Polymerisation of the different stereofoms results in materials with different properties. The polymers derived from the pure L,L-lactide or D,D-lactide monomers are semicrystalline, relatively hard materials with melting temperatures around 184°C and glass transition temperatures of about 55°C. The L,L-lactide and D,D-lactide are normally termed L-lactide and D-lactide, respectively. Polymerisation of the racemic (D,L)-lactide and meso-lactide results in an amorphous material with a glass transition similar to that of the semicrystalline counterparts. Polylactides are highly sensitive to heat, especially at temperatures

higher than 190 °C. Heating these materials above this temperature results in a noticeable decrease in weight-average molecular weight⁸. The samples synthesised in this study were prepared from (D,L)-lactide. The *in vitro* degradation of poly(L-lactide) is generally rather slow compared to the degradation of poly(D,L-lactide). The higher degradability is probably due to the greater water absorption in the amorphous domains. Copolymerisation is an important tool to modify the properties of the resulting copolymers and adjust them to the needs of a given application.

The study of the polymers' aging obtained through the characterisation by DSC, GPC and NMR showed stability in terms of the composition of the polymer chains. However, data relating to the calorimetric characteristics, studied by DSC, showed an increment of T_g values (Table 6.1). As regards the molecular weights and the polydispersity index, obtained by GPC analysis, the detected changes were minimal (Table 6.2). Finally, data concerning the molecular structure of polymers, obtained by NMR, showed results similar to those obtained in newly synthesised samples (Table 6.3). Thus, the aging of the polymer, stored at temperatures of 4 °C and in nitrogen, does not take place so rapidly. The DLS study of NP polymer dispersions reveals a good stability for up to 30 days. A variation in terms of the nanoparticles' size and dispersion stability is observed from their second month of life. In fact, the data obtained from the analysis of samples show non-overlapping curves with a variation of the dimensions and of PDI values and a reduction of the ZP values. The SEM images, in particular those of the sample with short-chain PLA (mPEO₁₁₃-b-PLA₃₀), show a complete loss of micellar morphology after about 100 days (Figure 6.3).

6.3 Chapter Summary

In Chapter 4, the aging issue of the mPEO-b-PLA_x system has been addressed in terms of the modifications of both the polymers and the nanoparticles as a function of time. The study of the polymers' aging obtained through the characterisation by DSC, GPC and NMR showed stability in terms of the composition of the polymer chains. However, data relating to the calorimetric characteristics, studied by DSC, showed an increase of T_g values. Molecular weights and the polydispersity indexes, obtained by GPC analysis, instead showed minimal variations. Finally, data concerning the molecular structure of polymers, obtained by NMR, showed results similar to those obtained in newly synthesised samples. By studying the aging of the polymer, stored at temperatures of 4 °C and in nitrogen, we find it does not take place so rapidly. As regards the study of NP polymer dispersion, the data reveal good stability up to 30 days. Measurements performed at 100 days instead showed total loss of particle organisation both by DLS and SEM.

6.4 References

1. Wu, C.S.; Characterizing Biodegradation of PLA and PLA-g-AA/Starch Films Using a Phosphate-Solubilizing Bacillus Species. *Macromol. Biosci.* **2008**, 8, 6, 560–567
2. Ishigaki, T.; Sugano, W.; Ike, M.; Kawagoshi, Y.; Fukunaga, I.; Fujita, M.; Abundance of polymers degrading microorganisms in a sea-based solid waste disposal site. *J. Basic Microbiol.* **2000**, 40, 3: 177-186.
3. Liu, L.; Fishman, M.L.; Hicks, K.B.; Liu, C.K.; Biodegradable composites from sugar beet pulp and poly(lactic acid). *J Agric. Food Chem.* **2005**, 53, 23: 9017-9022.
4. Tokiwa, Y.; Jarerat, A.; Biodegradation of poly(L-lactide). *Biotechnol Lett.* 2004, 26,10: 771-777.
5. Tokiwa, Y.; Jarerat, A.; Accelerated Microbial Degradation of Poly(L-lactide). *Macromolecular Symposia.* **2005**, 224,1: 367-376.
6. Lim, H.A.; Raku, T.; Tokiwa, Y.; A new method for the evaluation of biodegradable plastic using coated cellulose paper. *Macromol. Biosci.* **2004**,16, 4(9): 875-881.
7. Tsuji, H.; Miyauchi, S.; Enzymatic Hydrolysis of Poly(lactide)s: Effects of Molecular Weight, L-Lactide Content, and Enantiomeric and Diastereoisomeric Polymer Blending. *Biomacromolecules* **2001**, 2, 2: 597-604.
8. Cai, H.; Dave, V.; Gross, R. A.; Mccarthy, S. P.; Effects of physical aging, crystallinity, and orientation on the enzymatic degradation of poly(lactic acid). *J. Polymer Sci., Part B: Polym. Phys.* **1996**, 34, 16: 2701-2708.

CHAPTER 7

7.1 Conclusion and Future Outlook

In this thesis work, a protocol was developed for the synthesis and characterization of self-assembled polymeric NPs. We selected amphiphilic block copolymers of polyethylene oxide (PEO) and polylactic acid (PLA), two polymers already approved by the US Food and Drugs Administration (FDA) for medical use. The synthesis of the poly (lactic acid) block on a block of poly (ethylene oxide) has been carried out by means of ROP (Ring Opening Polymerization) catalyzed by 1,5-diazabicyclo[5.4.0]undec-5-ene (DBU). This completely metal-free synthesis avoids any potential issues of poor biocompatibility or allergenicity due to standard tin based ROP catalysts. The compositional characterization was carried out by solution Nuclear Magnetic Resonance (NMR) and Gel Permeation Chromatography (GPC). After polymerizing a great variety of PLA chains of different length (PEO₁₁₃-b-PLA_x- with x ranging from 30 to 1359), nanoparticles were assembled from different organic solvents: dimethylformamide (DMF), acetone, tetrahydrofuran (THF) and dioxane, using the technique of nanoprecipitation. NPs were then purified by dialysis and analyzed by Dynamic Light Scattering (DLS), obtaining for each sample a mean hydrodynamic diameter value and a value of dispersion diameters. Particle diameter ranges from 40 to 800 nm, with many of the polymers presenting different values as a function of the starting solvent. A plot of all samples in terms of the DLS variables displayed several clusters, ideally associated to different morphologies.

To verify the corresponding shapes, and then transform the plot into a morphological map that is able to guide the selection of the most promising nanocarriers for medical applications, investigation was necessary by microscopy. A crucial point, demonstrated by DSC measurements performed in bulk, is that the two blocks are actually miscible, and it is only the presence of water that keeps the particles stable.

Thus, only by Cryogenic Transmission Electron Microscopy (cryo-TEM) we could map the region of simple micelles (low diameter, low PDI) as well as a region of high PDI and diameter that was confirmed associated to polymersomes.

Cytotoxicity tests were performed on all samples and only the largest nanoparticles reduced cell viability. Finally, experiments have been carried out on the aging of both the polymer stored at low temperatures and in the anhydrous environment and the dispersed NPs. Both the polymer (average duration of about one year) and the solution nanoparticles (average duration about 30 days) showed good stability over time.

The great variety of morphologies that can be achieved by each mPEO₁₁₃-b-PLA_x polymer provided insight on the complexity of the self-assembly process that is often portrayed in literature as a simple phase separation due to the substitution of the good solvent with water. Instead, we portray a complex process where the reciprocal interactions between water, solvent and each block can modify the kinetic pathway and ultimately the morphology of the NP. Shaping the polymer particles offers the possibility to select for each application a form that simultaneously optimizes loading and interaction with the organs, to handle and transport the nanocarrier through the human body barriers. In the case of the transport of antitumor agents through BBB, preliminary studies were carried out (with C6 loading) in solvent mixtures, which will then be used for loading Paclitaxel. The "map" that connects simple measurements such as hydrodynamic radius and PDI (measured at DLS) has in this case allowed to identify as the most promising NPs for transporting the drug through BBB. These NPs belong to the family of micelles and have a diameter ranging from 40 to 100 nm.

Creating a map dedicated to the mPEO₁₁₃-b-PLA_x system has proven to be a useful tool for describing and representing this system in a synthetic and visual way, enabling understanding and organization of work. It would be interesting to check the correlation between DLS parameters and morphologies for other polymer systems to be used for drug delivery for nanotechnology applications in medicine.

The efficacy and the minimal toxicity of mPEO₁₁₃-b-PLA_x nanoparticles is an outcome that inspires future studies to improve the final application of these nanoparticles.

For example, optimizing the load level of C6 can further increase effectiveness. For this reason, further self-assembly experiments with solvent mixtures have been conducted in order to optimize the solubility of C6 without affecting the morphology of nanocarriers. In addition, numerous studies have shown that the size, rigidity and deformability of nanoparticles play a decisive role in their *in vivo* behavior^{1,2,3,4}. For example, when long-acting nanoparticles are prepared, there is a compromise between the half-life of the drug nanoparticles and the half-life of the drug. Smaller particles have a longer duration of circulation, but less load and a faster drug loss, while larger particles can improve drug loading and retain the drug better, but with less circulation^{5,6}. Softer particles are preferred due to their deformability allowing passage through capillary nets (diameter ranging from 5-10 μm) simulating physiological passage of red blood cells (diameter 7.5-8 μm) through the blood capillaries^{3,4} (Figure 7.1).

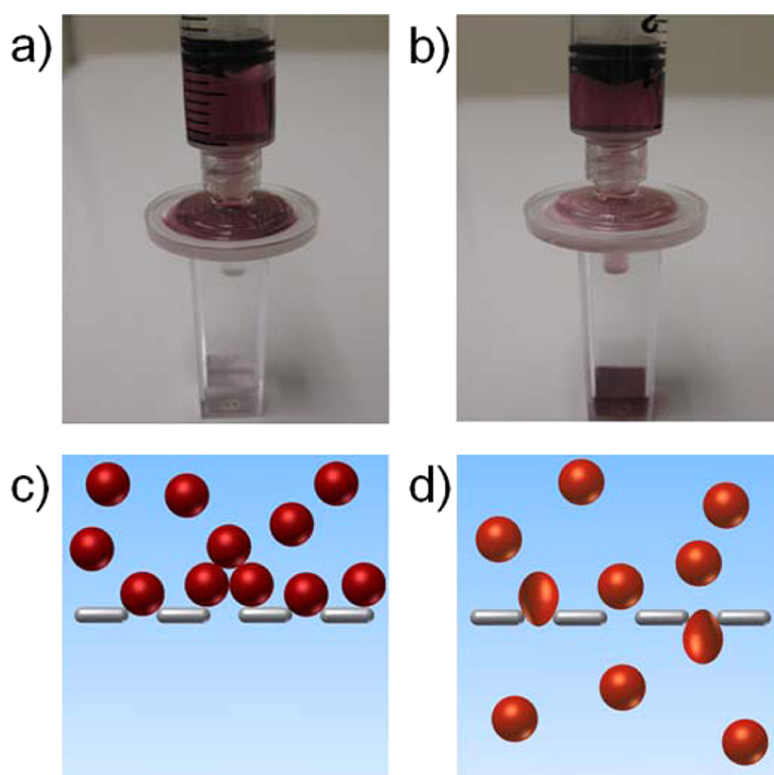


Figure 7.1. Photo images showing the ability of hard (a) and soft (b) NPs with a mean hydrodynamic size of 0.25 μm to pass filters with a pore size of 0.22 μm . Schemes showing the interactions of hard particles and soft particles with slits smaller than their size; the hard particles (c) are trapped by the slit, the soft particles (d) can deform and pass through the slit³.

A possible future work would be to enrich the already-drawn morphology map by superimposing a mobility map, made using techniques that allow locally measured mobility, such as photoluminescence of rotors.⁷

Further experiments could be conducted to evaluate the stability of lyophilized nanoparticles. Freeze-drying would allow nanoparticles to be used for longer periods and redispach them to the need without resorting to new preparation.

In addition, the use of stabilizers (eg. citrate, fatty acids, and other surfactant molecules) would help to ensures colloidal stability of NPs and modularize their interaction.⁸

The functionalization of the surface with specific ligands (eg. glucose⁹, mannose residue¹⁰ or mApoE^{11,12} : a modified fragment of human apolipoprotein E receptor would allow for easier crossing of biological barriers. The fields of application of the studied system, already widely used in the biomedical field, could be extended not only to drug delivery but also to the diagnosis of pathologies. For example, through the inclusion of paramagnetic particles in the polymeric structure¹³, obtained NPs dedicated to teranostics, or capable of simultaneously acting as contrast-NMR agents and drug carriers.

7.2 References

1. Banquy, X.; Suarez, F.; Argaw, A.; Rabanel, J-M.; Grutter, P.; Bouchard, J-F.; Hildgen P.; and Giasson S.; Effect of mechanical properties of hydrogel nanoparticles on macrophage cell Uptake. *Soft Matter*. **2009**, 5: 3984 -3991.
2. Merkel, T.J.; Chen, K.; Jones, S.W.; Pandya, A. A.; Shaomin Tian, S.; Napier, M.E.; William E. Zamboni, W.E.; DeSimone, J.M.; The effect of particle size on the biodistribution of low-modulus hydrogel PRINT particles. *Journal of Controlled Release* . **2012**: 37-44.
3. Zhang, L.; Cao, Z.; Li, Y.; Ella-Menye, J-R.; Bai, T.; and Jiang, S. Softer Zwitterionic Nanogels for Longer Circulation and Lower Splenic Accumulation. *ACS Nano*. **2012** , 6, 8: 6681-6686.
4. Cui, J.; Björnmalm, M.; Liang, K.; Xu, C.; Best, J.P.; Zhang, X.; and Caruso, F.; Super-Soft Hydrogel Particles with Tunable Elasticity in a Microfluidic Blood Capillary Model. *Adv. Mater*. **2014**, 26: 7295–7299.
5. Mohanraj, V. J.; Chen, Y. Nanoparticles;A Review. *Trop. J. Pharm. Res*. **2006**, 5, 561–573.
6. Redhead, H. M.; Davis, S. S.; Illum, L. Drug Delivery in Poly(lactide-co-glycolide) Nanoparticles Surface Modified with Poloxamer 407 and Poloxamine 908: In Vitro Characterisation and In Vivo Evaluation. *J. Controlled Release*. **2001**, 70, 353–363.
7. Vaccaro, G.; Bianchi, A.; Mauri, M.; Bonetti, S.; Meinardi, F.; Sanguineti, A.; Simonutti R.; Beverina, L.; Direct monitoring of self-assembly of copolymeric micelles by a luminescent molecular rotor. *Chemical Communication*, **2013**, 49, 76: 8474-8476.
8. Hrubý, M., Filippov, S. K., & Štěpánek, P. (2016). Biomedical Application of Block Copolymers. *Macromolecular Self-assembly*, 231-250.
9. Mamaeva, V.; Niemi, R.; Beck, M.; Özliseli, E.; Desai, D.; Landor, S.; Gronroos, T.; Kronqvist, P.; 9, Pettersen, I. KN; McCormack E.; 3,11, Rosenholm, J.M.; Linden M.; and Cecilia Sahlgren, C.; Inhibiting Notch Activity in Breast Cancer Stem Cells by Glucose Functionalized Nanoparticles Carrying γ -secretase Inhibitors. *Official journal of the American Society of Gene & Cell Therapy*. **2016**, 24, 5: 926-936.
10. Rieger, J.; Stoffelbach, F.; Cui D.; Imberty, A.; Lameignere,E.; Putaux,J-L.; Jérôme, R.; Jérôme, C.; and, and Auzély-Velty, R.; Mannosylated Poly(ethylene oxide)-b-Poly(ϵ -caprolactone) Diblock Copolymers: Synthesis, Characterization, and Interaction with a Bacterial Lectin. *Biomacromolecules*. **2007**, 8, 9: 2717-2725.
11. Gregori, M. Bertani, D.; Cazzaniga, E.; Orlando, A.; Mauri, M.; Bianchi, A.; Re, F.; Sesana, S.; Minniti, S.; Francolini, M.; Cagnotto, A.; Salmona, M.; Nardo L, Salerno, D.; Mantegazza, F.; Masserini, M.; Simonutti, R.; Investigation of Functionalized Poly(N,N-dimethylacrylamide)-block-polystyrene Nanoparticles As Novel Drug Delivery System to Overcome the Blood-Brain Barrier In Vitro. *Macromol Biosci*.**2015**,15, 12:1687-1697.
12. Saraiva, C.; Praça, C.; Ferreira, R.; Santos, T.; Ferreira, L.; Bernardino, L.; Nanoparticle-mediated brain drug delivery: Overcoming blood-brain barrier to treat neurodegenerative diseases. *J Control Release*. **2016**, 235: 34-47.
13. Balasubramaniam, S.; Kayandan, S.; Lin Y.N.; Kelly, D.F.; House M.J.; Woodward, R.C.; St. Pierre,T.G.; Riffle, J.S.; and Davis, R.M.; Toward Design of Magnetic Nanoparticle Clusters Stabilized by Biocompatible Diblock Copolymers for T₂-Weighted MRI Contrast. *Langmuir*, **2014**, 30: 1580-1587.

List of Abbreviations

Ac	Acetyl
Ace, Ace	Acetone
AFM	Atomic Force Microscopy
BBB	Blood Brain Barrier
BCP	Block Copolymer
°C	Degree Celsius
Cryo-EM	Cryo-Electron Microscopy
Cryo-TEM	Cryo-Transmission Electron Microscopy
DBU	1,8-diazabicyclo[5.4.0]-undec-7-ene
DCM	Dichloromethane
Diox	Dioxane
DDS	Drug Delivery Systems
DMF	Dimethylformamide
DSC	Differential Scanning Calorimetry
EtOAc	Ethyl Acetate
EtOH	Ethanol
FDA	Food and Drug Administration

List of abbreviation

FI	Fluorescence Index
g	Gram(s)
GPC	Gel Permeation Chromatography
h	Hour(s)
Hz	Hertz
HUVECs	Human Umbilical Vein Endothelial Cells
<i>i,i</i>	Isotactic, Isotactic
<i>i,s</i>	Isotactic, Syndiotactic
M	Molar
MAL	Maleimide
MeCN	Acetonitrile
Me	Methyl
MeOH	Methanol
MHz	Megahertz
min	Minute(s)
M_n	Number average molecular weight
mp, MP	Melting Point
MW	molecular weight
M_w	Weight average molecular weight

List of abbreviation

n.d.	none detected
ND	Not Determined
Nm	Nanometer(s)
NMR	Nuclear Magnetic Resonance
NP	Nanoprecipitation
NP, NPs	Nanoparticle, Nanoparticles
os	organic solvent
PDI	Polydispersity Index
PEO	Poly(ethylene oxide)
PLA	Poly(lactic acid)
ppm	parts per million
PTX	Paclitaxel
q	quartet, in NMR spectroscopy
Rac	Racemic
ROP	Ring Opening Polymerization
RES	Reticuloendothelial System
sec	second(s)
SEC	Size Exclusion Chromatography
SEM	Scanning Electron Microscopy

List of abbreviation

solv	solvent
TEM	Transmission Electron Microscopy
thf, THF	Tetrahydrofuran
ZP, ζ	Zeta Potential
1 D	one dimensional
2 D	two dimensional
3 D	three dimensional

Acknowledgements

Nanotechnology is a scientific crossroads where numerous disciplines converge. For this reason, it was not easy to take a road well articulated. These years of DdR, elapsed between the Department of Materials Science and the Department of Experimental Medicine, they have allowed me to open my eyes to "what we see" but mostly on "what we do not see." My doctor path in the world of nanotechnology and nanomedicine, has not been a challenge just for me, but also for who I was able to drive with extreme patience and great dedication. First, I thank my PhD coordinator, Prof. Gianfranco Pacchioni, who with great seriousness and professionalism has directed my training. The present work is the result of close cooperation between two groups of great scientific research, that of Prof. Roberto Simonutti and that of Prof. Massimo Masserini. To my supervisors, I extend my deepest gratitude for having introduced respectively to the study of nanotechnology and nanomedicine and for welcoming me in their laboratories. I thank my tutor: Dr. PhD Michele Mauri and Dr. PhD Maria Gregori who were able to send me with great enthusiasm and clarity on their knowledge. Thank you! For your time and expertise, he pointed in the right direction for my research and for having supported me in difficult times. Thank you: Dr. Daniela Bertani, Dr. Silvia Ferrario and Dr. Simone Murganti for the synthesis of the samples and Dr. PhD Roberto Marotta, ITT Genova for their cryo-TEM characterization.

Dr. PhD Alberto Bianchi is the great merit of having organized the work done in the laboratory, bringing order and discipline in our work activities: basic precondition for work well. I thank him also for his willingness to listen and giving me valuable advice. I thank Dr. Norberto Manfredi for all the advice relating to the proper thesis writhing. I sincerely thank Dr. Maria Fassina and Dott.ssa Caterina Giuliani for their kindness, helpfulness and competence that have made bureaucratic obstacles easy to overcome.

Acknowledgements

To all the friends of PosyLife Group: Dany and Silvia, Matteo , Simone Bonetti, Murali, Teffa, Valentina.

The group of Monza and in particular Carmen and Simona.

Last but not least: Andrea and Anna for sharing intensely every moment of these last years.

I thank my family for the love and support in my choices.

Thanks ... every one of you has a special place in my heart!

Publication list

In attached the detailed list of the scientific production during the PhD.

Oral Presentation:

Manzone, D.; Bertani, D.; Ferrario, S.; Mauri, M.; Simonutti, R.; ‘ **SELF-ASSEMBLY OF BIOCOMPATIBLE BLOCK COPOLYMERS FROM A VARIETY OF GOOD SOLVENTS**’. **EUPOC** - Block Copolymers for Nanotechnology Applications, 22 – 26 May 2016, Gargnano, lago di garda, Italy.

Poster:

Manzone, D.; Bertani, D.; Ferrario, S.; Mauri, M.; Gregori, M.; Marotta, R.; Masserini, M.; Simonutti, R ; ‘**BIOCOMPATIBLE BLOCK COPOLYMERS FOR NANOMEDICINE**’. **AIM- XXII National Conference**- 11-14, September 2017 Genova, italy.

Articles on peer-reviewed journals:

Bertani, D.; Marotta, R.; Ferrario, S.; Manzone, D.; Gregori, M.; Orlandi, A.; Michele Mauri, M; Masserini, M; Simonutti, R. PEO-*b*-PLA nanoparticles morphology reloaded. *Macromolecules*, **2017**.
Submitted

Appendix

Sample	Solvent	$\langle D_H \rangle_1$ (nm)	PDI ₁	$\langle D_H \rangle_2$ (nm)	PDI ₂
PEO₁₁₃-<i>b</i>-PLA₆₅	ACT	21	0.111	–	–
	DX	31	0.098	–	–
	THF	41	0.053	–	–
	DMF	34	0.112	–	–
PEO₁₁₃-<i>b</i>-PLA₃₀₅	ACT	33	0.070	–	–
	DX	34	0.114	–	–
	THF	65	0.143	–	–
	DMF	134	0.240	–	–
PEO₁₁₃-<i>b</i>-PLA₄₀₃	ACT	47	0.096	–	–
	DX	74	0.140	–	–
	THF	139	0.096	–	–
	DMF	138	0.161	1064	0.307
PEO₁₁₃-<i>b</i>-PLA₄₈₆	ACT	80	0.121	–	–
	DX	92	0.109	–	–
	THF	136	0.046	912	0.128
	DMF	109	0.062	831	0.173
PEO₁₁₃-<i>b</i>-PLA₁₃₅₉	ACT	620	0.194	–	–
	DX	123	0.150	–	–
	THF	42	0.075	832	0.168
	DMF	219	0.208	994	0.364

Table 1. Average hydrodynamic diameters ($\langle DH \rangle$) and PDIs of copolymer dispersions obtained from the four different solvents after dialysis. When multiple NP populations are present, each peak was considered separately.

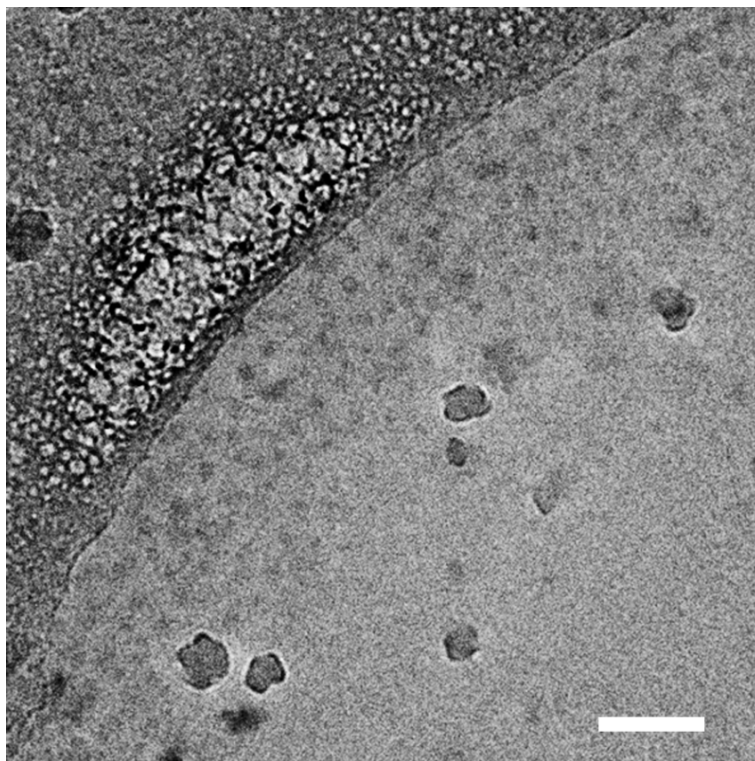


Figure 1. Single projection image showing PEO₁₁₃-*b*-PLA₆₅ many micelles (arrowheads). The arrows point to contaminations Scale bar 100 nm.

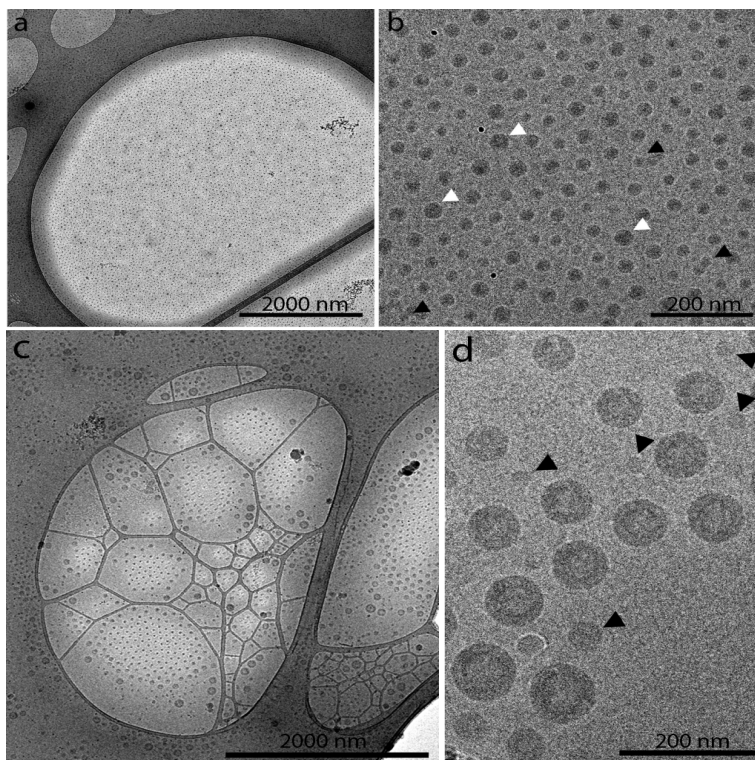


Figure 2. Cryo-EM projection images at different magnifications of PEO₁₁₃-*b*-PLA₁₃₅₉ assembled from THF [(a) and (b)] and PEO₁₁₃-*b*-PLA₄₈₆ assembled from DX [(c) and (d)].

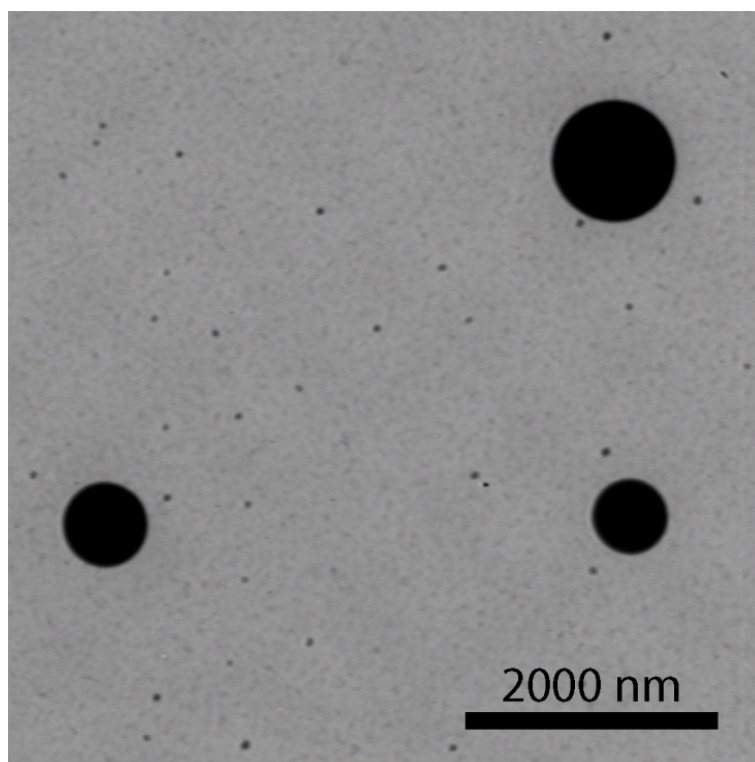


Figure 3. Room temperature TEM micrograph of large compound aggregates in $\text{PEO}_{113}\text{-}b\text{-PLA}_{1359}$ self-assembled from THF.